AD-A133 746 EFFECT OF CONTACT DAMAGE ON THE STRENGTH OF CERAMIC MATERIALS(U) NATIONAL BUREAU OF STANDARDS WASHINGTON DC B R LAWN ET AL. OCT 83 N00014-81-F-0002 1/2

UNCLASSIFIED F/G 11/2 NL

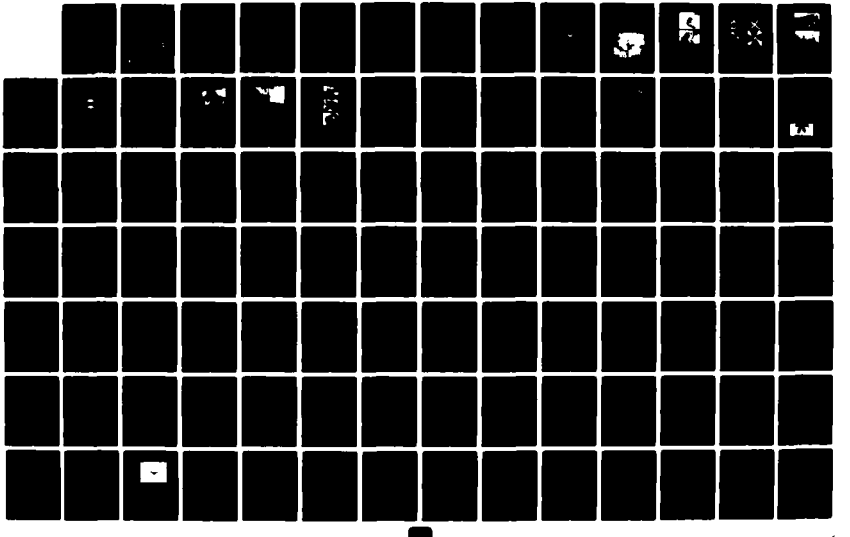

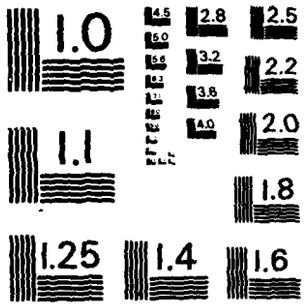

EFFECT OF CONTACT DAMAGE ON THE STRENGTH OF CERAMIC MATERIALS

B.R. Lawn, S.M. Wiederhorn

and

B.J. Hockey, R.F. Cook, H. Richter,
B.L. Symonds, J.P. Dabbs, C.J. Fairbanks,
H. Multhopp, A.C. Gonzalez, S.W. Freiman

Technical Report

ONR Contract No. N00014-81-F-0002
NBS Project No. 5610453

for

Office of Naval Research
Arlington, VA 22217

by

National Bureau of Standards
Washington, DC 20234

October 1983

EFFECT OF CONTACT DAMAGE ON THE STRENGTH OF CERAMIC MATERIALS

→ Contents:

INTRODUCTION

Work on this program during the past year has been directed towards the analysis of surface damage that occurs under different contact conditions, and the resulting strength of brittle materials containing such damage.

Sliding Friction Studies

A sliding friction apparatus has been completed for introducing cone fracture damage in brittle surfaces. The equipment translates a sphere across a specimen surface, thereby producing fracture tracks. The normal and tangential forces are continuously monitored during each run to allow for frictional characteristics to be specified. Temperatures up to 800°C can be achieved, with potential for modification to 1500°C. The strengths of specimens thus damaged are measured in 4-point bending.

Work thus far has concentrated on soda-lime glass. Damage tracks have been produced over a wide range of friction conditions, and over a range of normal contact loads. The strengths of the damaged specimens satisfy a simple relation, derived from fracture mechanics,

$$\sigma = K_c^{4/3} F(f)/P^{1/3}$$

where P is the normal load, F(f) is a function of the friction coefficient and K_c is toughness. The major finding is that F(f) is a slowly varying function, dropping by a factor of only about 2 as f increases from zero to unity. Thus strength is not a highly sensitive function of frictional properties, as has been implied by previous studies.

Preliminary data have been obtained on glass at elevated temperatures. Again, temperature is not a critical parameter, since K_c in the above formula is not temperature sensitive (until creep conditions prevail). Work is scheduled to begin on other materials in the coming year, to confirm the role of toughness in the strength relation.

Controlled Flaw Studies

Considerable effort is being directed to the use of indentation flaws for controlled strength studies. This approach allows one to obtain strength data with high reproducibility, from which accurate fracture mechanics parameters, such as toughness K_c and crack velocity exponent n, can be evaluated. The means by which indentation flaw techniques can be used in the assessment of reliability have been thoroughly investigated. The issues of point versus line flaws, equilibrium versus kinetic conditions of fracture, have been addressed. The role of residual stresses in the strength formulations has been given special attention.

One aspect of this work which is proving of particular interest is the influence of flaw size on strength behavior. The controlled flaw allows one to investigate such influences in a systematic manner. It is being found that when the flaw size approach the scale of the microstructure the strength properties show anomalous behavior. These anomalies relate to the effect of grain configurations on local microstresses, variations in the effective toughness, etc. Work is continuing on this part of the program.

Rate Effects

One of the most important variables in the contact fracture phenomenon is time. This is particularly the case in the critical conditions for initiating

radial cracks beneath point indenters. The threshold load for initiation is dramatically increased if the rate of contact, and the moisture content of the environment, are increased. Equipment for producing indentations down to $\sim$1 msec is now in full operation. This equipment includes a microscope facility for viewing the indentation events in situ.

Work on this part of the program over the past year has concentrated on determining the kinetics of the radial crack "pop-in" on exceeding the threshold. It is established that this pop-in can occur well after the indentation cycle is complete, once more emphasizing the role of residual stresses. Theoretical modelling of the phenomenon is underway. The work offers the promise of new light on the mechanisms by which cracks generate in brittle materials in the first place.

INDENTATION ANALYSIS: APPLICATIONS IN THE STRENGTH AND WEAR OF BRITTLE MATERIALS

B. R. Lawn, B. J. Hockey and H. Richter*

Fracture and Deformation Division
National Bureau of Standards
Washington, D.C. 20234, U.S.A.

---

* On leave from: Fraunhofer Institut fur Werkstoffmechanik
Freiburg, W. Germany

Journal of Microscopy, Vol. 130, *Pt* 3, *June* 1983, *pp.* 295–308.
Received 15 *July* 1982; *accepted* 30 *September* 1982

Indentation analysis: applications in the strength and wear of brittle materials

by B. R. LAWN, B. J. HOCKEY *and* H. RICHTER*, *Fracture and Deformation Division, National Bureau of Standards, Washington, D.C. 20234, U.S.A.*

KEY WORDS. Indentation analysis, strength, brittle materials.

SUMMARY

Some recent developments in the principles and applications of indentation fracture in brittle materials are surveyed. Attention is focused on 'sharp' indenters, for which precursor 'plasticity' is an essential element of the crack development. A major consequence of this plasticity is a residual contact stress field which exerts a dominant influence on ensuing mechanical behaviour. This influence is discussed in relation to strength and wear properties of brittle ceramics. Emphasis is placed on the advantages of the indentation method as a means of producing controlled cracks for evaluating material fracture parameters and for gaining insight into flaw micromechanics.

1. INTRODUCTION

Solids with large components of covalency and ionicity in their atomic bonding (ceramics, glasses, semiconductors) tend to be highly brittle at room temperature. The key to engineering design with this class of materials is thus the containment of crack growth. Nowhere is this susceptibility to fracture more apparent than in contact phenomena; for example, the inadvertent impingement of a single dust particle on to the pristine surface of an optical fibre can lead to a strength degradation of more than an order of magnitude. It is in this context that the widely expanding discipline of 'indentation fracture mechanics' (Lawn & Wilshaw, 1975) may be seen as establishing a basic scientific framework for analysing a broad range of strength- and wear-related properties.

In this paper we shall outline some of the more recent developments in indentation analysis, with particular emphasis on the microscopical aspects. Our discussion will focus on the damage patterns produced in ideally 'sharp' (i.e. plastic) as distinct from 'blunt' (elastic, e.g. Hertzian) contact. The former, quite apart from their greater topicality, offer certain advantages as a tool for materials testing: the patterns contain information on the modes of deformation, as well as on the fracture; since indentation fracture can be produced on the most pristine of surfaces above some threshold in the loading, the processes of crack nucleation, as well as propagation, can be investigated; the patterns are subject to a high degree of control in their geometry, scale and placement, and may be quantified entirely in terms of characteristic surface dimensions in conjunction with the contact load; the nature of the damage relates more closely to that which pertains in 'real' strength degradation and wear mechanisms under typical component fabrication and service conditions.

In our survey we shall first outline the mechanics of crack evolution during an indentation cycle, and then describe certain applications to practical properties. For the first of these, the

* On leave from: Fraunhofer Institut für Werkstoffmechanik Freiburg, West Germany.

vital interrelation between deformation and fracture processes will be a central theme. The most important manifestation of this interrelationship is the residual driving force exerted by the deformation zone on the cracks. For the applications, strength properties of pre-indented test pieces are considered, both for the insight they provide into the general micromechanics of flaws and for the element of control that may be exercised in the evaluation of material fracture parameters. A brief description of erosive wear properties is also included.

2. INDENTATION PATTERN IN SHARP CONTACT

2.1. *General features*

The indentation fracture patterns produced by sharp indenters (e.g. Vickers, Knoop) have been well characterized (Lawn & Swain, 1975; Evans & Wilshaw, 1976; Swain & Hagan, 1976; Hagan & Swain, 1978; Puttick, 1978; Arora *et al.*, 1979; Marshall & Lawn, 1979; Lawn *et al.*, 1980a). The general features of this type of pattern are shown in the schematic of Fig. 1. The indenter is loaded on to the surface at normal force P (or, equivalently, at incident kinetic energy U_K in impact loading). Immediately beneath the contact the material deforms irreversibly, giving rise to a 'plastic' enclave within the elastic half-space surround matrix; the scale of this

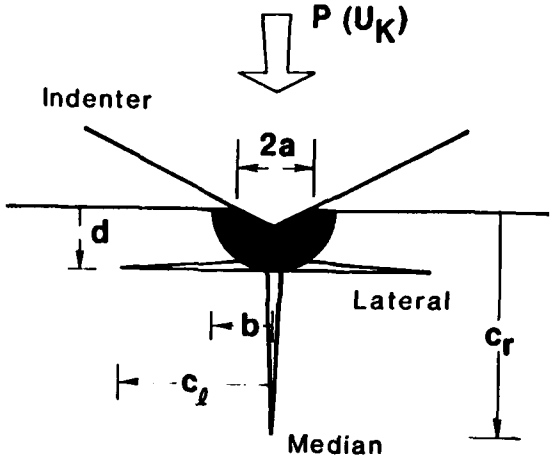

Fig. 1. Schematic of deformation/fracture pattern associated with a sharp indenter.

deformation is quantified by the characteristic dimensions a and b of the hardness impression and plastic zone, respectively. Two types of crack, both with essentially penny-like geometry, grow out of the deformation zone: median/radial cracks, on planes defined by contact normal and impression diagonal, characterized by dimension c_r (Lawn *et al.*, 1980a); lateral cracks, closely parallel to the specimen surface and centred on the base of the deformation zone, characterized by dimension c_l (Marshall *et al.*, 1982). The object of the fracture mechanics approach to the contact problem is to determine relations between the quantities defined in Fig. 1 and appropriate material parameters such as toughness, K_c, hardness, H, and Young's modulus, E.

Important modifications to the axial symmetry of the indentation pattern can ensue if a tangential component is added to the loading, as in sliding or rolling, or oblique impact. Some of these modifications are discussed in other papers in this volume.

2.2. *Deformation zone*

The deformation that occurs in highly brittle materials (especially those with a large component of covalent bonding) is typified by relatively large ratios of hardness (defined here as the mean contact pressure) to modulus, H/E. In silicon, for instance, $H/E \approx 0{\cdot}08$, implying stress

levels approaching the theoretical limiting strength of the structure. At these levels the conventional descriptions of slip and yield by classical dislocation glide must be regarded with caution. Hill & Rowcliffe (1974) prefer to consider the deformation process in silicon in terms of 'block' slip, in which shear takes place homogeneously and catastrophically across surfaces of maximum shear stress. A feature of this mode is that it does not depend critically on the existence of crystallographically favourable easy-glide planes. Accordingly, the concept is consistent with the recent identification of shear lines in indented soda-lime glass by Hagan (1980).

An important manifestation of such high-stress modes of deformation is the strong localization about the contact site (i.e. $b \approx a$ in the notation of Fig. 1). Materials in this category tend to show strong depth recovery at the unloaded impression, due to 'elastic springback' (Lawn & Howes, 1982). However, this recovery is never complete, in which case there exists a state of residual stress in the material. The intensity of such residual fields can be high, as is readily apparent from the TEM photograph of an indentation site in silicion (Fig. 2). (These fields are perhaps more commonly observed by virtue of their attendant birefringence patterns in transmission optical microscopy—see Fig. 4 later.) As we shall demonstrate, residual stresses can play a crucial role in the subsequent mechanical response of indented surfaces.

At sufficiently high rates of loading dynamic effects can become important (Evans & Wilshaw, 1977). Indeed, under impact conditions the plastic work rate can be so intense as to cause surface melting, in even the most refractory of ceramics (Lawn *et al.*, 1980b). Figure 3 shows evidence of this in glass and alumina impacted with silicon carbide particles.

Quantitative analysis of the deformation zone is a complex problem in solid mechanics. Elastic/plastic models based on the notion of an expanding internal cavity under pressure

Fig. 2. TEM of foil section in Vickers-indented silicon. Plane of specimen surface and of foil is (110). Note confinement of deformation about contact area.

Fig. 3. SEM views of surface of (a) glass, (b) Al_2O_3 (H.P.), impacted with 150 μm SiC particles at 90 m s^{-1}. Molten zones are evident.

(contact area), with immediate plastic and remote elastic surround volumes (embedded deformation zone), provide the most common starting point for obtaining a solution. It needs always to be remembered, however, that such models, based as they are on the underlying assumptions of spherical symmetry in the deformation geometry and a well-defined, continuous, homogeneous yield process, must inevitably be limited in their capacity to represent the inelastic indentation response of brittle solids.

2.3. *Cracks*

Above some threshold in the contact loading the crack system of Fig. 1 initiates spontaneously. Once developed, the radial and lateral cracks become highly stable. The physical processes actually responsible for the initiation remain somewhat obscure, although there is

growing evidence that the shear modes referred to in the previous subsection provide the essential crack nuclei (Hagan, 1980; Dabbs & Lawn, 1982).

Although the regular penny-like geometry of the well-developed cracks would seem to suggest a reasonably straightforward growth history through the contact cycle, direct observations reveal that this is far from so. Figure 4, a sequence of subsurface views of Vickers indentation in glass, illustrates the point. It is clear from this sequence that a significant portion of the radial crack evolution occurs during the unloading half-cycle (Marshall & Lawn, 1979). An important

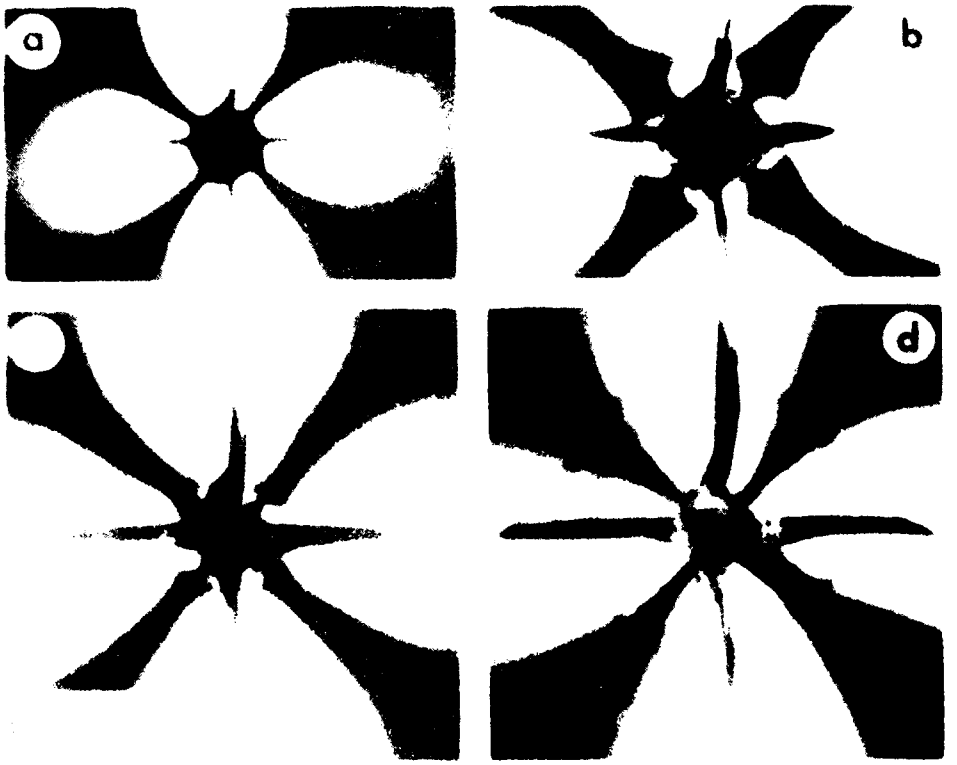

Fig. 4. Subsurface view, in crossed polars, of Vickers indentation in soda-lime glass in inert environment (N_2 gas). Showing full cycle, at loading (a) 47 N and (b) 90 N, and unloading (c) 30 N and (d) 0. Lateral cracks faintly visible in (d)

clue to such behaviour is the intense residual birefringence which remains about the contact site. It is the irreversible component of the stress field which drives the cracks outward into their ultimate circular symmetry; the reversible component is actually compressive over much of the prospective crack area, and accordingly acts as a constraint to growth while the load is applied (Lawn *et al.*, 1980a). The identification of the residual field as the critical component in the crack driving force is reinforced by the observation that the crack system can continue to expand (in the presence of a moist environment) long after the indentation cycle has been completed.

A closer look at the tip and interface regions of the indentation cracks reveals that the plasticity elements so critical to the initiation processes play absolutely no role in the micromechanisms of propagation; the brittle crack is atomically sharp, and extends in strict accordance with the classical picture of sequential bond rupture (Lawn *et al.*, 1980c; Lawn, 1983).

Fig. 5. TEM of ribbon segment of radial crack in sapphire: (a) dark field and (b) bright field conditions. Note misfit dislocation and stacking fault contrast at interface, absence of crack-tip plasticity.

Figure 5, showing TEM micrographs of a radial crack segment in an aluminium oxide foil, is a typical example of the configurations observed. There is clear evidence of network dislocations at the crack, but these are readily demonstrated to be associated with lattice misfit at a healed interface (Hockey, 1982). No slip dislocations are observed to emit from the crack tip. These observations are important because they establish the basis for theoretical descriptions of fundamental crack growth laws (Lawn, 1983).

The symmetry of the fully grown indentation cracks allows for straightforward fracture mechanics analysis. Accordingly, the residual driving force acting on the cracks may be quantified in terms of an appropriate stress intensity factor (Marshall & Lawn, 1979; Fuller *et al.*, 1982);

for the median/radial system this factor has the simple power-law form

$$K_r = \chi P / c_r^{r/2} \tag{1}$$

where $r = 3$ for 'point' loading and $r = 1$ for 'line' loading (it being understood that P is a force per unit length in the latter case), and $\chi \propto (E/H)^m$ is a dimensionless elastic/plastic parameter with $m \approx 0{\cdot}5$–$0{\cdot}7$ (Lawn *et al.*, 1980a); a similar relation, albeit somewhat more complex, is obtained for the lateral system (Marshall *et al.*, 1982). Recalling the tendency for these crack systems to continue in stable growth toward the end of the contact cycle (Fig. 4) we may, under suitably 'inert' (e.g. moisture-free) testing conditions, identify K_r in Eq. (1) with the critical stress intensity factor K_c for equilibrium extension, thereby providing the means for determinations of material toughness from simple radial crack traces (Anstis *et al.*, 1981).

3. INDENTATION CRACKS IN STRENGTH EVALUATION

3.1. *Controlled flaws*

The strength of brittle materials is governed by 'flaws', most commonly located in the surface. These flaws may be introduced by the processes of component fabrication, e.g. machining or polishing, or during service, e.g. via chance encounters with sharp, hard particles in the working environment. Indentation crack systems, in particular the more penetrative median/radial system, can be used to simulate such natural flaws. Simulations of this kind offer the advantage of almost absolute control of experimental conditions, namely in the scale (via the contact load), geometry and location of the critical failure origin. One then has the capacity for following the entire growth history of the flaw en route to instability, e.g. using optical techniques analogous to that shown in Fig. 4. As we shall indicate, studies along these lines reveal new types of flaw response, with important implications in the general theory of strength.

In the following subsections we distinguish between strength characteristics obtained under equilibrium and kinetic conditions of fracture.

3.2. *Equilibrium fracture: flaw stability*

In chemically inert testing environments (or at fast loading rates, or at low temperatures) the flaw system is in a state of mechanical equilibrium at failure. For a classical 'Griffith' flaw whose driving force for crack extension comes solely from a uniformly applied tensile stress, the configuration suddenly becomes unstable at a critical load, so failure occurs spontaneously. This concept forms the crux of modern-day theories of strength. Designing with brittle materials of given toughness then becomes a question of predetermination (often by statistical methods) of the size of the largest flaw.

However, when a residual field exists about the flaw centre a fundamentally different response to applied stresses becomes manifest. The local field, while adding to the total driving force on the crack, tends also to stabilize the growth. Consequently, the crack exhibits a distinctive precursor stage of stable crack growth prior to failure instability. This growth characteristic, first proposed by Cottrell (1958), is now well documented in indentation systems (Marshall *et al.*, 1979, 1981; Cook *et al.*, 1982; Marshall, 1982). Figure 6, which shows a Knoop indentation in silicon nitride before and during application of a bending force, is typical of the optical observations.

The precursor crack growth is readily amenable to fracture mechanics analysis (Marshall *et al.*, 1979). The stress intensity factor for the flaw loaded in an applied tension σ_a now has two components,

$$K = K_r + K_a = \chi P / c_r^{r/2} + \psi \sigma_a c_r^{1/2} \tag{2}$$

where χ in the residual component is defined as in Eq. (1) and ψ in the applied component is a dimensionless, material-independent, crack geometry term. The requirement for instability is $K = K_c$, $dK/dc_r = 0$, at which point $\sigma_a = \sigma_m$, $c_r = c_m$, where

$$\sigma_m = [r\,(r+1)]K_c / \psi c_m^{1/2} \tag{3a}$$

$$c_m = [(r+1)\,\chi P / K_c]^{2/r} \tag{3b}$$

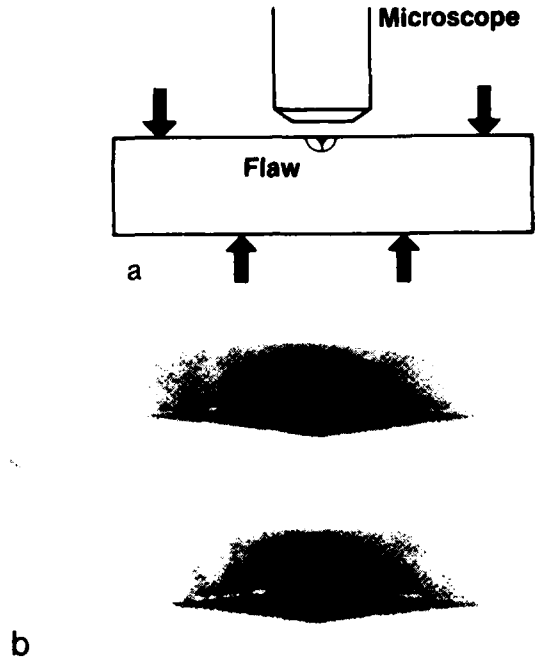

Fig. 6. Growth of radial cracks at indentations during stressing to failure. (a) Schematic of experimental arrangement for *in situ* viewing of cracks. (b) Micrographs showing Knoop-indented Si_3N_4 (H.P.) before (upper) and during (lower) stressing to failure. (Courtesy D. B. Marshall.)

defines the failure configuration. Eq. (2) may now be rearranged to provide an explicit formulation for the equilibrium precursor growth stage; inserting $K=K_c$ and combining with Eq. (3) we accordingly obtain

$$\sigma_a/\sigma_m = [(r+1)\,r]\,(c_m/c_r)^{1/2}[1-(c_m/c_r)^{r/2}/(r+1)] \tag{4}$$

An appropriately normalized plot of this applied-stress/crack-size function is shown in Fig. 7 for point flaws ($r=3$), along with representative Vickers and Knoop data on silicon nitride (Marshall, 1982). It is clear from this figure that the extent of the stable growth can be substantial.

It may be noted in Eq. (3) that all terms in crack size can be eliminated completely from the strength equation. By inverting this equation an expression may be obtained for K_c in terms of P and σ_m, two test variables which can be measured to relatively high accuracy. This provides an alternative avenue to toughness evaluation, without the need for monitoring the position of the crack tip (Chantikul *et al.*, 1981a).

An interesting study of surface cracks by Marshall and co-workers is throwing some light on to the micromechanics of machining damage. They find that the indentation crack extension shown in Fig. 6 correlates directly with the intensity of backscattered acoustic waves originating from a surface signal generator (Tien *et al.*, 1982). This correlation is particularly useful in the case of machining flaws which, by virtue of their small size and subsurface confinement, are not amenable to simple microscopical observation (especially, of course, in opaque materials). Marshall (1983) finds that, when stressed, the machining flaws show the same kind of strong acoustic wave scattering as do the indentation cracks. Since much of conventional mechanical testing of ceramic components is carried out on specimens in their as-machined state there is a clear need for a revised approach to the analysis of strength data (Lawn, 1982).

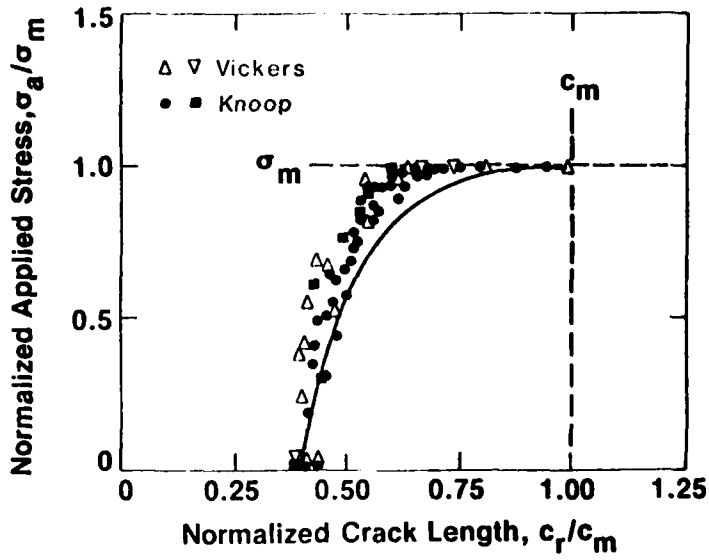

Fig. 7. Stable crack extension in Knoop- and Vickers-indented Si_3N_4 (H.P.) during stressing to failure. (Courtesy D. B. Marshall.)

3.3. *Kinetic fracture: fatigue*

In many brittle materials equilibrium fracture conditions are difficult to realize because of an extreme sensitivity to even minute traces of reactive chemical species in the environment, notably water. The chemical interactions take place specifically at the crack tip where the stress concentration is most intense. The major characteristic of this kind of fracture is a rate dependence which varies dramatically with the stress intensity factor. Thus cracks can extend subcritically with time until the instability requirement referred to in the previous subsection is met, at which point failure obtains. Since the strength under these conditions is lower than in a strictly inert environment, the material is said to show 'fatigue'. Accordingly, specimen 'lifetime' at given applied load becomes an important design concept for structural applications.

That the magnitude of the subcritical growth is by no means small is clearly seen in the micrographs of Fig. 8, showing fracture surfaces of Vickers-indented soda-lime glass stressed at a constant rate to failure in water (Marshall & Lawn, 1980). In the upper micrograph the indented surface was annealed prior to breaking to remove the residual contact stresses, and in the lower micrograph the specimen was broken in its as-indented state. The degree of extension relative to the initial flaw is clearly greater in the latter case, reflecting the additional component in the crack driving force. A more graphic demonstration of the time history of the crack growth to failure may be obtained by super imposing stress pulses on to the externally applied field, thereby leaving crack-front position markers of the kind shown in Fig. 9 (Kerkhof & Richter, 1969).

The existence of the residual stress term has a profound influence on the analysis of crack velocity parameters from fatigue strength data. Most commonly, the parameters sought are the exponent n and coefficient v_0 in the empirical velocity function (Wiederhorn, 1974)

$$v = v_0(K/K_c)^n \tag{5}$$

In combination with the stress intensity factor for indentation cracks, Eq. (2), at specified loading P and $\sigma_a(t)$, this function reduces to a differential equation in $c_r(t)$ (Marshall & Lawn, 1980; Chantikul *et al.*, 1981b; Lawn *et al.*, 1981; Cook *et al.*, 1982). The solution to this differential equation has to satisfy initial conditions $t = 0$, $K = K(c_0)$, and final conditions $t = t_f$, $K = K_c$ ($dK/$

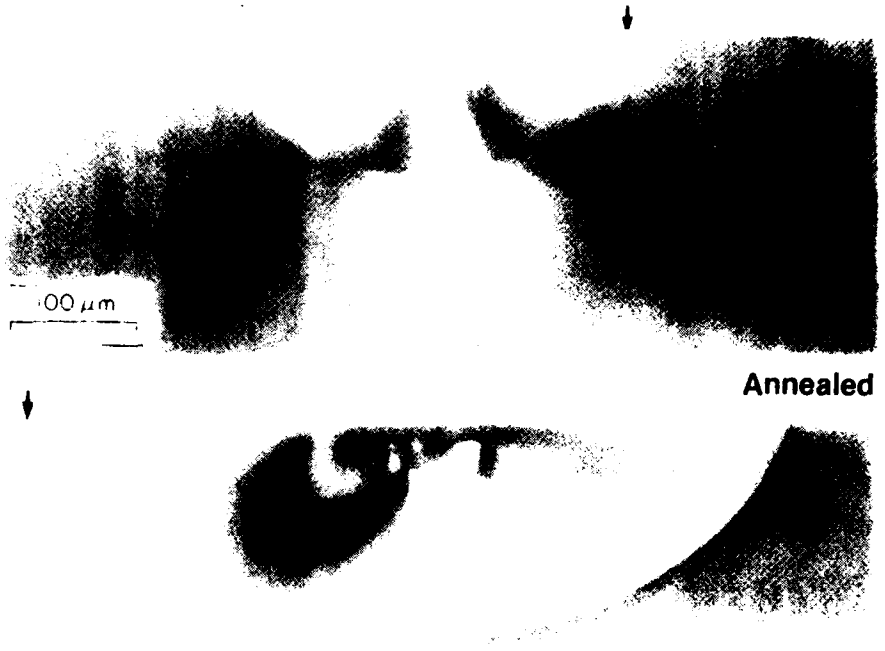

Fig. 8. Fracture surfaces of Vickers-indented soda-lime glass broken in water at fixed contact load and stressing rate. Arrows designate failure origins. Note greater extension in lower micrograph, reflecting the contribution of the residual contact field to the crack driving force.

$dc_r > 0$). For the special case $\sigma_a(t) = \text{const.} = \sigma_f$ the solution has the familiar closed form (Fuller *et al.*, 1982)

$$t_f = \lambda' / \sigma_f^{n'} \tag{6}$$

where the primes are to indicate parameters influenced by residual stresses. In the limiting case of zero residual stress ($\chi = 0$) the crack velocity exponent is found directly from the slope of a logarithmic plot of lifetime versus applied stress, i.e. $n' = n$. For non-zero residual stress ($\chi \neq 0$), however, the slope gives only an *apparent* velocity exponent, related to the *true* exponent via 'transformation' relations

$$n' = 3n\ 4 + 1\ 2 \qquad (r = 3) \tag{7a}$$

$$n' = n\ 2 + 1 \qquad (r = 1) \tag{7b}$$

Similar discrepancies are found in the intercept term used to evaluate the velocity coefficient.

Experimental confirmation of the above theoretical analysis is given in Fig. 10. The plot shows lifetime data for soda-lime glass in water, for both annealed and as-indented Vickers flaws (Chantikul *et al.*, 1981b). It is immediately clear that the lifetimes in the latter case are substantially reduced by the presence of the residual contact stresses. It is also apparent that the slopes are different for the two sets of data; from these slopes we obtain $n = 17{\cdot}9$ (annealed) and $n' = 13{\cdot}7$ (as-indented), which is entirely consistent (to within an experimental scatter of $\approx 3\%$) with the connecting relation Eq. (7a) for point flaws ($r = 3$).

Fig. 9. Fracture surface of Vickers-indented soda-lime glass broken in water, with ultrasonic markers imposed at 2 kHz.

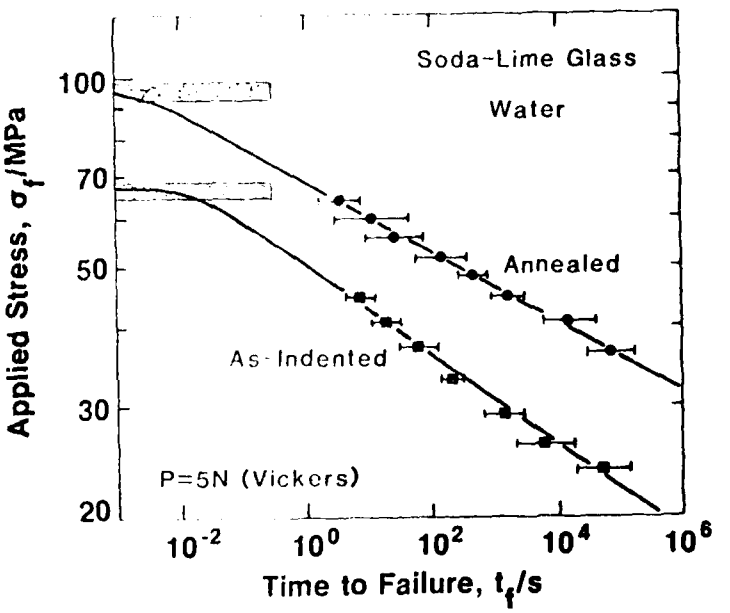

Fig. 10. Static fatigue data for Vickers-indented soda-lime glass tested in water. Shaded regions indicate inert strengths. Note shorter lifetimes of as-indented specimens compared to annealed specimens.

Bearing in mind the critically important role of the velocity exponent in lifetime designing with ceramics (Wiederhorn, 1974), it is essential that effects of the kind just discussed should be duly recognized. With machining flaws, for example, the connecting relation for line flaws ($r=1$), Eq. (7b), would seem to be more appropriate, in which event the discrepancies in n values could be as great as a factor of 2.

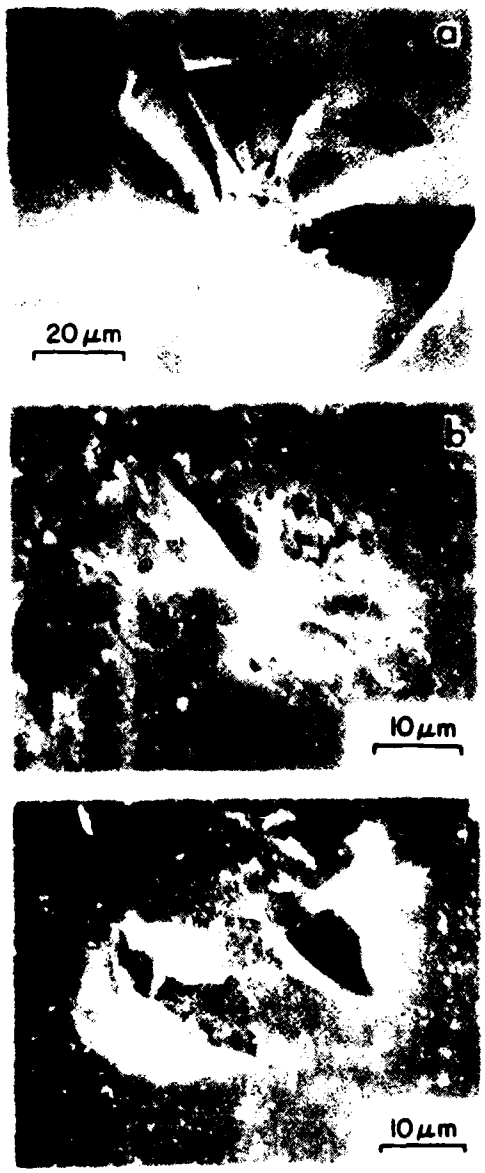

Fig. 11. SEM micrographs of ceramic surfaces impacted with 150 μm SiC particles at 90 m s^{-1}: (a) glass, (b) Al_2O_3 (H.P.), (c) Si_3N_4 (H.P.).

4. EROSIVE WEAR

The cumulation of a large number of surface contacts with sharp particles can lead to severe surface removal in brittle materials. This fact is, of course, exploited in the finishing of components, as in machining, abrasion and polishing. But these same removal processes can be highly deleterious in applications where a certain degree of surface integrity is vital to efficient

performance (e.g. infra-red windows); in some service environments it is difficult to avoid encounters with spurious particulate matter, particularly in airstreams.

Just as it is the median/radial crack system which controls the strength properties in brittle contact it is the lateral system which accounts for surface removal. The tendency for the lateral cracks to turn upward and intersect the surface is strong, especially at high velocity impact sites (Lawn & Swain, 1975; Hockey *et al.*, 1978; Wiederhorn & Hockey, 1982). Examples of the resulting chipping damage are shown in the SEM micrographs of Fig. 11 for three ceramic surfaces. These three materials are displayed in order of increasing toughness, and correspondingly show an increasing resistance to spalling. There is also clear indication of microstructural effects in the fracture removal process, particularly in the fine-grained alumina.

Theories of erosion based on lateral fracture mechanics generally begin with the postulate that the potential chip volume in a single contact event is determined by the characteristic radius c_l and depth d, Fig. 1, i.e.

$$\Delta V = \pi c_l^2 d \tag{8}$$

The radius is estimated from the lateral crack analogue of Eq. (1) for equilibrium conditions and the depth from the penetration of the deformation zone. Contact load is eliminated in favour of impact energy, U_K. The total volume removal is assumed to be the simple sum over all volumes ΔV in Eq. (1) (i.e. interactions are neglected). While this procedure appears reasonably straightforward the final expression obtained for the removal rate is highly sensitive to minor details in the analysis (note the strong, cube dependence on linear dimension in Eq. (8), relative to the square root dependence in strength equations). Furthermore, the scatter in erosion data is such that it is difficult to distinguish between different theories (Gulden, 1981; Wiederhorn & Hockey, 1982). Nevertheless, all such theories lead to more or less the same main conclusions, that the wear rate increases with particle kinetic energy and diminishes with material toughness, as intuitively expected.

5. CONCLUSION

We have discussed recent developments in indentation fracture, emphasizing the need to seek a proper understanding of basic micromechanical processes of deformation and fracture before attemping to analyse strength and wear properties. Our treatment has been somewhat selective in its coverage of practical topics; for instance, we have barely made reference to the existence of a fracture threshold in the contact mechanics, yet it is surely the domain of crack initiation which controls the strength of pristine optical fibres (Lawn, 1983). On the other hand, certain general conclusions may be drawn from the present analysis. Of these, the vital role of residual contact fields in the mechanics of surface damage in brittle materials is worthy of special mention.

ACKNOWLEDGMENTS

The authors gratefully acknowledge many discussions with D. B. Marshall on parts of this work. Funding for this project was provided by the Office of Naval Research, Metallurgy and Ceramics Program, and by the Deutsche Forschungsgemeinschaft.

REFERENCES

Anstis, G.R., Chantikul, P., Lawn, B.R. & Marshall, D.B. (1981) A critical evaluation of indentation techniques for measuring fracture toughness. I. Direct crack measurements. *J. Am. Ceram. Soc.* **64**, 533.

Arora, A., Marshall, D.B., Lawn, B.R. & Swain, M.V. (1979) Indentation deformation/fracture of normal and anomalous glasses. *J. non-Cryst. Solids*, **31**, 415.

Chantikul, P., Anstis, G.R., Lawn, B.R. & Marshall, D.B. (1981a) A critical evaluation of indentation techniques for measuring fracture toughness. II. Strength method. *J. Am. Ceram. Soc.* **64**, 539.

Chantikul, P., Lawn, B.R. & Marshall, D.B. (1981b) Micromechanics of flaw growth in static fatigue: influence of residual contact stresses. *J. Am. Ceram. Soc.* **64**, 322.

Cook, R.F., Lawn, B.R. & Anstis, G.A. (1982) Fatigue analysis of brittle materials using indentation flaws. II. Case study on a glass-ceramic. *J. Mater. Sci.* **17**, 1108.

Cottrell, A.H. (1958) Theory of brittle fracture in steel and similar metals. *Trans. Met. Soc. A.I.M.E.* **212**, 192.

Dabbs, T.P. & Lawn, B.R. (1982) Acid-enhanced crack initiation in glass. *J. Am. Ceram. Soc.* **65**, C-37.

Evans, A.G. & Wilshaw, T.R. (1976) Quasi-static solid particle damage in brittle materials. *Acta Met.* **24**, 939.

Evans, A.G. & Wilshaw, T.R. (1977) Dynamic solid particle damage in brittle materials: an appraisal. *J. Mater. Sci.* **12**, 97.

Fuller, E.R., Lawn, B.R. & Cook, R.F. (1982) Theory of fatigue for brittle flaws originating from residual stress concentrations. *J. Am. Ceram. Soc.*, in press.

Gulden, M.E. (1981) Correlation of experimental erosion data with elastic-plastic impact models. *J. Am. Ceram. Soc.* **64**, C-59.

Hagan, J.T. (1980) Shear deformation under pyramidal indentations in soda-lime glass. *J. Mater. Sci.* **15**, 1417.

Hagan, J.T. & Swain, M.V. (1978) The origin of median and lateral cracks at plastic indents in brittle materials. *J. Phys.* D, **11**, 2091.

Hill, M.J. & Rowcliffe, D.J. (1974) Deformation of silicon at low temperatures. *J. Mater. Sci.* **9**, 1569.

Hockey, B.J. (1982) Crack healing in brittle materials. In: *Fracture Mechanics of Ceramics* (Ed. by R. C. Bradt, A. G. Evans, D. P. H. Hasselman and F. F. Lange). Plenum Press, New York.

Hockey, B.J., Wiederhorn, S.M. & Johnson, H. (1978) Erosion of brittle materials by solid particle impact. In: *Fracture Mechanics of Ceramics* (Ed. by R. C. Bradt, D. P. H. Hasselman and F. F. Lange), Vol. 3, p. 379. Plenum Press, New York.

Kerkhof, F. & Richter, H. (1969) Investigation of the influence of water vapour on crack velocities in glass by ultrasonic fractography. In: *Proceedings of Second International Conference on Fracture, Brighton*, p. 463. Chapman & Hall, London.

Lawn, B.R. (1982) The indentation crack as a model surface flaw. In: *Fracture Mechanics of Ceramics* (Ed. R. C. Bradt, A. G. Evans, D. P. H. Hasselman and F. F. Lange). Plenum Press, New York.

Lawn, B.R. (1983) Physics of fracture. *J. Am. Ceram. Soc.*, **66**, 83.

Lawn, B.R., Evans, A.G. & Marshall, D.B. (1980a) Elastic/plastic indentation damage in ceramics: the median/radial crack system. *J. Am. Ceram. Soc.* **63**, 574.

Lawn, B.R., Hockey, B.J. & Wiederhorn, S.M. (1980b) Thermal effects in sharp particle contact. *J. Am. Ceram. Soc.* **63**, 356.

Lawn, B.R., Hockey, B.J. & Wiederhorn, S.M. (1980c) Atomically sharp cracks in brittle solids: an electron microscopy study. *J. Mater. Sci.* **15**, 1207.

Lawn, B.R. & Howes, V.R. (1982) Elastic recovery at hardness indentations. *J. Mater. Sci.* **16**, 2745.

Lawn, B.R., Marshall, D.B., Anstis, G.R. & Dabbs, T.P. (1981) Fatigue analysis of brittle materials using indentation flaws. I. General theory. *J. Mater. Sci.* **16**, 2846.

Lawn, B.R. & Swain, M.V. (1975) Microfracture beneath point indentations in brittle solids. *J. Mater. Sci.* **10**, 113.

Lawn, B.R. & Wilshaw, T.R. (1975) Indentation fracture: principles and applications. *J. Mater. Sci.* **10**, 1049.

Marshall, D.B. (1982) Controlled flaws in ceramics: a comparison of Knoop and Vickers indentation. *J. Am. Ceram. Soc.*, in press.

Marshall, D.B. (1983) Machining damage in ceramic materials. (In preparation.)

Marshall, D.B. & Lawn, B.R. (1979) Residual stress effects in sharp contact cracking. I. Indentation fracture mechanics. *J. Mater. Sci.* **14**, 2001.

Marshall, D.B. & Lawn, B.R. (1980) Flaw characteristics in dynamic fatigue: the influence of residual contact stresses. *J. Am. Ceram. Soc.* **63**, 532.

Marshall, D.B., Lawn, B.R. & Chantikul, P. (1979) Residual stress effects in sharp contact cracking. II. Strength degradation. *J. Mater. Sci.* **14**, 2225.

Marshall, D.B., Lawn, B.R. & Chantikul, P. (1981) Micromechanics of flaw growth in static fatigue: influence of residual contact stresses. *J. Am. Ceram. Soc.* **64**, 322.

Marshall, D.B., Lawn, B.R. & Evans, A.G. (1982) Elastic/plastic indentation damage in ceramics: the lateral crack system. *J. Am. Ceram. Soc.* **65**, 561.

Puttick, K.E. (1978) The mechanics of indentation fracture in polymethylmethacrylate. *J. Phys.* D, **11**, 595.

Swain, M.V. & Hagan, J.T. (1976) Indentation plasticity and the ensuing fracture of glass. *J. Phys.* D, **9**, 2201.

Tien, J.J.W., Khuri-Yakub, B.T., Kino, G.S., Marshall, D.B. & Evans, A.G. (1982) Surface acoustic wave measurements of surface cracks in ceramics. *J. appl. Phys.*, in press.

Wiederhorn, S.M. (1974) Subcritical crack growth in ceramics. In: *Fracture Mechanics of Ceramics* (Ed. by R. C. Bradt, D. P. H. Hasselman and F. F. Lange), Vol. 2, p. 613. Plenum Press, New York.

Wiederhorn, S.M. & Hockey, B.J. (1982) Effect of materials parameters on the erosion resistance of brittle materials. *J. Mater. Sci.*, in press.

DYNAMIC FATIGUE OF BRITTLE MATERIALS CONTAINING INDENTATION LINE FLAWS

Beth L. Symonds, R.F. Cook

Department of Applied Physics, School of Physics,
University of New South Wales, Kensington, N.S.W. 2033,
Australia

B. R. Lawn

Fracture and Deformation Division, National Bureau of
Standards, Washington, D.C. 20234, U.S.A.

JOURNAL OF MATERIALS SCIENCE 18 (1983) 1306–1314

Dynamic fatigue of brittle materials containing indentation line flaws

BETH L. SYMONDS, R. F. COOK
Department of Applied Physics, School of Physics, University of New South Wales, Kensington, NSW 2033, Australia

B. R. LAWN
Fracture and Deformation Division, National Bureau of Standards, Washington, DC 20234, USA

A study is made of the dynamic fatigue response of brittle materials containing indentation-induced line flaws. The theoretical fracture mechanics of "median" crack evolution to failure under applied tension are first developed, with special emphasis on the role of residual contact stresses. In particular, it is shown that use of fatigue curves to evaluate the exponent in an assumed power-law crack velocity function may result in systematic error, by as much as a factor of two, if proper account is not taken of this residual contact contribution. Data from strength tests on soda-lime glass bars in water, using a tungsten carbide cutting wheel to introduce the median pre-cracks, confirm the basic predictions. The results suggest that extreme care needs to be exercised when using surfaces with a contact history, e.g. as with machining damage, in fatigue test programmes for materials analysis.

1. Introduction

In a series of recent papers it has been shown how controlled indentation flaws can be used to obtain accurate and reliable fatigue strength data for brittle materials [1–6]. The capacity to predetermine the scale and location of the critical flaw is a key element in the fracture mechanics analysis, for the experimenter then has the unique opportunity of following the flaw at all stages of its evolution to failure. A major conclusion which emerges from such observations is that the Griffith concept of a well-defined microcrack driven exclusively by an applied tensile field is inadequate; the indentation flaw certainly does have the nature of a well-defined crack, but its driving force contains an important additional component, one associated with the residual stress field about the plastic contact zone [7–9]. The influence of this additional component is manifest in conventional fatigue plots, i.e. in plots of failure stress against stress rate ("dynamic fatigue") [1] or lifetime ("static fatigue") [2]. Thus whereas for flaws satisfying a power-law crack velocity function the linearity of such plots in logarithmic coordinates still holds to good approximation, the slope and intercept are significantly altered. The "apparent" exponent and coefficient of this velocity function evaluated from fatigue data need to be converted, via an appropriate set of "transformation equations" [3–6], to "true" parameters representative of macroscopic crack growth.

Although indentation crack systems might appear as somewhat contrived entities in the context of the strength of real materials, there is increasing evidence to suggest that such systems do, in many important practical cases, contain the essence of flaw response. This is especially so for flaws with a surface-contact history, e.g. particle impact [10, 11], where the analogy with an indentation process is obvious; however, insofar as the distinctive feature of the flaw description is the presence of a residual crack driving force, the modified fatigue analysis may have a far broader compass than this [6]. On the

0022–2461/83 $03.00 + .12

other hand, the analysis developed in the earlier studies [1–5] was restrictive in one important sense, that of flaw geometry; by considering only axisymmetric indentations, e.g. as produced by a normally loaded Vickers pyramid, the transformation relations derived were strictly applicable to just "point" flaw configurations. "Line" flaw configurations, e.g. as produced by translating a sharp indenter across a surface [12], are governed by different starting equations in the fracture mechanics formulation. In the most recent of the fatigue studies Fuller *et al.* [6] analysed the two geometrical types in some detail, and concluded that the line flaw was even more sensitive to residual-stress effects than its point-flaw counterpart. In particular, whereas for the latter case the apparent and true crack velocity exponents differed by a factor of about 4/3, for the former the corresponding factor was about 2. Discrepancies of this magnitude have indeed been reported by Pletka and Wiederhorn [13] in fatigue tests on surface-machined ceramics, although in their experiments no attempt was made to characterize the critical flaw.

In this paper we present the results of an experimental study of controlled line flaws aimed at testing the predictions of the residual stress theory. The test material is the same soda-lime glass as used in earlier work [1, 2], thereby providing a convenient base for data comparison. Line flaws are introduced by means of a glass-cutting wheel [14]. The failure tests are conducted at constant stressing rates in water. Analysis of the ensuing fatigue plot confirms the existence of a large discrepancy in the velocity exponents. It is concluded that extreme care needs to be exercised in the use of strength data from "natural" surfaces in the evaluation of materials for long-lifetime applications.

2. Theoretical background

Consider the line flaw system shown in Fig. 1. The contact event responsible for creating the flaw is characterized by the residual deformation track, half-width a, that it leaves on the specimen surface. There are two main ways in which such a track may be produced: (i) in wedge loading at normal force P_l per unit length along the contact line; (ii) in axisymmetric loading at normal force P, but with linear translation. Of these, the second, the case illustrated in Fig. 1, is more amenable to controlled experimentation, although it can be

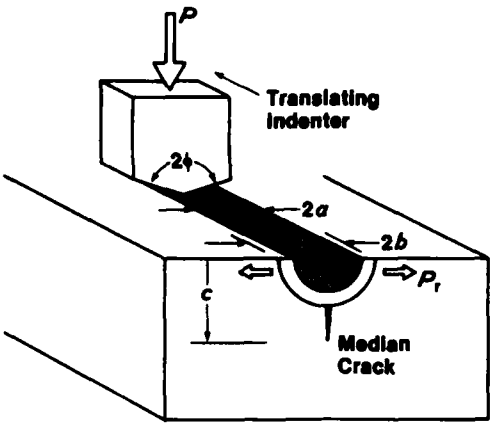

Figure 1 Schematic showing parameters of line flaw system.

argued that there is a certain equivalence between the two (Appendix I). Immediately below the deformation track a "median" crack, depth c, is formed. This crack leaves no characteristic "radial" trace on the specimen surface, as it does with point indentations [9]. In general, sideways-spreading "lateral" cracks (not shown in Fig. 1) also form below the deformation track [12]; these play only a secondary role in the strength degradation process, and will accordingly not be given detailed attention here.

The line flaw system thus produced is subjected to a subsequent applied tensile stress σ_a, which takes the median crack system to failure. The object of our exercise here is to determine the critical failure stress, σ_f, under dynamic fatigue conditions, i.e. $\dot{\sigma}_a$ = constant, in terms of appropriate indentation variables and crack velocity parameters.

2.1. Incorporation of residual contact term into basic fracture mechanics

In this section we write down a stress intensity factor for the line flaw configuration, placing special emphasis on the residual contact component. We also derive expressions for the "inert" strength to provide a reference baseline for analysis of the ensuing fatigue response.

Regardless of the way in which the linear deformation track is produced there will be a residual stress field of approximately cylindrical symmetry due to elastic/plastic mismatch. The source of this field lies in the accommodation of the contact impression volume by the elastic

matrix surrounding the plastic zone radius b [9]. A detailed analysis of the field intensity in terms of the elastic/plastic properties of the test material and the characteristic half-angle ϕ of the indenter is given in Appendix II. For present purposes it is sufficient to define a single, dimensionless material/indenter parameter χ which incorporates all these factors into a simple expression for the residual driving force on the median crack. Thus we may write a residual stress intensity factor of the general form for straight cracks generated by an "effective" line force P_l [12],

$$K_r = \chi P_l / c^{1/2}. \quad (1)$$

For static line loading P_l identifies with the *actual* line force on the indenter; for translating point loading we may talk of an *equivalent* line force (Appendix I). (It may be noted that the corresponding stress intensity factor for statically loaded point flaws differs only in the crack-size exponent, 3/2 instead of 1/2 [8].)

If the residual stress factor in Equation 1 were to be sufficient to maintain the median crack in a state of mechanical equilibrium after completion of the contact process, i.e. $K = K_c$, where K_c defines the material toughness, then

$$c_0 = (\chi P_l / K_c)^2 \quad (2)$$

would represent the initial crack depth in the subsequent strength testing. There are, however, several factors which effectively relax K_r below K_c, in which case Equation 2 underestimates the true crack depth, c_0' say. First, during the actual contact process there is an elastic component of the field which augments the residual component [7, 9]. Whereas for a line contact this component is zero at the median plane, for a point contact it is tensile [15]. In the latter case, therefore, the maximum crack driving force is attained at full loading, so that the crack must close up partially as the indenter is withdrawn. Second, the growth of lateral cracks, which tends to occur also upon indenter withdrawal, can relax the intensity of the residual field somewhat [1, 14, 16]. Third, the presence of a reactive environment can cause post-indentation, subcritical extension of the median crack [1, 17]. Clearly, the degree to which Equation 2 underestimates the initial crack depth in the failure test will depend on the elastic/plastic properties of the material, but other factors, such as the exposure time of the indented surface to the atmosphere, can have a significant effect.

Suppose now the median crack is subjected to the tensile stress σ_a. The stress intensity factor appropriate to this loading is of the familiar form

$$K_a = \psi \sigma_a c^{1/2} \quad (3)$$

where ψ is a crack geometry constant. Equations 1 and 3 may then be combined additively to yield the net stress intensity factor

$$K = K_r + K_a = \chi P_l / c^{1/2} + \psi \sigma_a c^{1/2}, \quad (c \geqslant c_0'). \quad (4)$$

The strength of the test piece is determined as the stress to take the crack from its initial size to an instability configuration, defined by the condition $K = K_c$, $dK/dc > 0$.

The strength under inert conditions of testing can be obtained immediately from Equation 4 by requiring that the crack should remain in a state of mechanical equilibrium in its approach to the instability. Accordingly, we insert $K = K_c$ into Equation 4, and rearrange to determine the equilibrium-stress/crack-size function

$$\sigma_a = (K_c / \psi c^{1/2})(1 - \chi P_l / K_c c^{1/2}). \quad (5)$$

For the limiting case $\chi = 0$, corresponding to ideal Griffith flaws, the failure is spontaneous at the initial flaw size, so the inert strength at $\sigma_i^0 = \sigma_a(c_0')$ is given by

$$\sigma_i^0 = K_c / \psi c_0'^{1/2} \quad (6)$$

in the absence of residual stresses.

For the more general case $\chi \neq 0$, the failure mechanics are more complex [8]. The function $\sigma_a(c)$ in Equation 5 now passes through a maximum at

$$c_m = (2\chi P_l / K_c)^2 \quad (7)$$

and the failure condition is contingent on whether c_0' is smaller or larger than this quantity. If smaller, the flaw must undergo a stage of stable, precursor crack growth prior to the critical instability. It is noted that c_m in Equation 7 exceeds c_0 in Equation 2 by a factor of 4; recalling that $c_0 \leqslant c_0'$ always, this factor represents the maximum degree of precursor extension possible. (We may note that the ratio c_m/c_0 for line flaws is substantially larger than that for point flaws [6, 8], namely, 2.52, reflecting a less rapid falloff in the function $K(c)$ in the former instance.) Insertion of Equation 7 back into Equation 5 gives the appropriate inert strength at $\sigma_i = \sigma_a(c_m) = \sigma_m$, i.e.

$$\sigma_i = K_c/2\psi c_m^{1/2} = K_c^2/4\psi\chi P_l, \quad (c_0' \leqslant c_m). \tag{8a}$$

If, on the other hand, c_0' is larger than c_m, the crack becomes critical without precursor extension; insertion of $\sigma_i = \sigma_a(c_0')$ into Equation 5 accordingly yields

$$\sigma_i = (K_c/\psi c_0'^{1/2})(1 - \chi P_l/K_c c_0'^{1/2}), \quad (c_0' > c_m). \tag{8b}$$

We note that the inital flaw size appears explicitly only in the second of these last two equations.

2.2. Dynamic fatigue formalism

In keeping with our previous course [1–6] we assume that in a reactive chemical environment the median crack can grow subcritically, i.e. at $K < K_c$, in accordance with the crack velocity function

$$v = v_0(K/K_c)^n \tag{9}$$

where the exponent n and coefficient v_0 are parameters to be determined empirically for any given material/environment system. In combination with Equation 4 this function yields, for a time-varying applied stress function $\sigma_a(t)$, a master differential equation for fatigue,

$$dc/dt = v_0[\chi P_l/K_c c^{1/2} + \psi\sigma_a(t)c^{1/2}/K_c]^n. \tag{10}$$

This equation has to be solved for the time to take the crack from its initial (stable) to its final (unstable) configuration, at which point the stress level defines the fatigue strength, $\sigma_a = \sigma_f$.

An analytical solution of Equation 10 is available only for the special case σ_a = constant = σ_f, with flaws in the precursor growth domain $c_0' \ll c_m$ [6]. However, this solution is of precisely the same form as obtained generally for Griffith-like flaws; there the effect of varying the function $\sigma_a(t)$ is manifest as a systematic change in the intercept of the appropriate (logarithmic) fatigue plot. On the assumption that the same generality holds for flaws with residual stress fields, we obtain the following result for the case of special interest here, namely $\dot{\sigma}_a = \sigma_a/t$ = constant = σ_f/t_f at specified contact load P_l [6]:

$$\sigma_f = (\lambda'\dot{\sigma}_a)^{1/(n'+1)} \tag{11}$$

where the slope on a plot of log σ_f against log $\dot{\sigma}_a$ relates to the true crack velocity exponent via the relation

$$n = 2n' - 2 \tag{12}$$

(cf. the case of Griffith flaws, for which $n = n'$); the intercept likewise relates to the velocity coefficient via

$$v_0 = (4\pi n')^{1/2}\sigma_m^{n'}c_m/\lambda'. \tag{13}$$

The validity of the generality assumption leading to this solution has been confirmed by numerical integrations of the master differential equation [3, 6].

Numerical analysis is also useful for investigating the effect of a varying initial flaw size on the fatigue behaviour [3]. Basically, it is found that the predicted $\sigma_f(\dot{\sigma}_a)$ response is insensitive to the value of c_0', up to c_m; beyond this point Equations 12 and 13 can no longer be relied upon to provide accurate crack velocity parameters. In the latter case, therefore, the advantage of a closed-form solution is lost, in addition to which additional, quantitative information on the initial crack condition is required. Notwithstanding these potential complications, Equation 12 serves to demonstrate the substantial discrepancies that can occur between "apparent" crack velocity parameters (i.e. as evaluated on the basis of zero residual stress) and "true" parameters pertinent to macroscopic crack laws.

3. Experimental

3.1. Procedure

Specimens of soda-lime glass, from the same batch as that used for the point-flaw studies of [1] and [2], were cut into bars 50 by 10 by 3 mm. These bars were annealed at 520° C for two days to remove any spurious surface stresses.

Line flaws were introduced along the transverse centre line of each prospective tensile surface for flexural strength testing. This was effected by mounting a bevelled tungsten carbide glass-cutting wheel of half-angle 66° and radius 3 mm onto the indenter arm of a standard hardness tester, allowing the wheel to bear down onto the specimen surface at a prescribed normal load, and translating the specimen support table at a velocity ≈ 0.5 mm sec^{-1}. The wheel traverse was stopped at a distance about 2 mm from opposite bounding faces of the specimen centre line, to avoid spurious edge chipping. The flaws thus produced were examined optically to ensure that the deformation tracks (see Appendix I) and the associated median cracks were sufficiently well defined. The flaws showed substantial birefringence in polarized light, consistent with the existence of an intense residual

contact field: an example is shown in Fig. 2. It was noted that at loads in excess of $P \approx 20$ N lateral crack growth became excessive to the point of causing occasional chipping. A normal load $P = 5$ N was thereby selected for all subsequent strength testing.

The strength tests themselves were conducted in four-point bending, with an outer span of 30.0 mm and an inner span of 7.0 mm. These were run about 30 min after indentation, to allow for saturation of post-contact slow crack growth (Section 2.1). Immediately prior to insertion into the bending fixture the indentation tracks were covered with either silicone oil, for inert strength testing, or water, for fatigue strength testing. The bending load delivered to the specimens was measured by a conventional strain-gauge instrumented cell for "slow" tests, i.e. for failure times > 10 sec, and by a piezoelectric cell for "fast" tests. Simple beam theory was used to evaluate the corresponding tensile stress on the flaw. All broken specimens were examined optically to confirm that failure had indeed initiated from the indentation site; those few exceptions, traceable to unusually large edge flaws, were rejected from the data accumulation.

3.2. Calibration tests

Some preliminary tests were carried out to investigate further the relative values of c_0' and c_m, bearing in mind the significant changes in the mechanical response of the crack system that are predicted once the former exceeds the latter (Sections 2.1 and 2.2). These tests also served to provide useful "calibration" parameters for the ensuing dynamic fatigue data analysis.

Accordingly, dummy specimens were prepared for crack depth measurements by section viewing. The sections were obtained by propagating large cracks from indentations on faces opposite to those containing the line flaws. This was most conveniently effected by stressing the specimens to failure in the bend apparatus, with the line flaws on the compression side to ensure no spurious extension of the primary crack system. An advantage of this procedure was that several line flaws could be placed on a given specimen. From 8 such flaws produced at the standard contact load of $P = 5$ N an initial flaw size $c_0' = 46 \pm 5\ \mu$m (mean and standard deviation) was measured.

In principle, a similar procedure could be used to gain an estimate of c_m, for systems in the domain $c_m > c_0'$. The method, successfully employed in an earlier study of point-indentation flaws [8], requires only that the crack system should be stressed to just below the critical instability prior to sectioning. However, comparative inert strength measurements for specimens with line flaws in the standard as-produced ($\chi \neq 0$) and re-annealed ($\chi = 0$) states [1] suggested that the condition $c_m > c_0'$ would be violated, thereby rendering this procedure ineffective. Thus, we obtained $\sigma_i = 81.0 \pm 9.5$ MPa and $\sigma_i^0 = 112.7 \pm 13.1$ MPa, respectively (mean and standard deviation, 10 specimens each series), corresponding to a ratio $\sigma_i/\sigma_i^0 = 0.72 \pm 0.17$. From Equations 6 to 8 we derive

$$c_m/c_0' = (\sigma_i^0/\sigma_i)^2/4, \qquad (c_0' \leqslant c_m) \tag{14a}$$

$$c_m/c_0' = 4(1 - \sigma_i/\sigma_i^0)^2, \qquad (c_0' > c_m) \tag{14b}$$

which gives us $c_m/c_0' = 0.31 \pm 0.24$; the line flaw system thus lies well outside the region where the fracture mechanics response is independent of initial conditions.

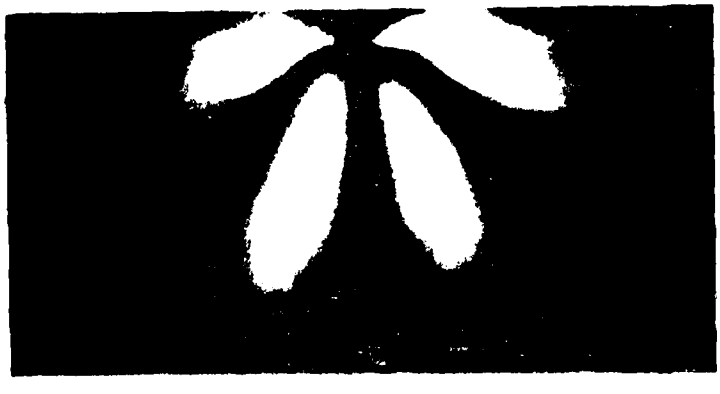

Figure 2 Section view of a linear flaw in glass, in crossed polars.

For the above determinations we may make two useful parameter evaluations. First, Equation 6 yields

$$\psi/K_c = 1/\sigma_i^0 c_0'^{1/2} = 1.31 \pm 0.17\ \mathrm{MPa}^{-1}\mathrm{m}^{-1/2}. \quad (15)$$

Then, in conjunction with Equation 8b, we obtain

$$\chi P_i/K_c = c_0'^{1/2}(1 - \sigma_i/\sigma_i^0) = (1.90 \pm 0.81) \times 10^{-3}\mathrm{m}^{1/2}. \quad (16)$$

4. Dynamic fatigue: results and analysis

The results of the dynamic fatigue tests are shown in Fig. 3. Each data point on this plot represents the mean and standard deviation, in logarithmic coordinates, of 10 to 15 specimens at the appropriate stress rate. The curve represents a numerical evaluation of the master differential equation, Equation 10, using the following parameters: ψ/K_c and $\chi P_i/K_c$, and the initial crack size c_0', as determined in Section 3.2; kinetic parameters $n = 17.9$ (± 0.5) and $v_0 = 2.4$ (± 0.6) mm sec^{-1} from the earlier study on the same glass/water system, but with re-annealed point flaws [1]. In comparing this curve with the data it should be noted that the evaluation of Equation 10 is sensitive to parameter input in the region $c_0' > c_m$; the large error quoted above for c_m/c_0' is especially pertinent in this context. With due acknowledgement of this point, we have been able to predict, to within the limits of experimental uncertainty, the fatigue response of specimens with contact-induced line flaws.

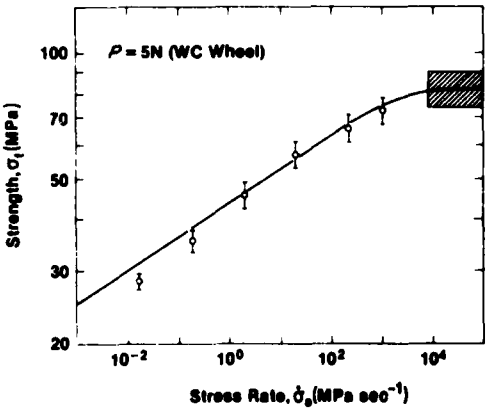

Figure 3 Dynamic fatigue of line-indented soda-lime glass in water. Curve through the data points represents evaluation of master differential equation, Equation 10, using "calibration" parameters (see text). Shaded region indicates inert strength limit.

It is perhaps worth reiterating at this point that the curve fit procedure just described takes full cognizance of a residual driving force in the fracture mechanics. If we were to adopt the normal course in fatigue analysis and treat the indentation cracks as ideal Griffith flaws we would compute an entirely different curve. It might be argued, for instance, that since $c_0' > c_m$ in our experiments the crack front could be considered sufficiently far removed from the actual source of residual stress for the system to be effectively dominated by the applied loading field. A test of this argument is to measure n' from a data fit to Equation 11: as indicated in Section 2.2, the prediction for Griffith flaws is $n' = n = 17.9 \pm 0.5$; the corresponding prediction for flaws under the full influence of a residual stress term (i.e. for $c_0' < c_m$) is, from Equation 12, $n' = n/2 + 1 = 10.0 \pm 0.3$. An actual least squares fit to the data shown in Fig. 2 gives $n' = 10.2 \pm 0.3$. It is clear that the residual stress effect is far from insignificant here.

5. Discussion

We have indicated that residual-contact terms can play a large role in the mechanics of line-flaw growth to failure. In particular, crack velocity exponents as estimated from slopes of fatigue plots can be in error by as much as a factor of two if such residual terms are omitted from the analysis. This factor is considerably greater than that for the corresponding point-flaw case [1], reflecting the greater range of influence of the residual stress intensity factor K_r in the line-flaw geometry [6]. Bearing in mind the key position occupied by crack velocity exponents in modern-day lifetime design schemes for brittle components [18, 19] it would seem reasonable to advocate more attention to characterization of strength-controlling flaws, especially in regard to their local configurational stress history [20]. In cases where direct observation of critical flaw evolution proves impractical during the actual failure testing, some alternative means of quantifying the residual stress effect, e.g. by comparing inert strengths for flaws in their as-produced and re-annealed states (Section 3.2), would appear desirable.

The results described above have important implications concerning the lifetime properties of ceramics whose surfaces have been finished by a contact-induced process, especially by machining.

Machining damage may be regarded in terms of a high density accumulation of near linear flaws. Generally, the critical, strength-degrading member of this accumulated population will experience a somewhat reduced residual crack driving force relative to that for an isolated median crack. For, in addition to the several relaxation factors mentioned in Section 2.1 in relation to the validity of Equation 2, neighbouring damage tracks will interact via their elastic/plastic fields so as to impose a countervailing, crack closure stress at the reference flaw [21]. Moreover, the enhanced lateral-crack chipping which facilitates the machining process might be expected to lead to physical removal of the deformation zone at the mouth of this flaw, and thereby of the very source of the residual field. Recent detailed investigations of machining damage in hot-pressed silicon nitride by Marshall [22] have nevertheless demonstrated that residual contact stresses can still play a dominant role in the failure mechanics. Indeed, in Marshall's strength experiments, conducted under effectively inert testing conditions, the critical median flaw always showed substantial precursor growth prior to reaching instability (i.e. $c_0' < c_m$, in the terminology of Section 2); the silicon nitride thus appears to be less influenced by residual-field relaxation processes than does our glass, presumably due to a relatively strong immunity to environmental slow crack growth effects. In this context it may be pointed out that much of present day ceramics strength analysis is carried out on test pieces with machined surfaces, in conjunction with conventional fatigue theory. It is clear now that crack velocity parameters obtained from this approach will generally not match those measured in macroscopic-crack test pieces [13], and, as such, will not provide a sound basis for lifetime design, particularly if the predictions involve extensive extrapolations beyond the data range.

Although the line-flaw test procedure described in this work is useful for emphasizing the importance of residual-stress terms in flaw micromechanics it suffers certain disadvantages, particularly in comparison with its point-flaw counterpart, as an avenue to routine materials evaluation. For a start, the median flaws remain subsurface along their length, and are therefore not amenable to optical examination in the simple manner of radial cracks at Vickers impressions. We have also noted that the growth of the line flaws tends to be somewhat erratic. Again, it would appear that line flaws are more susceptible to processes which partially relax the residual contact field, thereby leading to violation of the proviso $c_0' < c_m$ for validity of the closed-form fatigue solutions Equations 12 and 13.

Appendix I: Equivalence relations between normal-line and sliding-point loading

In this Appendix we investigate the connecting relation for the "effective" line force in two, essentially equaivalent, contact configurations: (i) wedge loading, at actual normal contact load P_l per unit length; (ii) axisymmetric loading, at normal contact load P but with linear translation.

To obtain the correspondence between the two cases we define hardness parameters in terms of the mean contact pressures:

$$H_l = P_l/2a \qquad \text{(line)} \qquad \text{(A1a)}$$

$$H = P/\alpha a^2 \qquad \text{(point)} \qquad \text{(A1b)}$$

where α is a geometrical constant of the point indenter. The condition for equivalence is that the track half-widths a should be identical in Equations A1a and A1b, i.e.

$$P_l = [2H_l/(\alpha H)^{1/2}]P^{1/2}. \qquad \text{(A2)}$$

Then insofar as the hardness parameters can be regarded as load invariant, which generally requires that the indenters should be of fixed profile (thereby preserving geometrical similarity) [23], we may use Equation A2 to evaluate the effective line force generated in translating-point contact.

We may note that the essence of this result, that $P_l \propto P^{1/2}$, is not addressed in the present experimental study, since all data are obtained at a single load $P = 5$ N.

Appendix II: Elastic/plastic analysis of residual line-contact field

Here we derive an expression for the dimensionless material/indenter parameter χ in Equation 1 of the main text, in terms of elastic/plastic properties of the material and the half-angle ϕ of the indenter. To do this we proceed exactly as for the point-contact configuration described in [9], simply replacing the model of an expanding spherical cavity used there with an analogous expanding cylindrical cavity, as appropriate to the plane-strain deformation geometry in Fig. 1.

Thus, we suppose that the plastic zone beneath the linear track may be considered to be of

circular cross-section, radius b. The residual force field associated with the formation of this zone may be estimated by the following hypothetical cut, operate and heal sequence:

(i) Starting with the original, unstressed elastic half-space, remove a cylindrical segment of radius b about the contact centre line.

(ii) Plastically deform the removed segment over the ultimate contact area to produce a characteristic line impression of half-width a, such that the plastic strain is accommodated as an outward radial displacement at the cylinder surface. Then, ignoring any depth recovery during unloading of the indenter [24], so that we may equate the impression depth to $a \cot \phi$, we obtain for the configurational bulk strain of the zone

$$\delta V/V \propto (a^2 \cot \phi)/b^2. \quad \text{(B1)}$$

(iii) Restore elastically the segment to its original radius by applying a hydrostatic pressure across the cylindrical boundary,

$$p_b \propto \kappa(\delta V/V) \propto E(a/b)^2 \cot \phi \quad \text{(B2)}$$

where in converting from bulk modulus κ to Young's modulus E we have omitted terms in Poisson's ratio.

(iv) Restore the cylinder to its original cavity in the half-space, allow the interface to heal, and allow the system to relax elastically. The cylinder will then exert an outward pressure on the encasing matrix. In the far-field approximation $c \gg b$ this pressure will be manifest as a residual mouth-opening line force

$$P_r \propto p_b b \propto [(a/b)(E/H_1) \cot \phi] P_1 \quad \text{(B3)}$$

where we have invoked Equation A1a to eliminate a in favour of P_1.

To proceed beyond this point we need to determine the dependence of the elastic/plastic cavity parameter a/b on material/indenter properties. For this we make recourse to Hill's analysis for the axially symmetric cylindrical problem [25]. His analysis provides an approximate normalized relation for the outward pressure p_0 acting on the internal cavity wall of radius r_0,

$$p_0/E = [1 + \ln (b/r_0)^2]/[(5 - 4\nu)(b/r_0)^2]. \quad \text{(B4)}$$

A plot of Equation B4 is shown, for Poisson's ratio $\nu = 0.25$, as the solid curve in Fig. B1. Over a greater part of the range of b/r_0 covered this function may be approximated by the dashed line

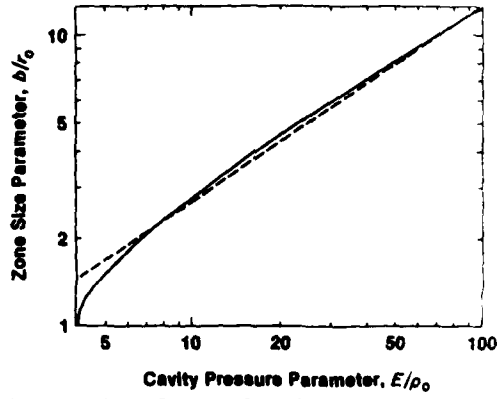

Figure B1 Plot of Equation B4, solid curve, and its power-law approximation, dashed line.

representation, which corresponds to a simple power-law relation

$$b/r_0 \propto (E/p_0)^m, \quad \text{(B5)}$$

where $m \approx 2/3$. If now we identify the internal pressure with the appropriate hardness parameter, $p_0 = H_1$, and equate the volume of the cavity with the volume of the wedge impression, $a \cot^2 \phi = \pi r_0^2$, we have

$$b/a \propto (E/H_1)^{2/3} (\cot \phi)^{1/2} \quad \text{(B6)}$$

The results from the expanding cylindrical cavity analysis are, in the far-field approximation considered here, pertinent to a straight-fronted crack of depth c loaded at its mouth by a concentrated line force P_r. The stress intensity factor for such a crack is of the form $K_r \propto P_r/c^{1/2}$ so, combining Equations B3 and B6, we obtain the required result for the master parameter in Equation 1 [9],

$$\chi = \xi(E/H_1)^{1/3} (\cot \phi)^{1/2} \quad \text{(B7)}$$

where ξ is a further dimensionless constant, but one which is independent of material or indenter properties.

Acknowledgements

The authors wish to thank D. B. Marshall for valuable discussions on this work. Funding was provided in part by the Australian Research Grants Committee and by the United States Office of Naval Research.

References

1. D. B. MARSHALL and B. R. LAWN, *J. Amer. Ceram. Soc.* **63** (1980) 532.

2. P. CHANTIKUL, B. R. LAWN and D. B. MARSHALL, *ibid.* 64 (1981) 322.
3. B. R. LAWN, D. B. MARSHALL, G. R. ANSTIS and T. P. DABBS, *J. Mater. Sci.* 16 (1981) 2846.
4. R. F. COOK, B. R. LAWN and G. R. ANSTIS, *ibid.* 17 (1982) 1108.
5. T. P. DABBS, B. R. LAWN and P. L. KELLY, *Phys. Chem. Glasses* 23 (1982) 58.
6. E. R. FULLER, B. R. LAWN and R. F. COOK, *J. Amer. Ceram. Soc.* in press.
7. D. B. MARSHALL and B. R. LAWN, *J. Mater. Sci.* 14 (1979) 2001.
8. D. B. MARSHALL, B. R. LAWN and P. CHANTIKUL, *ibid.* 14 (1979) 2225.
9. B. R. LAWN, A. G. EVANS and D. B. MARSHALL, *J. Amer. Ceram. Soc.* 63 (1980) 574.
10. D. B. MARSHALL and B. R. LAWN, *ibid.* 64 (1981) C-7.
11. S. M. WIEDERHORN and B. R. LAWN, *ibid.* 62 (1979) 66.
12. M. V. SWAIN, *Proc. Roy. Soc. Lond.* A366 (1979) 575.
13. B. J. PLETKA and S. M. WIEDERHORN, *J. Mater. Sci.* 17 (1982) 1247.
14. M. V. SWAIN, *J. Non-Cryst. Solids* 38–39 (1980) 445.
15. S. P. TIMOSHENKO and J. N. GOODIER, "Theory of Elasticity" (McGraw-Hill, New York, 1970) Chap. 4 and 13.
16. B. R. LAWN, D. B. MARSHALL and P. CHANTIKUL, *J. Mater. Sci.* 16 (1981) 1769.
17. G. R. ANSTIS, P. CHANTIKUL, B. R. LAWN and D. B. MARSHALL, *J. Amer. Ceram. Soc.* 64 (1981) 533.
18. J. E. RITTER, in "Fracture Mechanics of Ceramics" Vol. 4, edited by R. C. Bradt, D. P. H. Hasselman and F. F. Lange (Plenum, New York, 1978) p. 667.
19. S. M. WIEDERHORN and J. E. RITTER, in "Fracture Mechanics Applied to Brittle Materials", ASTM Special Technical Publication 678, edited by S. W. Freiman (ASTM, Philadelphia, 1979) p. 202.
20. B. R. LAWN and T. R. WILSHAW, "Fracture of Brittle Solids" (Cambridge University Press, London, 1975) Chap. 2.
21. R. F. COOK, B. R. LAWN, T. P. DABBS and P. CHANTIKUL, *J. Amer. Ceram. Soc.* 64 (1981) C-122.
22. D. B. MARSHALL, unpublished work (1982).
23. D. TABOR, "Hardness of Metals" (Clarendon Press, Oxford, 1951).
24. B. R. LAWN and V. R. HOWES, *J. Mater. Sci.* 16 (1981) 2745.
25. R. HILL, "The Mathematical Theory of Plasticity" (Oxford University Press, London, 1950) Chap. 5.

Received 6 September
and accepted 20 September 1982

CONTROLLED INDENTATION FLAWS FOR CONSTRUCTION OF TOUGHNESS AND FATIGUE MASTER MAPS

R. F. Cook*, Department of Applied Physics,
School of Physics, University of New South Wales,
Kensington, N.S.W. 2033, Australia

B. R. Lawn, Center for Materials Science,
National Bureau of Standards, Washington, DC 20234

*On leave at the National Bureau of Standards

ABSTRACT

A simple and economical procedure for accurate determinations of toughness and lifetime parameters is described. Indentation flaws are introduced into strength test pieces, which are then taken to failure under specified stressing and environmental conditions. By controlling the size of the critical flaw, via the contact load, material characteristics can be represented universally on "master maps" without the need for statistical considerations.

This paper surveys both the theoretical background and the experimental methodology associated with the scheme. The theory is developed for "point" flaws for dynamic and static fatigue, incorporating load explicitly into the analysis. A vital element of the fracture mechanics is the role played by residual contact stresses in driving the cracks to failure. Experimental data on a range of Vickers-indented glasses and ceramics are included to illustrate the power of the method as a means of graphic materials evaluation. It is demonstrated that basic fracture mechanics parameters can be measured directly from the slopes, intercepts and plateaus on the master maps, and that these parameters are consistent, within experimental error, with macroscopic crack growth laws.

KEY WORDS

Fatigue; indentation flaw; lifetime prediction; master maps; materials evaluation; strength; toughness; universal curves.

INTRODUCTION

The increasing use of glasses and ceramics as structural materials has prompted the development of new and accurate techniques for evaluating intrinsic fracture parameters. Chief among these parameters are the fracture toughness, K_c, and the crack velocity exponent, n, which respectively characterize the equilibrium and kinetic crack growth responses. In the context of brittle design it is essential to achieve an adequate level of precision in such parameter evaluations. This is particularly so in the consideration of component integrity under sustained stresses and chemical environments, where apparently minor uncertainties can translate into order-of-magnitude discrepancies in lifetime predictions.

A standard method of determining basic fracture parameters for design is to measure the strengths of representative test specimens in flexure. However, for specimens with typically as-received or as-prepared surfaces these strengths depend not only on the intrinsic material properties but on the flaw distributions as well. It is then not possible to investigate these two elements of the problem in any truly independent way. Evaluation of material parameters becomes a mere exercise in statistical data manipulation, with little or no physical insight into the nature of the critical flaws responsible for failure [1-2]. This probabilistic approach makes it difficult to assess the relative merits of different materials from the standpoint of intrinsic properties alone.

A controlled-flaw technique which effectively eliminates the statistical component from strength testing has been developed in a series of recent articles [3-12]. A single dominant flaw of predetermined size and geometry is introduced into the prospective tensile surface of each specimen using a standard diamond indenter. The specimens are then stressed to failure in the

usual way. With the indentation and flexure testing conditions held fixed any variations in the strength behavior can be taken as direct reflections of the intrinsic material response. The only need for statistical treatments then resides in the trivial accountability of random scatter in the data. Quite apart from the ensuing improvements in data reproducibility, the indentation procedure confers several advantages in strength analysis: (i) greater specimen economy is achieved; (ii) the location of the critical flaw is predetermined, thereby allowing for closer observation of the fracture mechanics to failure; (iii) indentations provide a reasonable simulation of the damage processes which are responsible for a great many brittle failures [13-15]. One apparent complication which attends the technique is the existence of a strong residual contact field about the elastic/plastic deformation zone, necessitating the incorporation of additional terms in the governing stress intensity factor. However, closed-form solutions of the fracture mechanics formulations are now available for both equilibrium [4] and kinetic [16] conditions of failure; analytical determinations of toughness and fatigue parameters from the strength data may accordingly be made in as straightforward a manner as for "Griffith" flaws without the residual stress term.

The capacity to control the scale of the critical flaw via the indentation load is a potent tool in the investigation of material fracture properties. The load actually replaces initial crack size as a variable in the fracture equations, thereby eliminating the need for onerous measurements of crack dimensions (although some observations of crack growth are useful for confirming the validity of the theory) [15]. Size effects in the micromechanics may then be studied systematically: important changes in the nature of low-load contact flaws have been thus revealed on reducing the crack

size to the scale of the deformation zone [17] or of the microstructure [18]. Systematic variations in the load dependence of indentation-strength characteristics can also be used to evaluate pre-existing stress states in brittle materials, e.g. in tempered glass [19]. Again, some materials may produce ill-defined indentation patterns outside certain ranges of flaw size, or be restricted in specimen dimensions, in which case the geometrical requirements of standard strength-testing procedures may make it impossible to operate at a single contact load. The theoretical analysis allows one to compensate for any such changes in the working contact conditions, effectively reducing all data to an "equivalent" load.

This paper illustrates a procedure for representing the intrinsic strength properties of brittle materials on an indentation "master-map". A suitable "normalization" scheme incorporating indentation load into the plotting coordinates allows for the reduction of all inert and fatigue strength data on to "universal" curves for the various test materials. In this sense the scheme is reminiscent of that developed earlier by Mould and Southwick [20], except that their use of relatively ill-defined abrasion flaws necessitated a totally empirical approach in the data reduction. On our master map the position of a given curve may be taken as a graphic indicator of the intrinsic toughness and fatigue susceptibility. Quantitative determinations may accordingly be made of K_c and n without recourse to statistically-based theories of strength.

BACKGROUND THEORY

Stress Intensity Factor for Indentation Cracks

The starting point in the analysis is the stress intensity factor for an indentation crack of characteristic dimension c produced at peak contact load P and subjected to subsequent applied tensile stress σ_a. For "point" flaws produced in axially loaded indenters the general form of this stress intensity factor is [4]

$$K = \chi P/c^{3/2} + \psi\sigma_a c^{1/2} \qquad (1)$$

where χ and ψ are dimensionless parameters. The second term in Eq. (1) is the familiar contribution from the applied field; ψ depends only on crack geometry, here assumed to be essentially "penny-like" [21]. The first term is the contribution from the residual contact field; for materials which deform irreversibly by a constant volume process

$$\chi = \xi\,(E/H)^{1/2} \qquad (2)$$

approximately [22], where E is Young's modulus, H is hardness and ξ is a numerical constant.

In the event of any pre-existent stress acting on the crack a third term would have to be included in Eq. (1) [4,9]. Other than to note that this potential complication needs to be heeded when preparing the surfaces of test specimens we shall consider it no further in our mathematical derivations.

Equilibrium Solutions: Inert Strengths

Equilibrium conditions of crack growth are closely realized experimentally by testing in an inert environment. In terms of fracture mechanics notation the criterion for equilibrium is that $K = K_c$; if $dK/dc < 0$ the equilibrium is stable, if $dK/dc > 0$ it is unstable. Now it is evident from Eq. (1) that K for given values of P and σ_a passes through a minimum in its functional dependence on c; thus at subcritical configurations $K(min) < K_c$ there is a stable and an unstable equilibrium, to the left and to the right of the minimum respectively [16]. In an inert strength test σ_a is increased steadily until these two equilibria merge at $dK/dc = 0$, which defines the critical variables

$$\sigma_m = 3K_c/4\psi c_m^{1/2} \tag{3a}$$

$$c_m = (4\chi P/K_c)^{2/3} \tag{3b}$$

at which crack growth proceeds without limit. We may note that any relaxation of the residual stress field, as reflected in a reduction in χ (or, more specifically, in ξ in Eq. (2)), will cause σ_m to expand and c_m thence to contract.

It can be shown that the ideal indentation crack is in a state of equilibrium immediately after completion of the contact cycle [22]. The size of this crack is found by setting $\sigma_a = 0$, $K = K_c$ in Eq. (1);

$$c_o = (\chi P/K_c)^{2/3} \tag{4}$$

From Eq. 3(b) we have $c_o \simeq 0.40\ c_m$. On subsequently applying the tensile stress the crack extends stably from c_o to c_m, whence spontaneous failure ensues at $\sigma_a = \sigma_m$ [4]. In reality, deviations from this ideal behavior are observed; relaxation effects can cause c_m to contract, as already mentioned, and subcritical, moisture-assisted crack extension within the residual contact field can cause c_o to expand , to c_o' say. Nevertheless, unless the condition $c_o' \leq c_m$ is violated some precursor crack growth will still precede failure, in which case σ_m remains a measure of the inert strength.

Equation (3) may then be conveniently rearranged to eliminate all terms in crack size, and then combined with Eq. (2) to yield

$$\sigma_m P^{1/3} = (3/4\psi)(1/4\xi)^{1/3}\ [(H/E)^{1/8} K_c]^{4/3}. \qquad (5)$$

This expression conveniently relates the test variables on the left side to the material properties, primarily the toughness, on the right side. We emphasize once more that this formulation is contingent on the absence of all spurious pre-present stresses.

Kinetic Solutions: Dynamic Fatigue

When cracks are exposed to moisture or other interactive environmental species extension can occur in the subcritical region, $K < K_c$. The major characteristic of this kind of extension is its rate dependence, which is in turn highly sensitive to the crack driving force. The basic equation of kinetic fracture accordingly takes the form of a crack velocity v(K). In the interest of obtaining closed-form solutions to the ensuing fracture mechanics relations we choose the empirical power-law function [23]

$$v = v_o(K/K_c)^n \tag{6}$$

where v_o and n are material/environment parameters. Materials with lower values of n are said to be more "susceptible" to kinetic crack growth effects.

The most practical loading arrangement for the systematic study of rate effects in strength properties is that of "dynamic fatigue", in which the time differential of stress is held fixed up to the point of failure, i.e. $\dot{\sigma}_a = \sigma_a/t = \text{const}$. We may thus combine Eqs. (1) and (6) to obtain a differential equation for this stressing configuration,

$$dc/dt = v_o\,[\chi P/K_c c^{3/2} + \psi\,\dot{\sigma}_a c^{1/2} t/K_c]^n. \tag{7}$$

This equation has to be solved at given P and $\dot{\sigma}_a$ for the time to take the crack from its initial configuration, $K = K(c_o')$, to its final configuration, $K = K_c$, at which point the stress level defines the dynamic fatigue strength, $\sigma_a = \sigma_f$ [16];

$$\sigma_f = (\lambda'\dot{\sigma}_a)^{1/(n'+1)} \tag{8}$$

where

$$n' = 3n/4 + 1/2 \tag{9a}$$

$$\lambda' = (2\pi n')^{1/2}\sigma_m^{\,n'} c_m/v_o. \tag{9b}$$

The solution in Eq. (8) is identical in form to that for "Griffith" flaws ($\chi = 0$) [23]. However, the slopes and intercepts from a linear plot of log σ_f against log $\dot{\sigma}_a$ are very different in the two instances. In the present case ($\chi \neq 0$) n' and λ' may be regarded as "apparent" fatigue parameters, in the sense that transformation equations are required to convert these to "true" crack velocity exponent and coefficient terms. Thus, Eq. (9a) may be inverted to obtain n directly from n', and Eq. (9b) similarly (in conjunction with measured values of σ_m and c_m) to obtain v_o from λ'. It is again seen that initial crack size does not enter the results, as long as the condition $c_o' \leq c_m$ remains operative [9].

Implicit in the derivation of Eq. (8) is the usual assumption that the prospective test surfaces are free of spurious stresses. The introduction of such stresses leads to nonlinearities in the dynamic fatigue plotting scheme, thereby destroying the basis for the above analysis [9,10].

It is convenient at this point to incorporate the indentation load as a working test variable into the dynamic fatigue relations. Whereas n' in Eq. (9a) is independent of all test variables, λ' in Eq. (9b) can be expressed as an explicit function of P via the quantities σ_m and c_m in Eq. (3). In this way we may write

$$\lambda' = \lambda_P' / P^{(n'-2)/3} \tag{10}$$

where λ' is a <u>modified</u> intercept term, totally independent of P, given by

$$\lambda_P' = (2\pi n')^{1/2} (3K_c/4\psi)^{n'} (K_c/4\chi)^{(n'-2)/3} / v_o. \tag{11}$$

Equation (10) tells us that fatigue data obtained on one material but using different indentation loads will fall on different straight lines, mutually translated but without change of slope. Now by inserting Eq. (10) into Eq. (11) we may appropriately modify the dynamic fatigue relation, thus

$$\sigma_f P^{1/3} = (\lambda'_p \dot{\sigma}_a P)^{1/(n'+1)}, \tag{12}$$

such that by plotting log $(\sigma_f P^{1/3})$ against log $(\dot{\sigma}_a P)$ all data should fall on to a universal fatigue curve. This plot would, of course, cutoff at a limiting level on the ordinate corresponding to the inert strength plateau defined in Eq. (5). The procedure for evaluating crack velocity parameters from the slopes and intercepts of such representations is the same as before, but with Eq. (10) serving as an intermediary to Eq. (9).

Kinetic Solutions: Static Fatigue

Of more practical interest from a design standpoint is the issue of component lifetime under fixed stress rather than stress rate. Ideally, it would seem desirable to formulate a universal static fatigue relation in direct analogy to Eq. (12) retaining, as far as possible, the same adjustable parameters. Lifetime predictions could then be made from dynamic fatigue data alone, without having to resort to delayed failure experiments. This formulation may be achieved in two steps. First, eliminate stressing rate in favor of time to failure, $\dot{\sigma}_a = \sigma_f/t_f$. This step introduces the lifetime concept without yet altering the status of Eq. (12) as a dynamic fatigue relation. Then, convert to equivalent static fatigue variables by replacing σ_f with σ_A, i.e. the level of the invariant applied stress, and t_f with $(n'+1)t_f$ [16]. The resulting static fatigue relation is

$$t_f/P^{2/3} = \lambda_p'/(n'+1)(\sigma_A P^{1/3})^{n'}. \quad (13)$$

We reiterate here, at the risk of laboring the point, that the variables P, σ_A and t_f in Eq. (13) relate to prospective static fatigue conditions, whereas the parameters n' and λ_p' are adjustables, as defined by Eqs. (9) and (10), to be determined from dynamic fatigue data.

EXPERIMENTAL

Materials Selection and Preparation

The materials in this study were chosen in accordance with two major criteria: first, they should cover a range of toughness and crack velocity characteristics, as determined by independent fracture techniques; second, they should be of some technical importance. Table 1 lists these materials and their pertinent properties.

All specimens were prepared in the usual manner for strength testing. However, particular attention was paid to surface preparation, bearing in mind our repeated assertion that pre-existing stress states can greatly influence the interpretation of strength data. The glass specimens were therefore annealed [19] and the ceramics surface-polished to a mirror finish with diamond paste [10] to ensure removal of any such stresses.

Indentation and Strength Testing Procedure

All specimens were routinely indented centrally along their length using a Vickers diamond pyramid indenter to produce dominant flaws for the subsequent failure tests. The Vickers geometry was chosen both for its proven

capacity to produce well-defined radial crack patterns and for its general availability in hardness testing facilities. The glasses were indented at several loads, ranging from 0.05 to 100 N, whereas the ceramics were each indented at single loads, 10, 20 or 100 N. In all cases the radial cracks extended well beyond the central hardness impression, but never to a length in excess of one tenth the specimen thickness.

The indented specimens were then broken in four-point flexure [24] in a universal testing machine at constant crosshead speed. Care was taken to center the indentation on the tension side, with one set of radial cracks aligned normal to the long axis. The breaking loads were recorded using conventional strain gage and piezoelectric load cells [10], and the corresponding rupture stresses thence evaluated from simple beam theory. Inert strengths, σ_m, were measured in dry nitrogen or argon or silicone oil environments, with the crosshead running at its maximum speed. Dynamic fatigue strengths, σ_f, were measured in distilled water over the allowable range of crosshead speeds. At least six specimens were broken in each strength evaluation, from which means and standard deviations were computed.

Measurement of Critical Crack Dimensions

For the purpose of confirming the necessary condition that the initial crack size c_o' should never exceed the instability value c_m for equilibrium failure, and for verifying certain aspects of the fatigue solutions presented earlier, an optical examination of representative critical indentations is recommended. The technique used here was to place three indentations instead of one on a given test surface, and then take the specimen to failure under inert conditions [10]. On the understanding that all three indentations must have had nearly identical growth histories, the procedure leaves two "dummies"

in the broken test piece from which to measure the required crack dimensions. The Vickers geometry proves particularly useful in this technique, for while the set of radial cracks perpendicular to the tensile direction provides a measure of c_m, the set parallel to this same direction remains free of external stress and hence provides a measure of c_o'.

In all materials studied in this work some precursor crack growth was indeed found to occur prior to failure.

RESULTS

Inert Strengths and Toughness

In this section we begin by examining the dependence of inert strength on indentation load for the three glasses studied. With this dependence established, we then investigate how the inert strength data may be reduced to a composite toughness parameter for all of the test materials.

Figure 1 accordingly shows σ_m as a function of P for the glasses. The straight lines are best fits of slope -1/3 in logarithmic coordinates, as per Eq. (5). This same dependence has been confirmed elsewhere for several other brittle materials [7,18,25,26].

Values of the composite parameter $\sigma_m P^{1/3}$ are thus evaluated for each of the glasses and ceramics, and are plotted as a function of $(H/E)^{1/8}K_c$ (from Table 1) in Fig. 2. The straight line is a fit of logarithmic slope 4/3 in accordance with Eq. (5), using a "calibration" value $(3/4\psi)(1/4\xi)^{1/3} = 2.02$ from an earlier, more comprehensive study [7]. The trends in Fig. 2 appear to be in reasonable accord with prediction, although some deviations are evident, particularly for the fused silica and borosilicate glasses. Estimates of the

"indentation toughness" obtained directly from $\sigma_m P^{1/3}$ by inverting Eq. (5) are included in Table 1 for comparison with the independently determined values.

Dynamic Fatigue and Crack Velocity Parameters

We consider now the dynamic fatigue responses, again beginning with the glasses to examine the functional influence of contact load, and outline the procedure for determining the exponent and coefficient in the crack velocity function.

Figure 3 shows these responses for the glass compositions in water. The straight lines drawn through individual sets of data at fixed P are best fits to Eq. (8), regressed for each glass on all the data consistent with the intercept relation Eq. (10). Thus we obtain families of lines of constant slope, with systematic displacements to lower strength levels with increasing load. Analogous plots are shown in Fig. 4 for the five ceramics in the same water environment, but now for a single load in each case. The inert strength limits are included in all plots as a reference baseline for assessing the degrees of fatigue.

From the regressed slopes and intercepts we obtain values of the apparent fatigue parameters n' and λ' in Eq. (8). Inversion of Eq. (9) (together with the inert strength data) then allows us to evaluate the true crack velocity parameters, n and v_o. These evaluations are summarized in Table 1; comparisons may be made in this tabulation with independent measurements of the crack velocity exponent.

Master Maps

We have set the base for determining universal fracture curves for the materials studied, and thence to construct master maps. We do this for dynamic and static fatigue conditions in turn.

The presentation of the dynamic fatigue results on a single master map requires conversion of all data to appropriate load-adjusted variables $\sigma_f P^{1/3}$ and $\dot{\sigma}_a P$ in Eq. (12). Figure 5, an appropriate composite of all data thus converted from Figs. 3 and 4 (but with error bars omitted for clarity), is such a map. Each material is now conveniently represented by a universal curve, independent of the contact loads used to obtain the data. The curves plotted in this diagram represent numerical solutions of the basic fatigue differential equation, Eq. (7), obtained for the ranges of P and $\dot{\sigma}_a$ covered experimentally for each material, using the inert and kinetic parameters already determined along with the measured initial crack sizes [10]. The fact that the curves regenerated in this way are effectively coincident with the data is, of course, no real surprise, since the regression analyses used in the parameter evaluations were performed in accordance with the solutions of the differential equation in the first place. An exercise of this kind nevertheless serves two useful purposes: (i) to confirm that the solutions referred to, which are of closed form, are indeed reasonably reliable; (ii) to show how closely the curves remain linear in the fatigue region, and then plateau out at the inert strength levels, $\sigma_m P^{1/3}$ (Fig. 2).

The equivalent construction for static fatigue is obtained from the constant stressing rate results using the rationale described earlier in the derivation of Eq. (13). Thus we generate the plots shown in Fig. 6 directly from the best-fit values of n' and λ' (or more strictly, via Eq. (10), λ'_p) determined by the data regressions shown in Figs. 3 and 4. Cutoff levels on

the abscissa again correspond to inert strength limits. Because the construction in Fig. 6 is not obtained this time from regenerated solutions of the basic differential equation we are unable to plot the curved transition between the fatigue and inert regions; however, the abruptness of the corresponding crossover points in Fig. 5 suggests that we may reasonably ignore any such curvature in the lifetime maps.

DISCUSSION

Quantitative Evaluation of Fracture Parameters

The scheme presented here for reducing fatigue data to universal curves for any specified material/environment system, and thence for constructing master maps to facilitate comparisons between these curves, provides an attractive route to simple, accurate and economical evaluation of fracture parameters for design. In the following subsections we discuss how these constructions may be used as a quantitative tool for parameter determinations in different regions of the curves.

Inert Strength Levels. The position of the inert strength cutoff level, $\sigma_m p^{1/3}$, may be taken as an indicator of material toughness, K_c. Intrinsically tougher materials will therefore exhibit cutoffs further toward the top of a dynamic fatigue map (Fig. 5) and toward the right of a static fatigue map (Fig. 6).

It should be emphasized that the correspondence implied here is not exact. To clarify this point we may invert Eq. (5) to obtain an explicit expression for toughness,

$$K_c = (256\psi^3\xi/27)^{1/4} (E/H)^{1/8} (\sigma_m p^{1/3})^{3/4}. \qquad (14)$$

Thus, K_c depends on the elastic/plastic term E/H as well as on $\sigma_m P^{1/3}$. On the other hand, since E/H varies only between 10 and 25 over the range of materials listed in Table 1, the use of an invariant, representative mean value $\langle (E/H)^{1/8} \rangle = 1.50$ in Eq. (5) would lead to errors of no more than 10%. Another potential source of discrepancy lies in the implicit assumption that geometrical similarity is preserved in the indentation pattern from material to material, as reflected in the constancy of the parameters ξ and ψ. We have already pointed out that relaxation effects in the residual contact field can lead to reductions in the ξ term. Systematically low values of ξ will also be manifest in materials which deform by other than a constant-volume process or which exhibit plastic pile up at the impression edges [22]. Fused silica and borosilicate glass, which tend to deform by densification [27], fall into this category, thereby explaining the tendency for the data points representing these two materials to lie above the general trend in Fig. 2. Finally, it has been taken as given that the radial crack patterns are always well defined, and in the materials used here this has generally found to be so. In materials where the microstructure is comparable in scale with the indentation event, however, the symmetry of the crack pattern can become severely disrupted [8,28], with consequent variations in both ξ and ψ.

It may be argued that the "effective" toughness reckoned from the cutoff position on a master map, while perhaps not an accurate measure of its macroscopically determined counterpart, may nevertheless characterize more closely the response of "natural" flaws. This is certainly likely to be so where the strength-controlling flaw in a component is created by a surface contact event, as in sharp-particle impact or in a machining operation. In this sense the master map approach might well be expected to serve more

appropriately as a source of design parameters than the more conventional methods involving large-scale fracture specimens.

Fatigue Curve Slopes. We have noted from Eqs. (12) and (13) that the slope of a universal fatigue curve is a measure of the intrinsic susceptibility to slow crack growth. Thus materials with lower values of the crack velocity exponent n, and hence of n', Eq. (9a), will have greater slopes on dynamic fatigue master maps and, conversely, lower (negative) slopes on static fatigue maps.

As with the toughness, certain caution needs to be exercised when using master map data to determine n values. This is because in applying the inverted form of Eq. (9a),

$$n = 4n'/3 - 2/3 \ , \qquad (15)$$

it is implicit that certain necessary conditions are met. The most important of these is the proviso $c_o' < c_m$, which we have considered at some length in this work. It is interesting to note that if this proviso is satisfied even the "anomalous" glasses which deform by non-volume-conserving processes may be analyzed in terms of Eq. (15); the fatigue properties are not sensitive to the origin of the residual contact field, as long as this field is of sufficient intensity to generate some precursor crack growth [11]. If such a precursor stage were not to be evident in the failure mechanics the "apparent" term n' would tend closer in value to the true n [5,9,12,13]. A second condition that needs to be met is that the flaws should indeed be produced in axial loading; other indentation loading systems, e.g. linear translation, give rise to flaws

which are governed by a transformation equation with coefficients significantly different to those in Eq. (15) [12,16].

It is seen in Table 1 that the exponents obtained from this study agree well with the independent determinations for the glasses, but not for the ceramics. The relatively good agreement in the case of the glasses is attributable in part to the "model" behavior of this class of materials: transparency, isotropy, absence of microstructural complication and ease in specimen preparation are factors which contribute to this behavior. Also, the n values of the glasses are comparatively low, so fatigue effects show up more strongly. This last point, coupled with a growing realization that conventional testing techniques used to obtain macroscopic velocity data are themselves subject to uncertainty (particularly the double torsion specimen [29]), could account for the discrepancies evident in the data for the ceramics.

Fatigue Curve Intercepts. The intercept terms in the master map representations do not have such a simple interpretation in terms of basic fracture parameters. This is clear from Eq. (11); λ_p' is a function of several quantities. Given the fatigue slope and inert strength evaluations as described in the two previous subsections, along with a direct measurement of the critical flaw size c_m, λ_p' effectively determines the crack velocity coefficient v_o. Due to the compounding of errors (particularly from the n' exponent), determinations of this kind are subject to gross uncertainty. There accordingly seems to be little value in trying to retain v_o as a design parameter, particularly since the λ' terms, which can usually be determined to within 15% from dynamic fatigue data, may be used directly in lifetime

formulae. In studies of the basic physics and chemistry of crack growth, of course, v_o remains a useful coefficient for scientific analysis.

Practical Implications of Master Maps

The major appeal of the master map construction advocated here lies in the provision of a graphic indicator of the intrinsic toughness and fatigue properties of brittle materials. Each material is represented by a universal curve, the relative position of which determines the merit of that material for structural applications. The marked superiority of such materials as silicon carbide and alumina become vividly apparent in the maps of Figs. 5 and 6. Useful distinctions may also be made between materials which cross over within the data range, e.g. soda-lime glass and PZT. On the basis of straight inert-strength testing we might reckon the first of these as the stronger material, whereas for applications involving sustained stresses it is the second which would tend to the larger lifetimes. Such crossovers would not be so obvious from the raw fracture mechanics parameters. It will be appreciated that this kind of intercomparison is made on the basis of "equivalent" flaw sizes: in this respect the indentation method, through its control over the flaw severity via the contact load, is unique in its capacity for reducing strength data to a common denominator.

In arguing the merits of this approach we do not mean to imply that it is only the intrinsic fracture properties which play an important role in the determination of component strengths and lifetimes; the effective sizes of the naturally occurring flaws which ultimately cause failure must also be known. Our procedure, by introducing flaws greater in severity than any of these natural flaws, automatically excludes information concerning the latter from the data. What our scheme effectively allows us to do is to determine the

intrinsic parameters in a truly independent manner. All necessary extrinsic flaw parameters should be obtainable from straightforward inert strength tests (run at a single stressing rate), in the form of the usual statistical distribution functions. Lifetime predictions for as-prepared components could then be made without ever having to accumulate vast quantities of fatigue data [2]. In adopting this strategy one needs to keep in mind the strong influence that any persisting residual stress concentrations associated with the original initiation processes (in our case the elastic/plastic deformation) might exert on the subsequent flaw evolution. In the absence of information as to this aspect of flaw characterization steps should be taken to design conservatively, on the basis of "worst-case" configurations wherever possible. This last point will be dealt with in greater detail elsewhere in this volume [25].

It has been indicated at several points that the existence of any spurious stresses incurred during the mechanical, chemical or thermal history of a material would necessitate a third contribution to the starting stress intensity factor in Eq. (1), with consequent deviations from the currently determined toughness and fatigue relations. The fact that such deviations were not observed in the materials studied here may be taken as evidence that this potential complication has been successfully avoided. Again, it may be well to emphasize that it may not be so simple to confirm the elimination of spurious stresses from surfaces whose strengths are controlled by natural flaws, particularly in materials with typically wide flaw distributions; nor, of course, may we wish to eliminate them, bearing in mind that these stresses are most often compressive.

Finally, a comment may be made concerning the convenience of indentation load as a variable for investigating fundamental flaw size effects. By

systematically reducing the load we can produce corresponding smaller flaws, thereby providing a link between macroscopic and microscopic crack behavior. Any change in the nature of the indentation flaw will then become evident as deviations from universal plots, much as just described in relation to the spurious stress influence. In this way it has been possible to demonstrate that indentation flaws in glasses undergo an abrupt transition in properties below a threshold load (corresponding to a flaw size $\approx\mu m$): above this threshold the macroscopically determined laws of crack growth remain perfectly valid, regardless of scale, provided the residual contact term is duly accounted for [11]; below the threshold the universal curves no longer apply, and failure becomes dominated by initiation micromechanics [17,30]. The indentation technique should prove similarly useful for studying size effects in ceramics, particularly for polycrystalline materials with relatively coarse microstructures.

CONCLUSIONS

(1) The indentation-flaw technique provides an attractive route to the evaluation of intrinsic fracture parameters. Coupled with independent determinations of natural flaw distributions, the approach offers the prospect of accurate lifetime predictions with optimum specimen economy.

(2) The control over the nature, shape and, above all, the size (via the contact load) of the indentation flaw allows for the derivation of a universal fracture formulation. Each material is represented by a single curve which

incorporates the toughness and fatigue properties. Composite plots of these curves produce master maps, affording a simple graphic format for materials comparisons.

(3) The inert strength cutoff on such a master map is a measure of effective material toughness. For "well-behaved" materials this effective toughness is consistent with macroscopically measured K_c values. In cases where inconsistency is observed the toughness reckoned from indentation data may provide a more reliable indication of the response of the typical natural flaw.

(4) The slope of the fatigue curve on a master map is a measure of the susceptibility of a material to subcritical crack growth. The crack velocity exponent determined from this slope is an apparent value, n', which is converted to the true value, n, via a simple transformation equation.

(5) Deviations from universality on a master map indicate an extraneous influence in the fracture mechanics, e.g. spurious stress states, microstructure/crack interactions, and threshold size effects.

ACKNOWLEDGEMENTS

The authors thank T. P. Dabbs for providing raw fracture data on the glasses, and L. Respall and S. J. Mann for help with specimen preparation. Funding was provided by the Australian Research Grants Committee and the United States Office of Naval Research (Metallurgy and Ceramics Program).

REFERENCES

[1] Wiederhorn, S.M., Fuller, E.R., Mandel, J. and Evans, A.G., Journal of the American Ceramic Society, Vol. 59, 1976, pp. 404-411.

[2] Ritter, J.E., Bandyopadhyay, N. and Jakus, K., Ceramic Bulletin, Vol. 60, 1981, pp. 798-806.

[3] Marshall, D.B. and Lawn, B.R., Journal of Materials Science, Vol. 14, 1979, pp. 2001-2012.

[4] Marshall, D.B., Lawn, B.R. and Chantikul, P., ibid, pp. 2225-2235.

[5] Marshall, D.B. and Lawn, B.R., Journal of the American Ceramic Society, Vol. 63, 1980, pp. 532-536.

[6] Chantikul, P., Lawn, B.R. and Marshall, D.B., ibid, Vol. 64, 1981, 322-325.

[7] Anstis, G.R., Chantikul, P., Lawn, B.R. and Marshall, D.B., ibid, pp. 533-538.

[8] Chantikul, P., Anstis, G.R., Lawn, B.R. and Marshall, D.B., ibid, pp. 539-543.

[9] Lawn, B.R., Marshall, D.B., Anstis, G.R. and Dabbs, T.P., Journal of Materials Science, Vol. 16, 1981, pp. 2846-2854.

[10] Cook, R.F., Lawn, B.R. and Anstis, G.R., ibid, Vol. 17, 1982, pp. 1108-1116.

[11] Dabbs, T.P., Lawn, B.R. and Kelly, P.L., Physics and Chemistry of Glasses, Vol. 23, 1982, pp. 58-66.

[12] Symonds, B.L., Cook, R.F. and Lawn, B.R., Journal of Materials Science, in press.

[13] Marshall, D.B. and Lawn, B.R., Journal of the American Ceramic Society, Vol. 64, 1981, pp. C6-C7.

[14] Marshall, D.B., Evans, A.G., Khuri-Yakub, B.T., Tien, J.W. and Kino, G.S., to be published.

[15] Lawn, B.R. in Fracture Mechanics of Ceramics, R.C. Bradt, A.G. Evans, D.P.H. Hasselman and F.F. Lange, Eds., Plenum, New York, 1982, Vol. 5.

[16] Fuller, E.R., Lawn, B.R. and Cook, R.F., Journal of the American Ceramic Society, in press.

[17] Dabbs, T.P. and Lawn, B.R., Physics and Chemistry of Glasses, Vol. 23, 1982, pp. 93-97.

[18] Cook, R.F., unpublished work.

[19] Marshall, D.B. and Lawn, B.R., Journal of the American Ceramic Society, Vol. 61, 1978, pp. 21-27.

[20] Mould, R.E. and Southwick, R.D., ibid, Vol. 42, 1959, pp. 542-547, 582-592.

[21] Lawn, B.R. and Fuller, E.R., Journal of Materials Science, Vol. 10, 1975, pp. 2016-2024.

[22] Lawn, B.R., Evans, A.G. and Marshall, D.B., Journal of the American Ceramic Society, Vol. 63, 1980, pp. 574-581.

[23] Wiederhorn, S.M., in Fracture Mechanics of Ceramics, R.C. Bradt, D.P.H. Hasselman and F.F. Lange, Eds., Plenum, New York, 1974, Vol. 2, pp. 613-646.

[24] "Flexure Testing of Glass", A.S.T.M. Annual Book of Standards, A.S.T.M., Philadelphia, 1979, Part 17, C158-C172

[25] Gonzalez, A.C., Multhopp, H., Cook, R.F., Lawn, B.R. and Freiman, S.W., this volume.

[26] Lawn, B.R., Marshall, D.B., Chantikul, P. and Anstis, G.R., Journal of the Australian Ceramic Society, Vol. 16, 1980, pp. 4-9.

[27] Arora, A., Marshall, D.B., Lawn, B.R. and Swain, M.V., Journal of Non-Crystalline Solids, Vol. 31, 1979, pp. 415-428.

[28] Smith, S.S. and Pletka, B.J., in Fracture Mechanics of Ceramics, R.C. Bradt, A.G. Evans, D.P.H. Hasselman and F.F. Lange, Eds., Plenum, New York, 1982.

[29] Pletka, B.J., Fuller, E.R. and Koepke, B.G., in Fracture Mechanics Applied to Brittle Materials, S.W. Freiman, Ed., A.S.T.M. Special Technical Publication 678, A.S.T.M., Philadelphia, 1978, pp. 19-37.

[30] Dabbs, T.P. Fairbanks, C.J. and Lawn, B.R., this volume.

[31] Wiederhorn, S.M., Journal of the American Ceramic Society, Vol. 52, 1969, pp. 99-105.

[32] Wiederhorn, S.M., unpublished work.

[33] Ritter, J.E. and Sherbourne, C.L., Journal of the American Ceramic Society, Vol. 54, 1971, pp. 601-605.

[34] Cook, R.F., Lawn, B.R., Dabbs, T.P., Reeve, K.D., Ramm, E.J., and Woolfrey, J.L., Journal of the American Ceramic Society, Vol. 65, 1982, pp. C172-C173.

[35] Gonzalez, A.C. and Freiman, S.W., unpublished work.

[36] McHenry, K.D., Yonushonis, T. and Tressler, R.E., Journal of the American Ceramic Society, Vol. 59, 1976, pp. 262-263.

[37] Koepke, B.G., unpublished work.

[38] Pletka, B.J. and Wiederhorn, S.M., Journal of Materials Science, Vol. 17, 1982, pp. 1247-1268.

TABLE 1. Materials used in this study.

	Independent Parameters				Indentation Parameters		
Material	E GPa	H GPa	K_c MPa $m^{\frac{1}{2}}$	n	K_c MPa $m^{\frac{1}{2}}$	n	log v_o ms^{-1}
Soda-Lime Glass[a]	70	6.6	0.74*	16-19*	0.97	18	-1.6
Borosilicate Glass[b]	89	6.5	0.77*	31-37*	1.2	36	1.6
Fused Silica[c]	72	7.6	0.81*	38*	1.2	44	2.2
Synroc[d]	190	10.3	1.9	-	1.8	35	0.2
P.Z.T.[e]	88	3.1	0.87	-	1.0	43	-0.5
Alumina[f]	400	16	4.4	46*	3.8	59	1.7
Silicon Carbide[g]	435	24	4.1*	118*	3.7	222	8.4
Glass Ceramic[h]	108	8.4	2.5*	63,* 84*	2.2	117	5.0

*Determinations by other workers. (See references, below).

[a]Schott-Ruhrglas GMBH [11,31,32].

[b]Schott-Ruhrglas GMBH [11,31,32].

[c]Schott-Ruhrglas GMBH [31,33].

[d]Synroc B, Australian Atomic Energy Research Establishment [34].

[e]Lead Zircon Titanate, Plessey Australia.

[f]F99, Friedrichsfeld GMBH [35].

[g]NC203, Norton Co. [7,36].

[h]Pyroceram C9606, Corning Glass Co. [7,10,37,38].

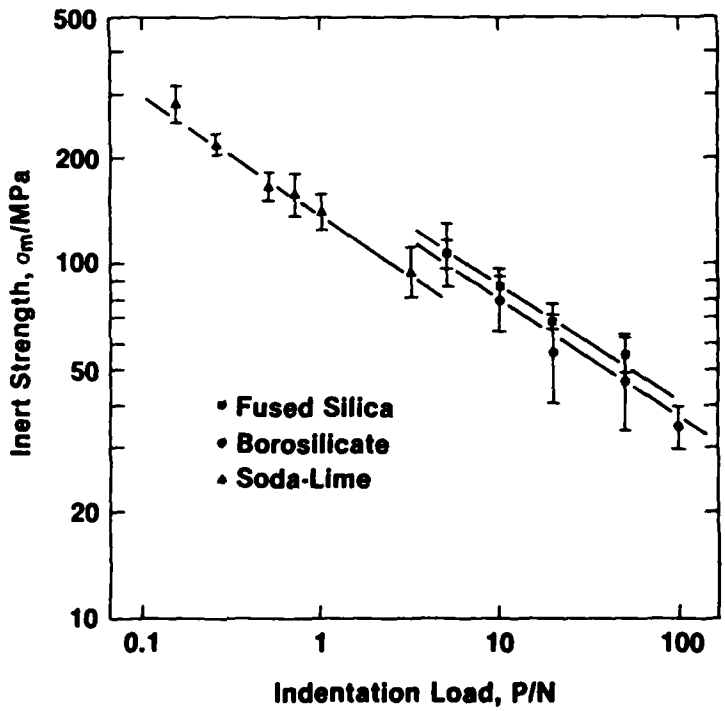

1. Inert strength as function of indentation load for the silicate glasses. (Data courtesy T.P. Dabbs.)

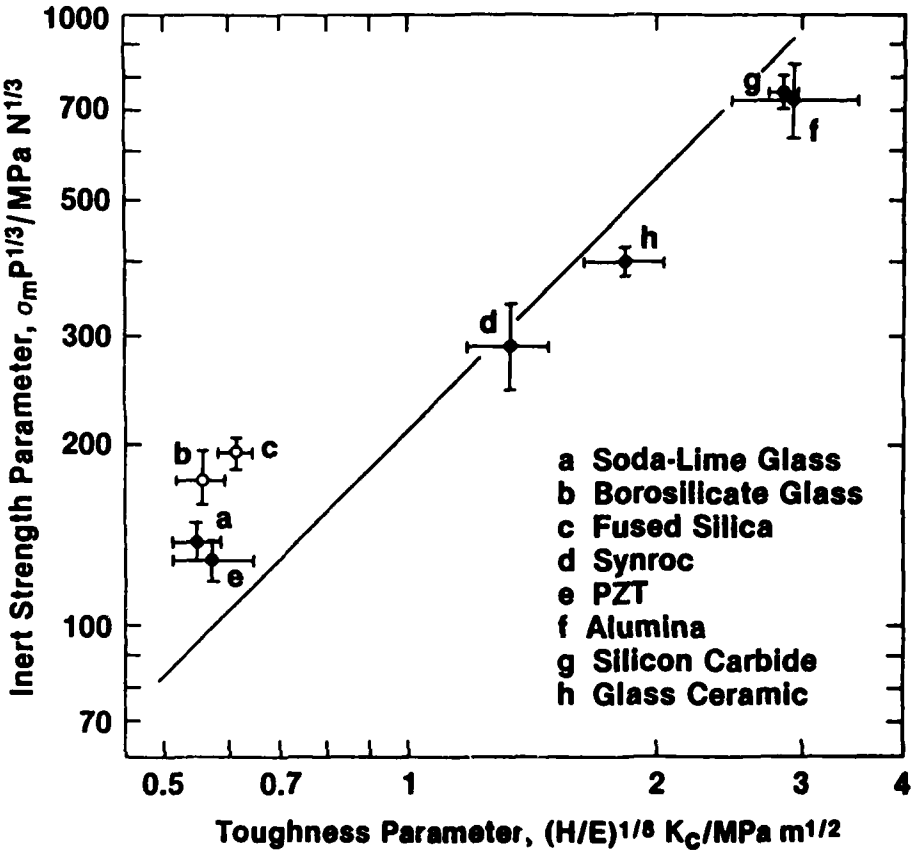

2. Inert strength parameter $\sigma_m P^{1/3}$ as function of toughness parameter $(E/H)^{1/8} K_c$ for the glasses and ceramics.

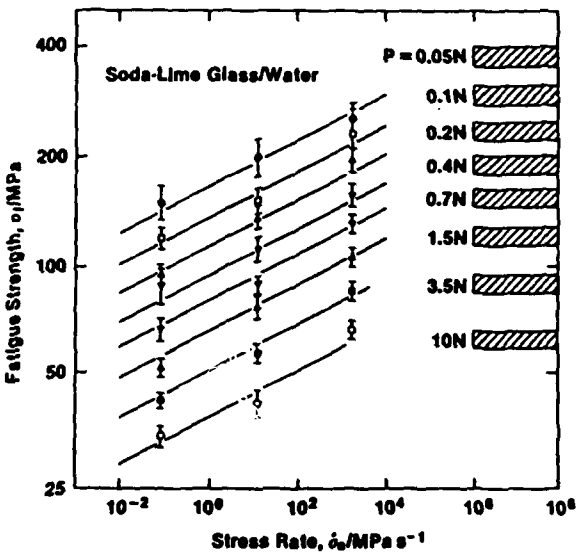

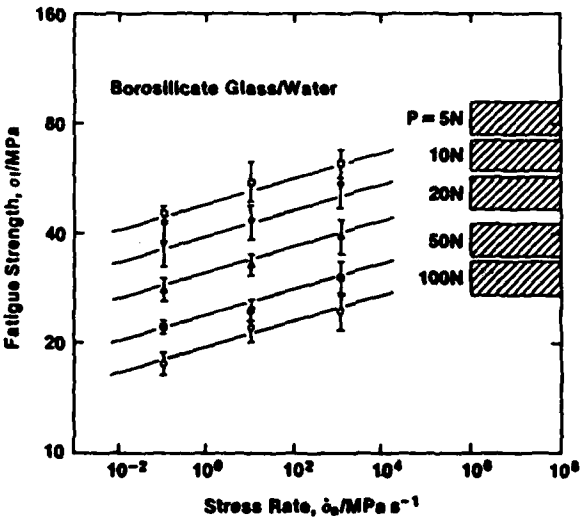

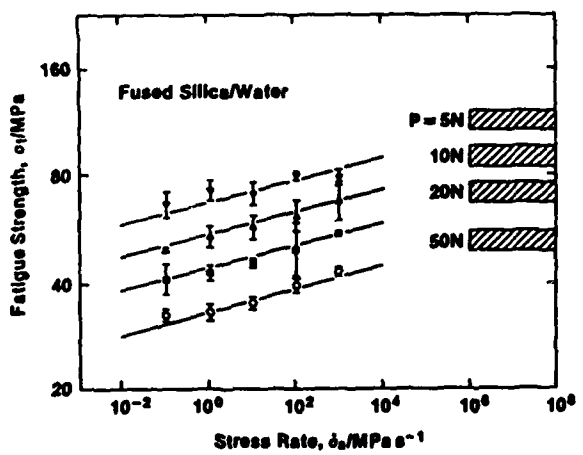

3. Dynamic fatigue responses of glasses indented at different loads. The hatched bands indicate inert strength levels. (Data courtesy T.P Dabbs.)

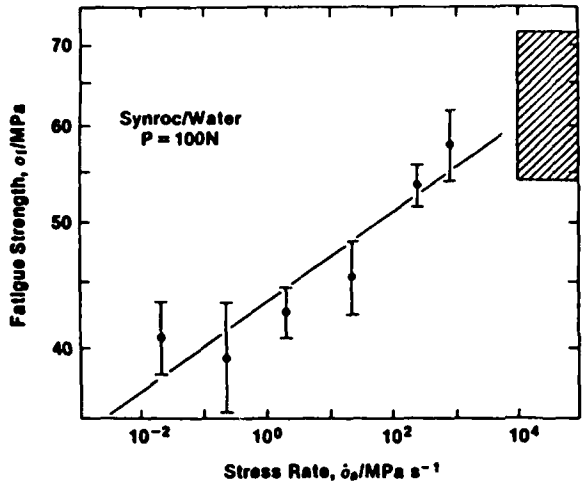

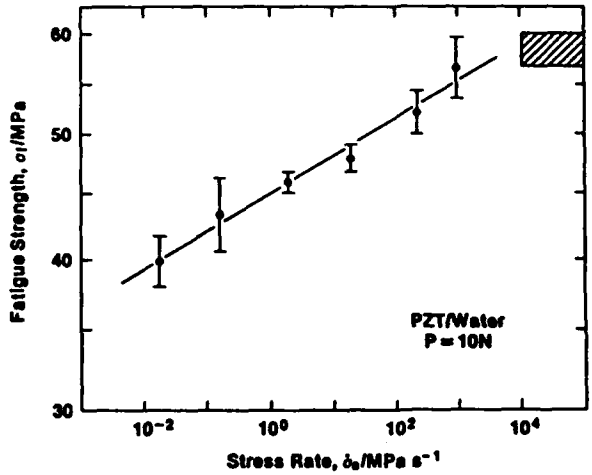

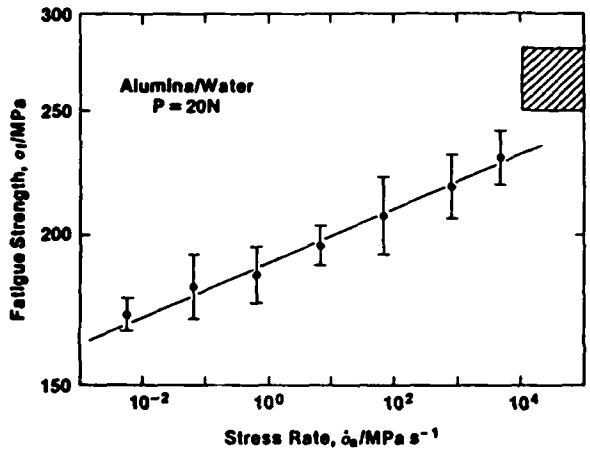

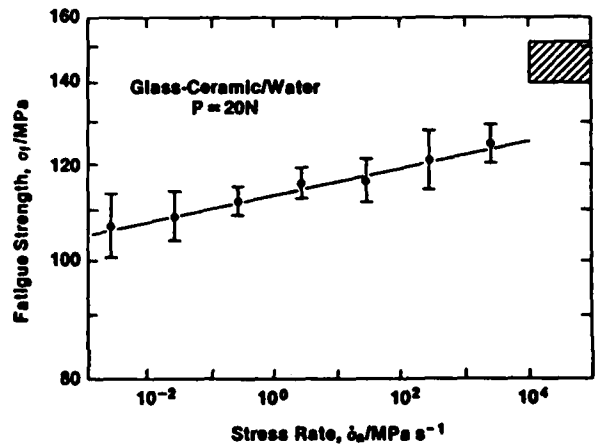

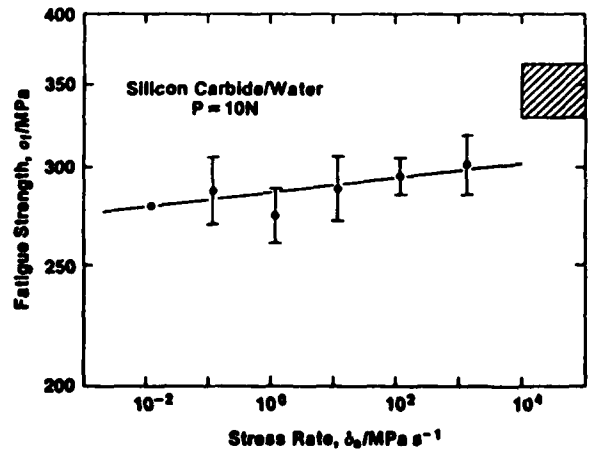

4. Dynamic fatigue responses of cerami
indented at single loads. Hatched
bands indicate inert strength level

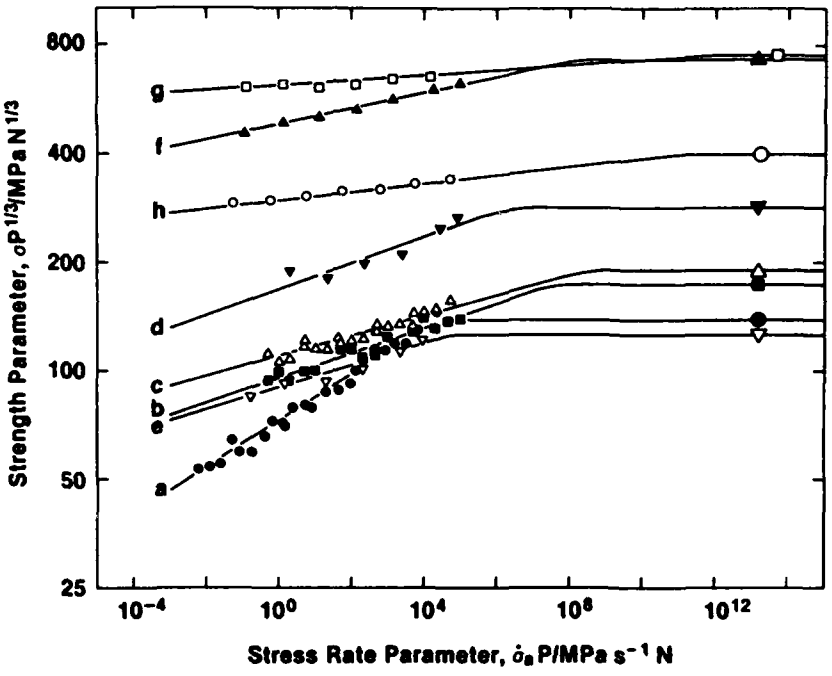

5. Dynamic fatigue master map. Error bars omitted from data points for clarity. See Table 1 for key to materials.

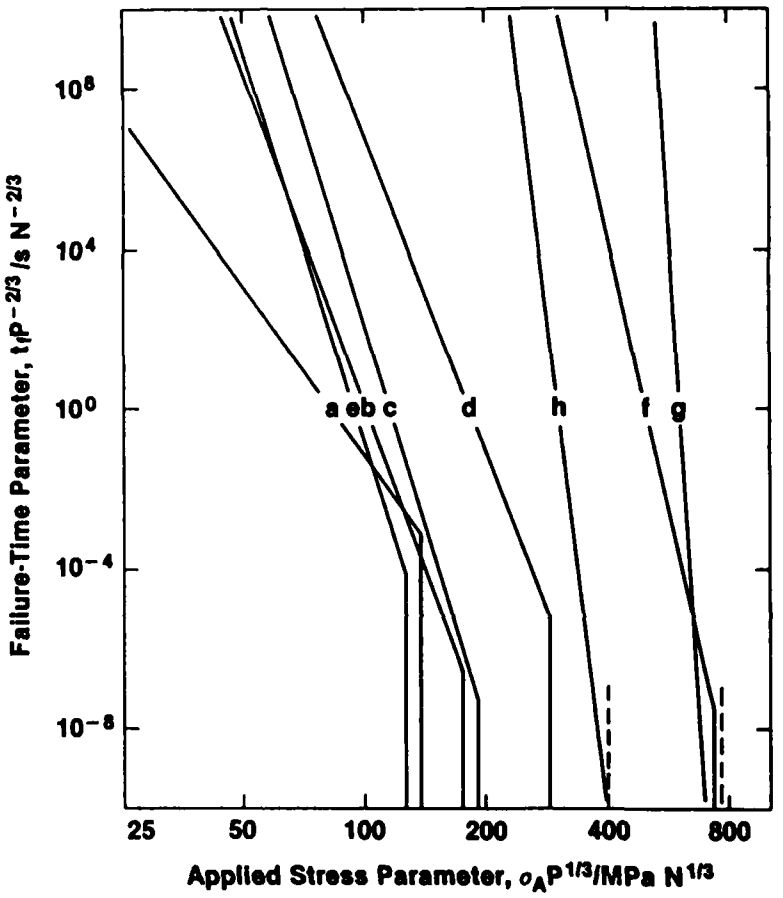

6. Static fatigue master map, generated from Fig. 5. See Table 1 for key to materials.

FATIGUE PROPERTIES OF CERAMICS WITH NATURAL AND CONTROLLED FLAWS: A STUDY ON ALUMINA

A.C. Gonzalez, H. Multhopp, R.F. Cook,* B.R. Lawn, S. W. Freiman

Center for Materials Science, National Bureau of Standards,
Washington, DC 20234

*On leave from the University of New South Wales

ABSTRACT

A systematic study of the fatigue properties of an as-fired polycrystalline alumina containing either "natural" (sawing damage) or indentation-induced (Vickers) strength-controlling flaws has been made. All fatigue strengths were measured in four-point bending in water. The study is presented in three steps: first, comparative Weibull analyses are made of inert strength data for the two flaw types, both to demonstrate the reduction in scatter that attends the indentation method and to characterize the flaw distributions for the as-sawn surfaces; next, fatigue data are taken on indented surfaces to determine relatively accurate fracture parameters for the alumina and to confirm that constant stressing rate tests can be used as a base for predicting the response in static loading; finally, the results from the two previous, independent steps are combined to generate lifetime responses for the surfaces with natural flaws, and fatigue data taken on such surfaces are used to evaluate these predictions. It is emphasized that residual stresses about the critical flaws, associated either with the preceding contact events responsible for creating the flaws or with extraneous processing, preparation or service conditions, can play a crucial role in the fracture mechanics. Notwithstanding this complication, the present approach offers a new design philosophy, with the potential for predicting responses relating to flaws generated after, as well as before, any laboratory screening tests.

KEY WORDS

Alumina; fatigue; indentation flaw; lifetime prediction; residual stresses; strength testing.

INTRODUCTION

In the preceding paper [1] a case was made for using indentation flaws to investigate the fracture properties of candidate materials for structural applications. The indentation method allows for complete control over the forces used to generate the critical flaws, provides knowledge of the local stress state of these flaws prior to strength testing, and reduces the scatter in the ensuing failure stresses. Most importantly, it separates the general strength problem into its two constituent parts, facilitating truly independent determinations of intrinsic material parameters and extrinsic flaw distribution characteristics. This opens the way to a new approach to design, whereby much of the empiricism and statistical data handling associated with conventional strength testing might be avoided.

In this study we demonstrate the approach on a commercial alumina. Alumina was chosen because of its widespread use as a structural ceramic, its availability in large quantities, its relatively simple microstructure and, above all, its well-documented susceptibility to slow crack growth. This last point is a key one, for it highlights the variability which can bedevil fracture mechanics measurements in ceramics; evaluations of the crack velocity exponent n, using both macroscopic crack specimens [2-7] and fatigue strength tests [6-9], lie anywhere between 30 and 90. Part of this variability is no doubt attributable to differences in the source materials, but the increasing recognition that most techniques in current use for monitoring crack growth are subject to systematic error [10], coupled with the strong influence that any residual stress fields about the critical flaws have on the slopes of fatigue curves [1], can also account for significant discrepancies. The recent comparative study by Pletka and Wiederhorn of double torsion and strength tests on common-source aluminas and other ceramics suggest that such

discrepancies could easily exceed a factor of three [9]. There would appear to be a need for a greater awareness of the oversimplistic assumptions that are implicit in our present descriptions of crack growth laws, at both the macroscopic and microscopic levels.

The central aim of the present work is to characterize the strength properties of alumina specimens containing "controlled" flaws in order to optimize the amount of testing that must be carried out on similar specimens with "natural" flaws. More specifically, it is intended that crack growth parameters for the alumina should be obtained from dynamic fatigue results on indented surfaces, and flaw distribution parameters from independent inert strength tests on as-prepared surfaces, enabling the two vital elements of the lifetime prediction problem to be treated separately. Predictions made using this approach will be tested against representative fatigue data from the latter, natural surfaces.

EXPERIMENTAL PROCEDURE

Preparation of Specimens With Different Flaw Types

The aluminum oxide used in this study was a roll-compacted, sintered substrate material with 4% additive component,* having an average grain size ≈10μm. It was obtained as plates 1.3 mm thick in its as-fired state, and was diamond-sawn into strips 30 mm long and 5 mm wide. Inspection of these strips in the optical microscope revealed chipping damage at the edges. One group of specimens was immediately selected out, at random, and set aside for testing in the as-received state.

---

*AD96, Coors Porcelain, Colorado

The remaining specimens were used for "controlled-flaw" testing. Each member of this group was indented at a face center with a Vickers diamond pyramid, taking care to orient the impression diagonals parallel to the specimen edges. A "standard load" of P = 5N was chosen for this purpose, this representing a compromise between the requirements that the radial cracks extending from the impression corners should be sufficiently large compared to the scale of the impression itself and yet sufficiently small compared to the specimen thickness [11]. All indentations were made in air, and were allowed to sit ≈1 hr prior to strength testing. Optical and scanning electron microscopical examination of representative examples on surfaces pre-polished through 3 μm diamond paste showed that the crack patterns thus produced were not generally of the ideal radial geometry, due to microstructural complications [12], as is evident in the micrograph of Fig. 1. The indentations were nevertheless sufficiently well formed to allow hardness determinations, and to a lesser extent crack size measurements, to be made.

Strength Testing

The alumina bars prepared as above were loaded to failure in four-point flexure, outer span 27 mm and inner span 9 mm, with the surfaces containing the indentation flaws on the tension side. Inert strengths were measured in nitrogen gas or silicone oil, fatigue strengths in water. The inert strength and dynamic fatigue tests were run using a crosshead loading machine, the former at the fastest available rate. Breaking loads were measured by strain-gage and piezoelectric cells [11]. For the static fatigue tests the load was applied pneumatically [13], with a nominal rise time 8 s and a maximum fluctuation 1 % at hold. Simple beam theory was used to evaluate the stresses from the recorded loads.

All broken test pieces were examined by optical microscopy to confirm the sources of failure. As expected, those specimens with controlled flaws broke from the indentation sites, those without from the as-sawn edges.

Efforts were also made to run double torsion tests on the alumina, to obtain crack velocity parameters as a check on the strength analysis. However, it was found impossible to produce well-behaved cracks in this configuration, presumably due to instabilities in the propagation [7]. Double-cantilever beam specimens were also unsatisfactory, owing to the difficulty in locating the crack tips.

RESULTS

Inert Strength Tests

Inert strength tests were run to determine flaw statistical parameters, to check for spurious pre-existing stresses in the specimen surfaces, and to obtain appropriate toughness parameters for later fatigue analysis.

The first runs were made on specimens from each of the two groups, i.e. as-sawn and indented. The data from these runs were analyzed in accordance with the usual two-parameter Weibull probability function

$$F = 1 - \exp\left[-(\sigma_m/\sigma_o)\right]^m \qquad (1)$$

where σ_m is the inert strength and m and σ_o are adjustable parameters. It is seen that the spread in results is indeed smaller for the surfaces with indentation flaws (m = 12.9) than for those with natural flaws (m = 9.8). Nevertheless, this spread in the former case is by no means insignificant, consistent with the inherent variability in the crack pattern of Fig. 1.

The next runs were made on indented specimens as a function of the contact load, P. Figure 3 shows the results. The data points represent strengths at 50 ± 32% Weibull failure probability (equivalent to standard deviation limits for a normal distribution) for at least 10 specimens per load, and the straight line is a best fit of slope -1/3, in logarithmic coordinates, from which we obtain $\sigma_m P^{1/3} = 590 \pm 47$ MPa $N^{1/3}$ (mean and standard deviation). The constancy of this quantity over the load range covered is an indication of the absence of prepresent stresses in the as-fired surfaces [1,14]. It is noted that the as-sawn strength level in Fig. 3 corresponds to an "effective" indentation load 3.3 ± 1.4 N.

Some additional tests were made on pre-polished surfaces containing 5 N "dummy" indentations [1,11]. In these tests, on 10 specimens, failure occurred from one of three near-identical contact sites located along the specimen within the inner span, leaving two dummies intact for the determination of the important crack dimensions, Thus, measurements of the set of radial cracks parallel to the tensile directive gave the initial crack dimension $c_o' = 28 \pm 4$ μm, while those of the perpendicular set gave the critical dimension $c_m = 33 \pm 5$ μm. The crucial proviso for validity of the fracture mechanics formulation in Ref. 1 is therefore satisfied.

With the underlying basis of the equilibrium fracture description thereby established we may insert the value of $\sigma_m P^{1/3}$ obtained above, together with H = 15.5 ± 1.0 GPa measured directly from the hardness impressions and E = 303 GPa specified by the manufacturer, into the expression for toughness [1,15]

$$K_c = \eta\,(E/H)^{1/8}\,(\sigma_m P^{1/3})^{3/4} \qquad (2)$$

where $\eta = 0.59$. This gives $K_c = 3.2 \pm 0.2$ MPa $m^{1/2}$, which may be compared with the value 3.31 ± 0.07 obtained by other workers [16] on similar material using a chevron-notched rod technique.

Dynamic and Static Fatigue of Specimens with Controlled Flaws

Dynamic and static fatigue data were collected on the alumina specimens with standard 5 N indentation flaws, with the purpose of testing the theoretically predicted interrelationships between the two stressing modes.

Figure 4 shows the dynamic fatigue results. The data points are 50 ± 32 % Weibull evaluations of the strengths, σ_f, for at least 10 specimens at each of the prescribed stressing rates, $\dot{\sigma}_a$. It is immediately evident that the fatigue strengths are substantially less than the inert strength level, even at the fastest stressing rates. The straight line is a best fit to all individual test results, in accordance with the prediction [1,17,18]

$$\sigma_f = (\lambda' \dot{\sigma}_a)^{1/(n'+1)}. \qquad (3)$$

Bearing in mind the precursor growth stage apparent in the equilibrium failure mechanics referred to in the previous subsection (i.e. $c_o' < c_m$), it is important to emphasize that the slope and intercept terms, n' and λ', relate to "apparent" crack velocity parameters. Appropriate transformation equations for converting these to corresponding "true" parameters obtain from the modified stress intensity factors for "point" flaws with residual contact terms incorporated [1,18],

$$n' = 3n/4 + 1/2 \qquad (4a)$$

$$\lambda' = (2\pi n')^{1/2} \sigma_m^{n'} c_m / v_o \qquad (4b)$$

where n and v_o are exponent and coefficient, respectively, in the usual power-law crack velocity relation (Eq. 6 in Ref. 1). Thus, from the data analysis we obtain $n' = 54.9 \pm 4.9$ which converts, via Eq. (4a), to $n = 72.5 \pm 6.5$; also, $\log \lambda' = 133 \pm 12$ (in the units used in Fig. 4) which, in conjunction with the inert strength data from the preceding subsection, yields $\log v_o = 4.0 \pm 0.5$ (velocity in m s^{-1}).

The corresponding results for the static fatigue tests are shown in Fig. 5. In this case the data are plotted as median values of the times to failure, t_f, over 10 tests at each of the prescribed holding stresses, σ_A, to accommodate null tests in which the specimens either broke during the loading ramp or survived the two-week cutoff. The straight lines are predictions using the static analogue of Eq. (3) [1,18], i.e.

$$t_f = \lambda'/(n'+1)\sigma_A^{n'} \qquad (5)$$

where the terms n' and λ' have the same values as above. As discussed in Ref. 1, the procedure is equivalent to inverting the dynamic fatigue curve in accordance with the relation $t_f = \sigma_f/\dot{\sigma}_a$, identifying σ_f with σ_A, and translating the intercept through n'+1 in logarithmic space. In the spirit of this description we have generated 17 % and 83 % failure probability limits directly from the corresponding Weibull band for the inert strengths in Fig. 5. The level of agreement between data and predictions in this figure may be taken as a measure of the confidence with which we might use the fatigue equations to analyze the response of less well-defined flaws.

Lifetimes of Specimens with Natural Flaws

In this part of the study a priori predictions were made of the lifetime characteristics for surfaces with the natural (sawing damage) flaws, using the results of the preceding subsections. Fatigue data were then taken on such surfaces as a check against these predictions.

In adopting this course we find ourselves confronted immediately by an apparent obstacle, namely our lack of foreknowledge of the flaw characteristics. If we could assume that the natural flaws were to behave in essentially the same way as the Vickers-induced radial cracks the procedure would be straightforward enough. Then, one could make use of the "effective" load evaluated at the intersection point of the indentation line, $\sigma_m P^{1/3} =$ const., with the inert strength level in Fig. 3 to characterize the flaw severity. The appropriate lifetime relation would follow directly from Eq. (5), using the same slope parameter n' as determined for the indentation flaws but with a load-adjusted intercept parameter [1]

$$\lambda' = \lambda'_p / P^{(n'-2)/3} \qquad (6)$$

where λ'_p is a modified, load-independent term, also to be evaluated from the indentation fatigue data. This prediction is plotted as the solid line in Fig. 6. As in Fig. 5, failure probability limits may be generated directly from the plotted 50 ± 32 % Weibull band for the inert strengths, but these are omitted from the present plot for the sake of clarity.

Unfortunately, the assumption that the strength properties of real materials may be described in terms of ideal point contact flaws does not always hold to good approximation [1]. If the past history of the controlling flaws is such that residual driving forces do indeed persist to stabilize the

initial crack growth, but the flaw has essentially linear rather than point geometry, the mechanics will reflect the same kind of stress augmentation, but with even greater intensity [19]. Or, if for some reason the residual influence is diminished to an insignificant level, the mechanics will tend closer to those for "Griffith" flaws (i.e. zero residual stress) [20,21]. In either case, the procedure for generating a lifetime prediction remains much the same as before, in that Eq. (5) may be retained as the basic starting formula but with the slope term n' in Eq. (4a) and the intercept term λ' in Eq. (4b) replaced by appropriate analogues [18]. Expressions for these replacement terms are given in the Appendix; suffice it to say here that evaluations may still be made from the independently obtained dynamic fatigue data on the indented control specimens and inert strength data on the actual specimens with natural flaws. The predictions for these alternative, extreme flaw types are plotted as the broken lines in Fig. 6.

These various predictions for the natural surfaces may be reckoned against the data points from the confirmatory fatigue tests. Initially it was intended that all such data should be obtained directly from tests at constant applied stress, but the problems with loading-ramp failures and "runouts" referred to in connection with Fig. 5, magnified in the case of natural surfaces by the wider spread in flaw severity (i.e. lower Weibull modulus), imposed severe limitations on specimen and time economy. Therefore, supplementary data were collected in the constant stressing rate mode, using the "inversion and translation" operation which interrelates Eqs. (3) and (5) to evaluate "equivalent" lifetimes. A difficulty here, of course, is that this conversion operation is contingent on the quantity $n'+1$, which we cannot specify a priori. In our case we have obtained a working evaluation by regressing on the pooled dynamic fatigue results, in accordance with Eq. (3).

Accordingly, the data points in Fig. 6 represent median values for 20 to 40 tests at each static holding stress or 50 ± 32 % probability bounds for 10 to 15 tests at each predetermined dynamic stress rate.

DISCUSSION

We have presented results of a strength study on alumina surfaces with both controlled and natural flaws in the context of lifetime design. Currently, it is widely accepted that the most reliable route to this end is via the exclusive and extensive testing of specimens with the same preparation as that of the structural component, regarding Eqs. (3) and (5) as empirical relations to be used in conjunction with statistically determined flaw distributions [22]. We have argued for an alternative philosophy, in which inert strength tests on as-prepared surfaces are retained to determine the flaw distributions, but independent tests are run on indented surfaces to evaluate toughness and crack velocity parameters. The most apparent advantage of this approach is a substantial reduction in the uncertainty in the intrinsic, material component of the strength formulation, so that many less specimens should need to be broken to attain a specified tolerance in predicted lifetimes.

The one major obstacle which we face in adopting this alternative course is the general inability to predetermine the true nature of the strength-controlling flaw in any prospective structural component. We have seen in Fig. 6 that the presence of residual stresses about the flaw center and the geometrical aspect of this flaw configuration can be decisive factors in lifetime response. In the present tests on as-sawn specimens the results would appear to indicate a relatively minor role for these factors. This is

not altogether unreasonable, for, although diamond-sawing is a contact-related process, the basic removal mechanism is one of "lateral-crack" chipping [23], and such chipping modes can greatly relieve the residual contact fields [20]. In principle, the extent of such relief mechanisms may be quantified by comparing strength values before and after a full anneal treatment of the natural surfaces, as has been done in glass [20,21,24]. With many ceramics, however, annealing is impractical, in which case the prudent designer would presume that residual stress components remain fully active. Indeed, in certain cases, e.g. with machined surfaces, it might well be advisable to adopt the ultra-conservative path and work on the assumption that the flaws also have essentially linear geometry. There is clearly the prospect of overdesign with this approach, which may be unacceptable in applications where the limits of material performance are an absolute necessity. Any decision to design on a less conservative basis should, on the other hand, be backed up with confirmatory fatigue data, e.g. as in Fig. 6. Then, of course, we shall have had to revert, at least in part, to precisely the kind of testing we have sought to supplant in the first place.

With due acknowledgement of the complication just discussed, we may now reinforce our case for the controlled-flaw procedure advocated in this work by emphasizing some of the unique advantages which attend the broad field of indentation fracture mechanics [25-27]. Most importantly, the approach offers, via its physical insight into the underlying micromechanics of flaw development, the prospect of accommodating changes in the flaw characteristics subsequent to the laboratory screening tests within the design specifications. Such changes can be particularly dangerous if they are associated with the spontaneous initiation of new flaws, due, for example, to interactions with a hostile mechanical [26,28,29] or chemical [30] service environment. Under

these conditions any amount of laboratory testing on as-prepared surfaces would be totally useless if the new flaws were to be dominant. However, provided that the potential service environment is specifiable, indentation fracture mechanics provides us with the facility for estimating an equivalent indentation load for any such flaw; in a particle erosion field, for instance, the load is readily calculable in terms of the incident particle energy and quasistatic component hardness [29]. The problem is thereby reduced to the level of the pre-present natural flaw, whence Eq. (6) may be invoked, as before, to obtain a lifetime prediction from Eq. (5).

Another distinctive advantage of the indentation flaw method is that one can check routinely for spurious stresses in the as-prepared surfaces. The presence of such stresses becomes manifest as a breakdown in the fracture mechanics formalism used earlier in this work, most conveniently in the inert strength response as a departure from the load independence of the quantity $\sigma_m P^{1/3}$ [1]. (Indeed, quantitative information on surface compression stresses has been determined in this manner for tempered glasses [31,32]). Insofar as the lifetime predictions in Fig. 6 are concerned, the effect of a superposed spurious stress may be regarded in terms of an appropriate displacement of all plotted points, in absolute terms, along the horizontal axis, thereby introducing a greater or lesser degree of curvature in the logarithmic representation [17]. This curvature may pass unnoticed in tests on natural surfaces, depending on the scatter in data and range in failure times covered, yet lead to significant discrepancies in long-term extrapolations.

ACKNOWLEDGEMENTS

The authors thank Dan Briggs of Coors Porcelain Co. for supplying the alumina plates used in this study. Funding was provided by the Office of Naval Research (Metallurgy and Ceramics Program).

APPENDIX

In interpreting the fatigue results for specimens with natural flaws it was indicated that Eqs. (3) and (5) may be retained as the basis for analysis, provided that the quantities n' in Eq. (4a) and λ' in Eq. (4b) for point flaws with residual stresses are suitably replaced to match the specific flaw characteristics. Reference is made to the paper by Fuller, Lawn and Cook [18] for details.

One of the distinctions we shall be required to make in effecting these conversions is that between geometrical factors for the point and line configurations. The relation between inert strength, σ_m, and critical crack size, c_m, for the standard point indentations,

$$\sigma_m = 3K_c/4\psi_p c_m^{1/2}, \tag{A1}$$

provides us with the means for doing this; here ψ_p is a dimensionless factor to be evaluated from the experimental data. An equivalent evaluation for line flaws may then be made purely on theoretical grounds, using an appropriate "modification" relation [33]

$$\psi_\ell = (\pi/2)\,\psi_p. \tag{A2}$$

Consider now the case of linear flaws with fully persistent residual stresses. The replacement quantities in the fatigue equations are

$$n'' = n/2 + 1 \tag{A3a}$$

$$\lambda'' = (4\pi n'')^{1/2}\sigma_m^{n''}c_m/v_o \tag{A3b}$$

where it is understood that σ_m and c_m now pertain to measurements on the natural surfaces. Since crack sizes are not readily measured for failures from natural flaws it is convenient to eliminate c_m from Eq. (A3b) using the line-flaw analogue of Eq. (A1),

$$\sigma_m = K_c/2\psi_\ell \; c_m^{1/2}. \tag{A4}$$

Thus, given the "calibrated" values of ψ_ℓ and K_c from the standard indentation tests, we are left with the natural inert strength as the controlling variable in Eq. (A3b). Equation (A3) may then be coupled with its indentation-flaw counterpart, Eq. (3) in the text, to eliminate n and v_o, thus to complete the conversion operation.

For flaws with zero residual stress, conventional theory applies. The replacement quantities are

$$n_o = n \tag{A5a}$$

$$\lambda_o = [2/(n-2)] \; \sigma_o'^{\,n} \; c_o'/v_o \tag{A5b}$$

where σ_o' is the inert strength conjugate to the initial flaw size c_o'. In this case the "apparent" and "true" crack velocity exponents are identical. The crack size may be eliminated via the familiar inert strength relation

$$\sigma_o' = K_c/\psi c_o'^{1/2} \tag{A6}$$

where ψ identifies with the geometrical factor for point or line flaws as appropriate. Thereafter, the procedure is the same as that outlined in the previous example.

REFERENCES

[1] Cook, R.F. and Lawn, B.R., this volume.

[2] Freiman, S.W., McKinney, K.R. and Smith, H.L., in Fracture Mechanics of Ceramics, R.C. Bradt, D.P.H. Hasselman and F.F. Lange, Eds., Plenum, New York, 1974, Vol. 2, pp. 659-676.

[3] Evans, A.G., Linzer, M. and Russell, L.R., Materials Science and Engineering, Vol. 15, 1974, pp. 253-261.

[4] Bansal, G.K. and Duckworth, W.H., Journal of Materials Science, Vol. 13, 1978, pp. 215-216.

[5] Ferber, M.K. and Brown, S.D., Journal of American Ceramic Society, Vol. 63, 1980, pp. 424-429.

[6] Koepke, B.J., unpublished work.

[7] Pletka, B.J. and Wiederhorn, S.M., Journal of Materials Science, Vol. 17, 1982, pp. 1247-1268.

[8] Rockar, E.M. and Pletka, B.J., in Fracture Mechanics of Ceramics, R.C. Bradt, D.P.H. Hasselman and F.F. Lange, Eds., Plenum, New York, 1978, Vol. 4, pp. 725-735.

[9] Ritter, J.E. and Humenik, J.N., Journal of Materials Science, Vol. 14, 1979, pp. 626-632.

[10] Freiman, S.W., in Fracture Mechanics of Ceramics, R.C. Bradt, A.G. Evans, D.P.H. Hasselman and F.F. Lange, Eds., Plenum, New York, 1982.

[11] Cook, R.F., Lawn, B.R. and Anstis, G.R., Journal of Materials Science, Vol. 17, 1982, pp. 1108-1116.

[12] Anstis, G.R., Chantikul, P., Marshall, D.B. and Lawn, B.R., Journal of the American Ceramic Society, Vol. 64, 1981, pp. 534-538.

[13] Gonzalez, A.C. and Freiman, S.W., unpublished work.

[14] Marshall, D.B. and Lawn, B.R., Journal of Materials Science, Vol. 14, 1979, pp. 2001-2012.

[15] Chantikul, P., Anstis, G.R., Lawn, B.R. and Marshall, D.B., Journal of the American Ceramic Society, Vol. 64, 1981, pp. 539-543.

[16] Barker, L.M., in Fracture Mechanics of Ceramics, Eds. R.C. Bradt, D.P.H. Hasselman and F.F. Lange, Eds., Plenum, New York, 1978, Vol. 3, pp. 483-494.

[17] Lawn, B.R., Marshall, D.B., Anstis, G.R. and Dabbs, T.P., Journal of Materials Science, Vol. 16, 1981, pp. 2846-2854.

[18] Fuller, E.R., Lawn, B.R. and Cook, R.F., Journal of the American Ceramic Society, in press.

[19] Symonds, B.L., Cook, R.F. and Lawn, B.R., Journal of Materials Science, in press.

[20] Marshall, D.B. and Lawn, B.R., Journal of the American Ceramic Society, Vol. 63, 1980, pp. 532-536.

[21] Chantikul, P., Lawn, B.R. and Marshall, D.B., ibid, Vol. 64, 1981, pp. 322-325.

[22] Ritter, J.E., in Fracture Mechanics of Ceramics, R.C. Bradt, D.P.H. Hasselman and F.F. Lange, Eds., Plenum, New York, 1982.

[23] Marshall, D.B., Lawn, B.R. and Evans, A.G., Journal of the American Ceramic Society, Vol. 65, 1982, pp. 561-566.

[24] Marshall, D.B. and Lawn, B.R., Journal of the American Ceramic Society, Vol. 64, 1981, C6-C7.

[25] Lawn, B.R. and Wilshaw, T.R., Journal of Materials Science, Vol. 10, 1975, pp. 1049-1081.

[26] Lawn, B.R., in Fracture Mechanics of Ceramics, R.C. Bradt, D.P.H. Hasselman and F.F. Lange, Eds., Plenum, New York, 1978, Vol. 3, pp. 205-229.

[27] Lawn, B.R., ibid, 1982.

[28] Hockey, B.J., Wiederhorn, S.M. and Johnson, H., ibid, 1978, Vol. 3, pp. 379-402.

[29] Wiederhorn, S.M. and Lawn, B.R., Journal of the American Ceramic Society, Vol. 62, 1979, pp. 66-70.

[30] Dabbs, T.P., Fairbanks, C.J. and Lawn, B.R., this volume.

[31] Marshall, D.B. and Lawn, B.R., Journal of the American Ceramic Society, Vol. 61, 1978, pp. 21-27.

[32] Chantikul, P., Marshall, D.B., Lawn, B.R. and Drexhage, M.G., ibid, Vol. 62, 1979, pp. 551-555.

[33] Lawn, B.R. and Wilshaw, T.R., Fracture of Brittle Solids, Cambridge University Press, London, 1975, Ch. 3.

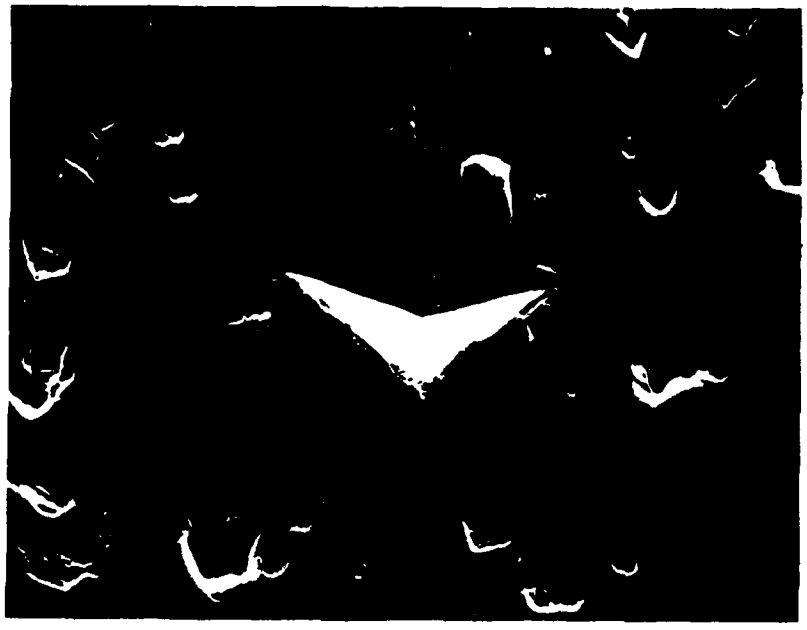

1. Scanning electron micrograph of Vickers indentation flaw in alumina. Note transgranular nature of radial cracking about hardness impression. Indentation load P = 5N, width of field 150 μm.

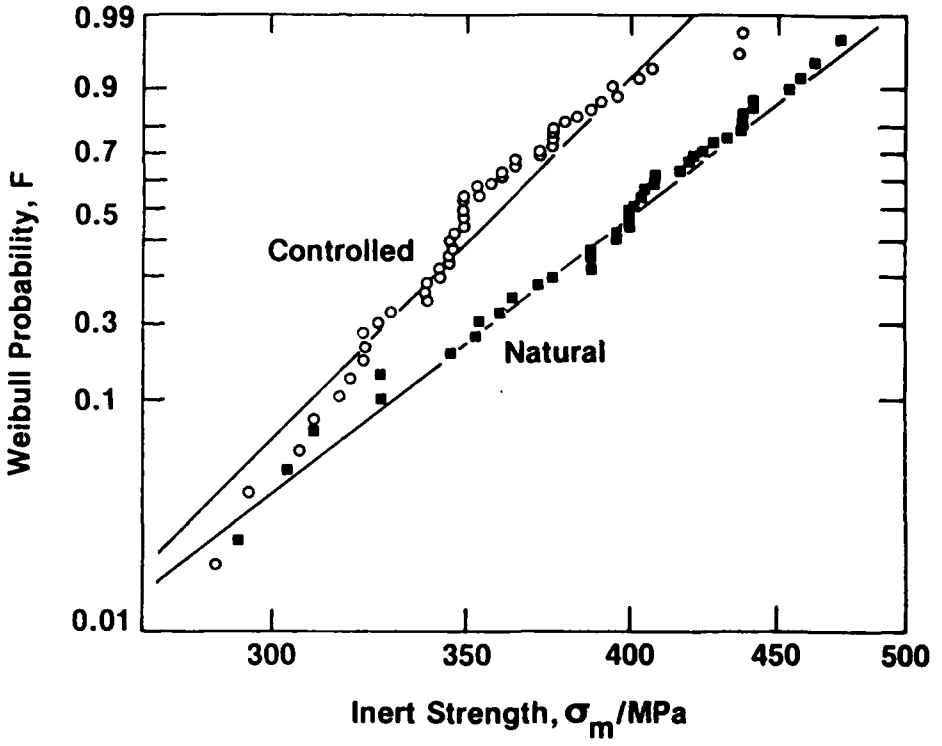

2. Weibull plot of inert strengths on alumina surfaces with natural (sawing damage) and controlled (5N Vickers indentation) flaws.

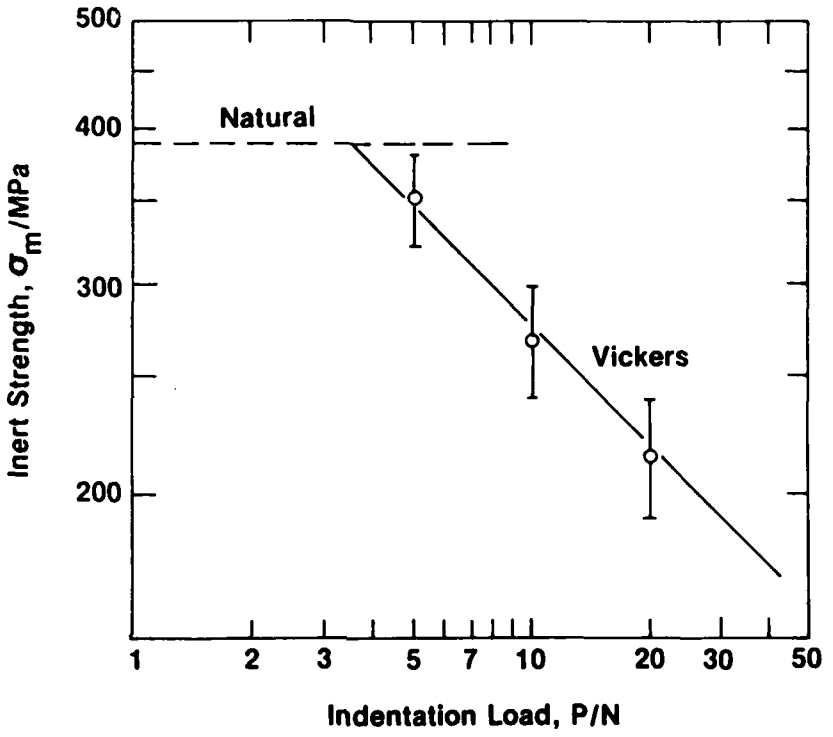

3. Inert strength of alumina as function of Vickers indentation load.

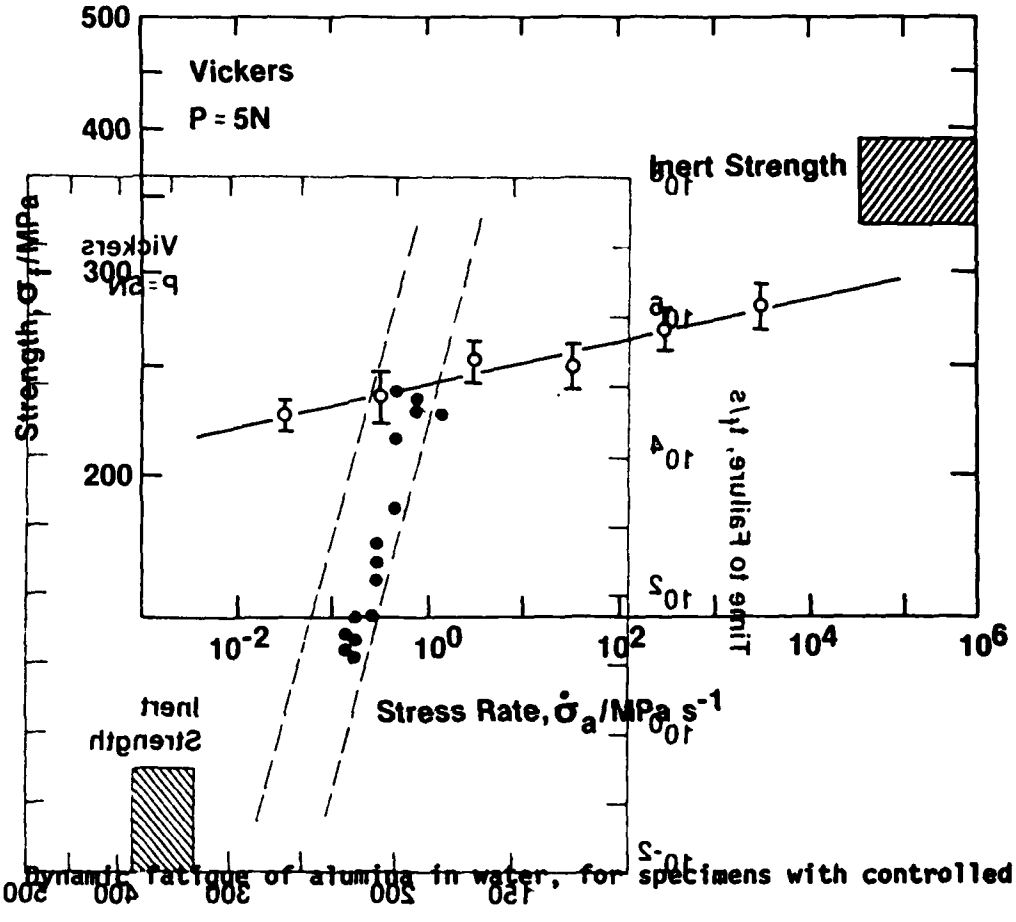

4. Dynamic fatigue of alumina in water, for specimens with controlled flaws.

5. Static fatigue of alumina in water, for specimens with controlled flaws.

5. Static fatigue of alumina in water, for specimens with controlled flaws.

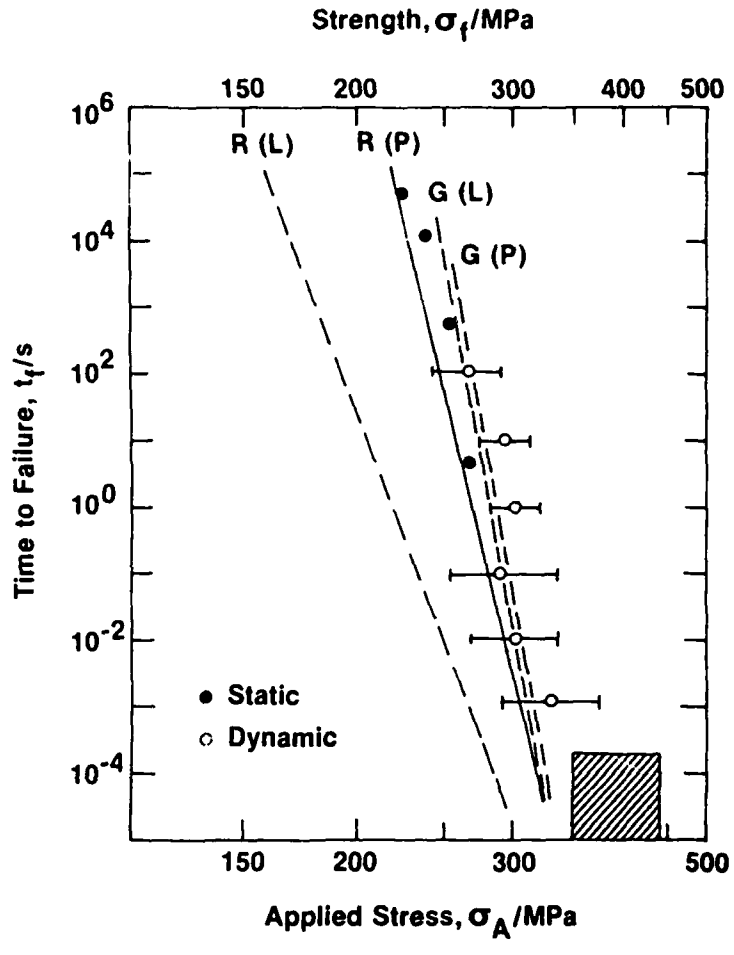

6. Lifetime diagram for alumina in water, for surfaces with natural flaws. Lines are predictions based on indentation-calibrated fracture mechanics formulas: R refers to flaws with residual stress, G to conventional Griffith flaws; P and L denote flaws with point and line geometry, respectively. Points are confirmatory static and dynamic fatigue data.

SUBTHRESHOLD INDENTATION FLAWS IN THE STUDY OF FATIGUE PROPERTIES OF ULTRA-HIGH STRENGTH GLASS

T.P. Dabbs,* C.J. Fairbanks, B.R. Lawn

Center for Materials Science, National Bureau of Standards,
Washington, DC 20234

*On leave from the University of New South Wales

ABSTRACT

The rate-dependent characteristics of subthreshold indentation flaws in glass are surveyed. In the first part, the kinetics of radial crack initiation within the indentation field are described. It is shown that an incubation time must be exceeded in the contact process for a critical crack nucleus to develop. This incubation time decreases as the contact load and the water content in the environment increase. Even if incubation is not achieved during the contact, delayed pop-in may occur after the contact due to the action of residual stresses. Scanning electron microscopic evidence shows that the radial cracks initiate from precursor shear faults within the deformation zone. In the second part of the presentation, the fatigue properties of specimens with indentation flaws on either side of the threshold are discussed. The subthreshold flaws differ significantly from their postthreshold counterparts in these properties: the applied stresses at failure are higher, the susceptibility to water is stronger, and the scatter in individual data points is wider. These features are discussed in relation to the preceding crack-initiation kinetics. Finally, the implications of the results concerning design criteria for the ultra-high strength domain of optical fibers are considered.

KEY WORDS

Crack initiation; fatigue; glass; indentation flaw; optical fibers; radial crack; shear fault; strength

INTRODUCTION

In an earlier paper in this volume [1] a strong argument was presented for the use of indentation flaws in the investigation of intrinsic fracture parameters and flaw characteristics. One major advantage cited was the facility to control the scale of the flaw, via the contact load, in order to check for size effects in macroscopically-determined crack growth laws. Such size effects would be apparent as deviations from the proposed "universal" plotting schemes. In view of the growing concern that microscopic flaws might differ in some significant respects from true cracks [2,3], particularly in the region of ultra-high strengths (i.e. approaching the theoretical limit), there would appear to be a need for systematic studies of flaw response at a fundamental level.

Accordingly, we survey here the results of some recent Vickers indentation studies on glass [4-6]. The original driving force for this work came from a pilot study on optical fibers [7], in which it was found that the strengths of specimens with indentations abruptly increased as the contact load diminished below some threshold. This threshold corresponded to a critical flaw configuration for crack initiation; the "pop-in" of radial cracks from the impression corners appeared to require the development of a sufficiently large precursor deformation zone [8,9]. Nevertheless, even though the subthreshold indentations were free of visible cracks, they still provided preferred sites for failure. It was therefore clear that the mechanics, if not the mechanisms, of failure were different at the subthreshold level. Thus, insofar as indentation flaws could be expected to simulate the broad features of natural flaws in glass fibers, the conclusion could be drawn that extrapolations from macroscopic to microscopic domains, as is implicit in most (statistically based) strength analyses, may well be

unjustified. The reported observation that the "apparent" crack velocity exponent evaluated from optical fiber fatigue data are distinctly lower (by about a factor of two) than the corresponding parameter obtained from large-scale fracture specimens [10-12] serves to reinforce this conviction.

Our presentation will be made in two major parts. First, we shall summarize the results of some recent observations made on the kinetics of radial crack initiation in soda-lime glass. It will be seen, from scanning electron micrographs of the indentations, that shear faults within the deformation zone act as the initiation precursors for the radial cracks. The threshold for pop-in is found to be highly sensitive to the contact period, and to the presence of water. Then, fatigue data on specimens indented at different loads, embracing the threshold, will be presented. These data are interpreted in terms of the initiation kinetics. The relevance of the interpretations to the mechanical behavior of optical fibers will remain an underlying motivation for the study.

INITIATION KINETICS OF INDENTATION CRACKS

Microscopy of Flaws

In this section we discuss what we know about the nature of indentation flaws near the threshold load, as revealed by direct microscopical observations. The broader features of the typical deformation/fracture pattern, shown schematically in Fig. 1 for the Vickers indentation geometry, are readily discerned by conventional optical techniques; the scale of the flaw at radial crack pop-in is generally of the order 10 μm for glass. It is this amenability to optical observation that has led to the relatively

advanced state of our understanding of flaw response in the postthreshold region, Ref. 1.

To understand the response in the subthreshold region, however, it becomes necessary to focus attention on events within rather than without the deformation zone. For this purpose one must go to higher resolution techniques, such as scanning electron microscopy. Figures 2 and 3 are appropriate micrographs of indentations in soda-lime glass. In the first of these figures we see two simple top views of the same, postthreshold indentation before and after etching in dilute hydrofluoric acid. The etching reveals the detailed structure of the hardness impression more clearly, although one must be careful here in drawing conclusions about the immediate post-indentation configuration; it is apparent from a comparison of Fig. 2(a) and (b) that the acid treatment has caused additional pop-in events to occur at the indentation corners, under the action of the residual stress field [13]. In Fig. 3 we see both top and side views (obtained by positioning the Vickers pyramid across a pre-existing hairline crack and then running this crack through the specimen [6]) of a subthreshold indentation. Again, there is evidence of considerable fine structure in the deformation zone, particularly in the subsurface section.

The features of greatest interest in the scanning electron micrographs are the well-defined "fault" traces on the free surface areas which define the irreversible deformation zone. These faults appear from their geometry to be shear-activated, much the same as classical dislocation slip processes in crystalline materials, although they operate at stress levels close to the theoretical limit of cohesive strength. One may conceive of the faulting configurations in terms of an intermittent "punching" mode, whereby catastrophic slip takes place at periodic intervals along shear stress

trajectories to accommodate the intense strains exerted by the penetrating indenter [6]. For further geometrical details of the fault patterns reference is made to the important papers by Hagan and Swain [14,15] on the subject.

The pertinent conclusions that we derive from the study of the micrographic evidence are as follows [6]:

(1) The freshly created fault walls tend to recontact due to strongly compressive normal stresses within the contact zone, and thence to heal at the interface. This healing is nevertheless incomplete, since the faults remain susceptible to preferential etching.

(2) Faults generated in different quadrants of the contact area can intersect to produce high stress intensifications (notwithstanding a certain ability for the faults to interpenetrate [15]), thus providing favorable sites for crack nucleation.

(3) The tendency for fault production to be intermittent (possibly due to the availability of suitable defect centers for the initial generation) leads to a certain variation in the geometrical disposition of the pattern from indentation to indentation (and even from quadrant to quadrant), thus giving rise to an element of scatter in the distribution of crack nuclei.

Kinetics of Crack Pop-in

It was indicated in the preceding subsection that optical techniques, although of insufficient resolution to observe the finer details of the precursor initiation processes, are usually adequate for observing the actual pop-in event itself. Here we describe the results of such observations made

AD-A133 746 EFFECT OF CONTACT DAMAGE ON THE STRENGTH OF CERAMIC MATERIALS(U) NATIONAL BUREAU OF STANDARDS WASHINGTON DC B R LAWN ET AL. OCT 83 N00014-81-F-0002 2/2

UNCLASSIFIED F/G 11/2 NL

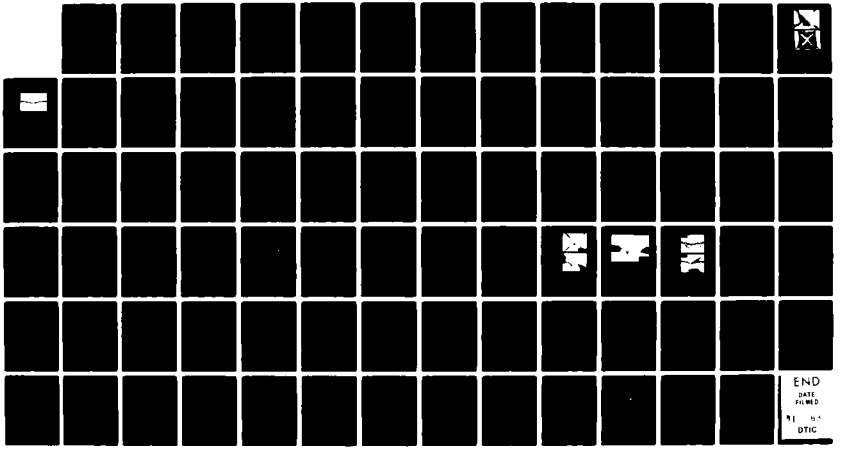

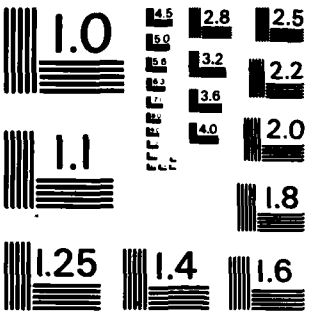

in situ through a microscope objective located immediately below the indentation site [6]. In our set-up a sinusoidal load-time pulse is applied to the Vickers indenter, and the time for radial pop-in, t_c, after the start of contact is recorded in relation to the indentation period, T. The functional interdependence of these two time variables then characterizes the kinetic response of the indentation flaws.

Typical results are shown in Fig. 4 for soda-lime glass tested in air at a prescribed maximum load, P. It is immediately clear that the threshold condition is rate-sensitive. At long contact periods pop-in occurs *during* the indentation cycle, specifically at a reproducible point 0.3 P on the unload half-cycle. At short contact periods, however, pop-in occurs *after* the contact, generally with extensive delays, $t_c >> T$, and with large scatter. These results show that the driving force for initiation is greatest while the indenter is under load, but is nevertheless far from insignificant in the residual field. One may interpret the transition from short-contact to long-contact behavior in terms of an *incubation* time for development of a critical nucleus from the shear fault configuration. This incubation time is found to diminish as the peak contact load or the water content of the environment increase [6], consistent with the general fatigue experience.

Observations of this type lead us to the following picture, based on the two-step process of precursor shear faulting and subsequent tensile crack pop-in, of initiation kinetics [6]:

(1) Newly formed shear faults become exposed to moisture in the environment, which penetrates into the interfaces and reduces the (already incomplete) cohesion. The penetration and decohesion mechanisms are both rate dependent, and therefore have the potential for controlling the kinetics. As

this stage progresses the stress intensifications at mutual fault intersection points increase, thereby building up the driving forces on the crack nuclei centers. It can be shown that the shear stress component responsible for activating the fault mechanisms reaches its maximum at the peak of indenter penetration, but remains in force, albeit at reduced intensity, after completion of the cycle, consistent with the observations in Fig. 4.

(2) The crack nuclei form close to the specimen surface, and are therefore similarly exposed to environmental moisture. Thus, unless the stress conditions are such that the nuclei propagate spontaneously to the fully-developed radial configuration, the system will be subject to slow crack growth. The normal stresses on such nuclei remain compressive through most of the indentation cycle, becoming tensile only at the 0.3 P unload point: if the incubation time has been exceeded by the time this point is reached the critical nucleus, released of its constraint, becomes free to propagate immediately; if not, the incubation process continues in the weakened, residual stress field, in which case the pop-in kinetics become subject to the variability in nucleation centers alluded to earlier.

According to this description, either of the two steps above could control the rate at which the critical stress intensification develops at the initiation center. Further work is needed to establish the relative importance of the shear fault and tensile crack concepts in the initiation kinetics.

FATIGUE OF GLASS WITH POSTTHRESHOLD AND SUBTHRESHOLD INDENTATION FLAWS

We now examine the results of dynamic fatigue studies of soda-lime glass containing postthreshold [4] and subthreshold [5] flaws. These studies were carried out using annealed rod specimens of 4 to 5 mm diameter, the surfaces of which had been pre-etched to remove large handling flaws and had been coated with protective lacquer over all but a central region ≈3 mm wide. Vickers indentations were placed in these uncoated test areas at prescribed peak loads, and were examined after 30 min to determine whether radial cracks had or had not popped in. The specimens were then stressed at constant rates in four-point flexure in water, with the indentation oriented for maximum tension, and their fatigue strengths duly recorded. In each case the broken specimens were checked to confirm that the failures had indeed originated from the indentation site; those that had not were omitted from the data accumulation.

Figure 5 shows the results for both postthreshold and subthreshold flaws, plotted in accordance with the "master map" scheme advocated in Ref. 1. We recall from this earlier source that, for indentations with well-developed cracks, the dynamic fatigue response for any given material may be represented by the expression

$$\sigma_f P^{1/3} = (\lambda_p' \dot{\sigma}_a P)^{1/(n'+1)} \qquad (1)$$

where P is the indentation load, $\dot{\sigma}_a$ is the stressing rate, σ_f is the strength, and n' and λ_p' are adjustable parameters. Both n' and λ_p' are load-independent, so plotting in the coordinates of Fig. 5 should reduce all the data to a universal curve, regardless of the scale of the flaws. It is clear that there

is a breakdown in this universality as one traverses the threshold into the low-load region:

(1) The strengths are substantially higher, by a factor 3 to 4, consistent with the earlier study on fibers [7].

(2) The scatter in data is wider, in correlation with the element of variability observed in the initiation kinetics (Fig. 4).

(3) The susceptibility to fatigue is stronger; cf. apparent crack velocity exponents $n' = 9.0 \pm 0.8$ for subthreshold and $n' = 14.0 \pm 0.3$ for postthreshold.

Equation (1) is derived on the basis of specific assumptions concerning the flaw configuration, notably that the critical crack extension occurs in the far field of the initiation zone [1], so it should not be altogether surprising that the subthreshold data plot onto a different curve in Fig. 5. The characteristics of the data in the two regions are nevertheless sufficiently diverse to suggest that we are dealing with two entirely different failure mechanisms, corresponding to a transition from propagation to initiation-controlled instabilities. In this context it may be noted that the inert strength level for postthreshold flaws lies below the fatigue strength for subthreshold flaws over a large portion of the stressing rate range; so that, when radial cracks do initiate during a fatigue test, failure must occur spontaneously from the precursor shear fault configuration.

It is useful to replot the data in Fig. 5 in a way which brings out the scale effect more clearly. This is done in Fig. 6. To obtain this plot we

have made use of the lifetime analog of Eq. (1) [1], i.e. substituting $\dot{\sigma}_a = \sigma_f/t_f$ and identifying σ_f with the constant applied stress σ_A, rearranged thus

$$t_f \sigma_A^{n'} = \lambda_p'/P^{(n'-2)/3} \qquad (2)$$

as an explicit function of load. Each point in Fig. 6 accordingly represents a composite evaluation of $t_f\sigma_A^{n'}$ from all data at a given P, taking the two regions separately but using n' from the postthreshold curve fit in Fig. 5 as an appropriate fatigue exponent. The rationale for this choice of a common exponent is that, as mentioned above, the derivation of Eqs. (1) and (2) is strictly based on the assumption that failure occurs from well-developed cracks. Thus, flaws which violate this assumption would be expected to show systematic departures from the baseline data curve, and this is indeed observed to be the case in Fig. 6. The solid line in this figure is equivalent to the prediction we would make using macroscopic crack laws (with due account of residual stress terms [1]); it is seen that such a prediction, extrapolated into the subthreshold domain, underestimates the lifetime at a fixed level of applied stress by several orders of magnitude.

It is useful to view the threshold phenomenon in Fig. 6 in terms of flaw size rather than indentation load. We have accordingly included a scale of the hardness impression $\underline{a}$ on the abscissa, using the hardness relation $H = P/2\underline{a}^2 = 5.5$ GPa for Vickers indentations on glass as the basis for conversion. In the present case the threshold occurs in the range $\underline{a} = 1$ to 10μm, although it needs to be remembered that this range can scale up or down, depending on the kinetic history of the flaw. The overlap between the subthreshold and postthreshold data is attributable to the variability in

the shear fault configurations discussed earlier. Thus it is conceivable that a particular flaw could be substantially smaller in its characteristic dimension than many of its possible competitors in a given specimen, and yet still control the strength properties by virtue of some uniquely favorable crack initiation conditions. Of course, the potential always remains in such instances for delayed pop-in from some of these larger flaw centers, with consequent degradation in the overall lifetime response.

IMPLICATIONS CONCERNING OPTICAL FIBERS

We conclude this discourse by examining the implications of the results on the fatigue properties of ultra-strong silica fibers. The data presented here were obtained on rod rather than fiber specimens, and on soda-lime rather than high-silica glass: although we have taken precautions to eliminate pre-existing handling flaws on our rod specimens, we can never be certain that the pristine surfaces of freshly drawn fibers would have responded in exactly the same way; and it is now well known that soda-lime and high-silica glasses differ significantly in their indentation behavior [16], the latter being regarded as "anomalous" in this respect. Nevertheless, it may be recalled that our very first observations of threshold effects in the strength behavior were on actual optical fibers [7], so we may feel justified in making certain predictions, if only of a qualitative nature.

One point that comes out clearly in the present work is the need to identify the flaw region which characterizes the operating stress range for a given component. Thus, if we wished to use the type of glass represented by the data in Figs. 5 and 6 as a structural material at ultra-high strengths, it would hardly be efficient to design on the basis of extrapolations from the

macroscopic crack region. (On the other hand such extrapolations, in this case at least, would suffice in applications calling for extreme conservatism in lifetime predictions.) These comments would appear to reinforce the conviction held by many, that, as far as practically possible, design evaluations should be made using data taken on surfaces which have the same finish as those to be placed in service and which embrace the required lifetime. This is particularly so when adopting empirical approaches to flaw characterization, especially those based on statistical distribution functions, where the underlying processes responsible for creating the flaws in the first place are disregarded.

The point just made about designing within the time range of the fatigue data bears further elaboration here, for, as we have seen, flaws can continue to evolve long after their inception. Accordingly, where it is necessary to make extended lifetime predictions from relatively short term fatigue data, the possibility exists for premature failures. Any amount of fatigue testing of control samples, or proof testing of actual components, will count for nothing if surfaces with subthreshold flaws are subsequently exposed to service environments conducive to crack initiation. There is some evidence from the optical fiber literature [17,18] that small-scale natural flaws can indeed suffer abrupt increases in severity with prolonged exposure to water, although in these cases direct observations of the flaws themselves could not be made to establish the nature of the transition. There would accordingly seem to be a strong case for advocating more controlled studies of fatigue failure in optical fibers, using flaws introduced by indentation or other artificial means, so that the fundamental lifetime-controlling processes might ultimately be identified and studied in a more systematic manner.

ACKNOWLEDGEMENTS

The authors gratefully acknowledge many useful discussions with R.F. Cook. Funding was provided by the U.S. Office of Naval Research (Metallurgy and Ceramics Program).

REFERENCES

[1] Cook, R.F. and Lawn, B.R., this volume.

[2] Lawn, B.R., Journal of the American Ceramic Society, in press.

[3] Jakus, K., Ritter, J.E., and Babinski, R.C., this volume.

[4] Dabbs, T.P., Lawn, B.R., and Kelly, P.L., Physics and Chemistry of Glasses, Vol. 23, 1982, pp. 58-66.

[5] Dabbs, T.P. and Lawn, B.R., ibid, pp. 93-97.

[6] Lawn, B.R., Dabbs, T.P., and Fairbanks, C.J., Journal of Materials Science, to be submitted.

[7] Dabbs, T.P., Marshall, D.B., and Lawn, B.R., Journal of the American Ceramic Society, Vol. 63, 1980, pp. 224-225.

[8] Lawn, B.R. and Evans, A.G., Journal of Materials Science, Vol. 12, 1977, pp. 2195-2199.

[9] Lawn, B.R. and Marshall, D.B., Journal of the American Ceramic Society, Vol. 62, 1979, pp. 347-350.

[10] Ritter, J.E. and Jakus, K., ibid, Vol. 60, 1977, p. 171.

[11] Kalish, D. and Tariyal, B.K., ibid, Vol. 61, 1978, pp. 518-523.

[12] Gulati, S.T., Helfinstine, J.D., Justice, B., McCartney, J.S., and Runyan, M.A., American Ceramic Society Bulletin,, Vol. 58, 1979, pp. 1115-1117.

[13] Dabbs, T.P. and Lawn, B.R., Journal of the American Ceramic Society, Vol. 65, 1982, pp. C37-C38.

[14] Hagan, J.T. and Swain, M.V., Journal of Physics D: Applied Physics, Vol. 11, 1978, pp. 2091-2102.

[15] Hagan, J.T., Journal of Materials Science, Vol. 15, 1980, pp. 1417-1424.

[16] Arora, A., Marshall, D.B., Lawn, B.R., and Swain, M.V., Journal of Non-Crystalline Solids, Vol. 31, 1979, pp. 415-428.

[17] Chandan, H.C. and Kalish, D., Journal of the American Ceramic Society, Vol. 65, 1982, pp. 171-173.

[18] Gupta, P.K., in Fracture Mechanics of Ceramics, R.C. Bradt, A.G. Evans, D.P.H. Hasselman and F.F. Lange, Eds., Plenum, New York, 1982.

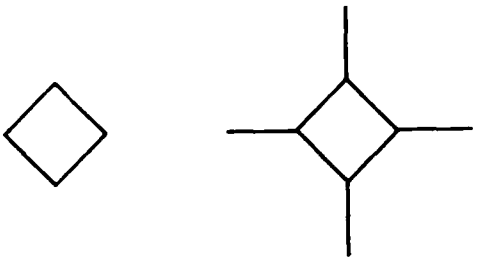

1. Schematic of Vickers indentation geometry. Cracks pop-in spontaneously at threshold to well-developed radial configuration.

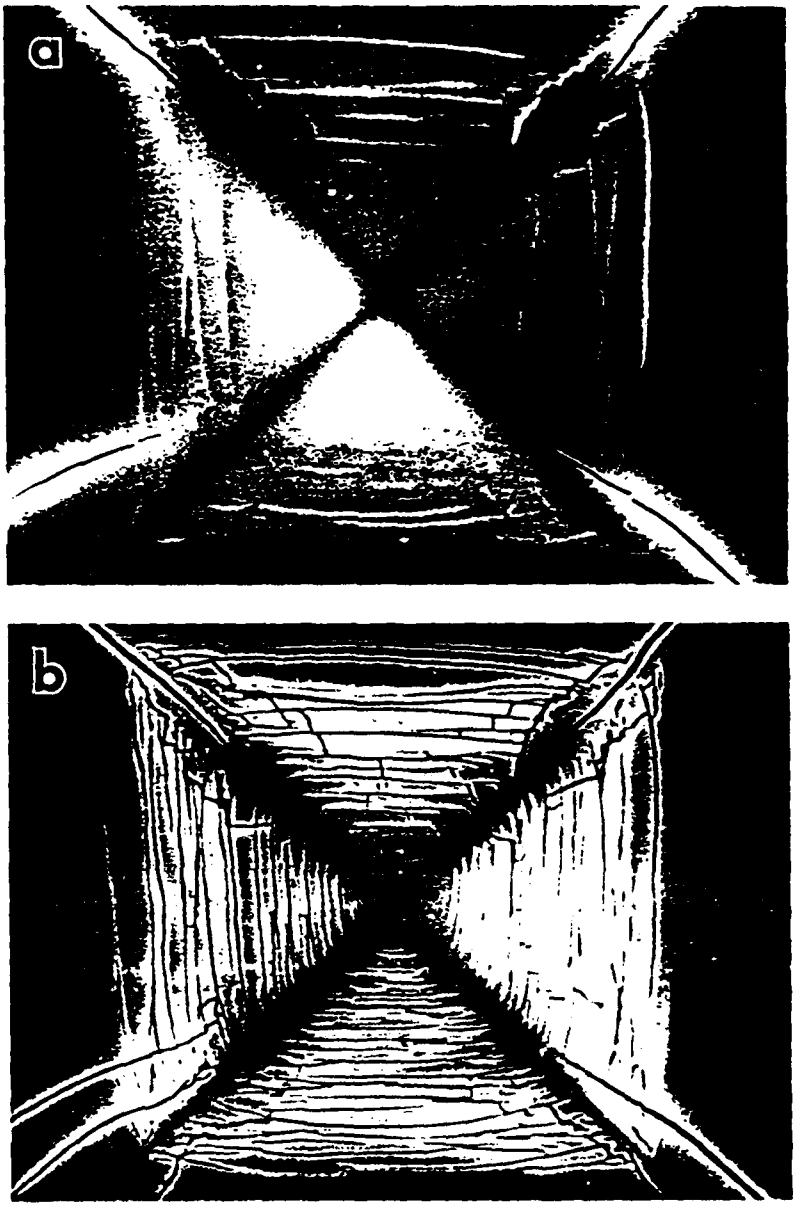

2. Scanning electron micrographs of Vickers indentation in soda-lime glass. Top views, (a) unetched and (b) etched. Indentation load 4 N, width of field 40 μm. Radial cracks initiate from shear fault structure in hardness zone.

3. Scanning electron micrograph of Vickers indentations in soda-lime glass. Simultaneous top and side view. Indentation load 1 N, width of field 25 μm. Shear faults are evident below hardness impression.

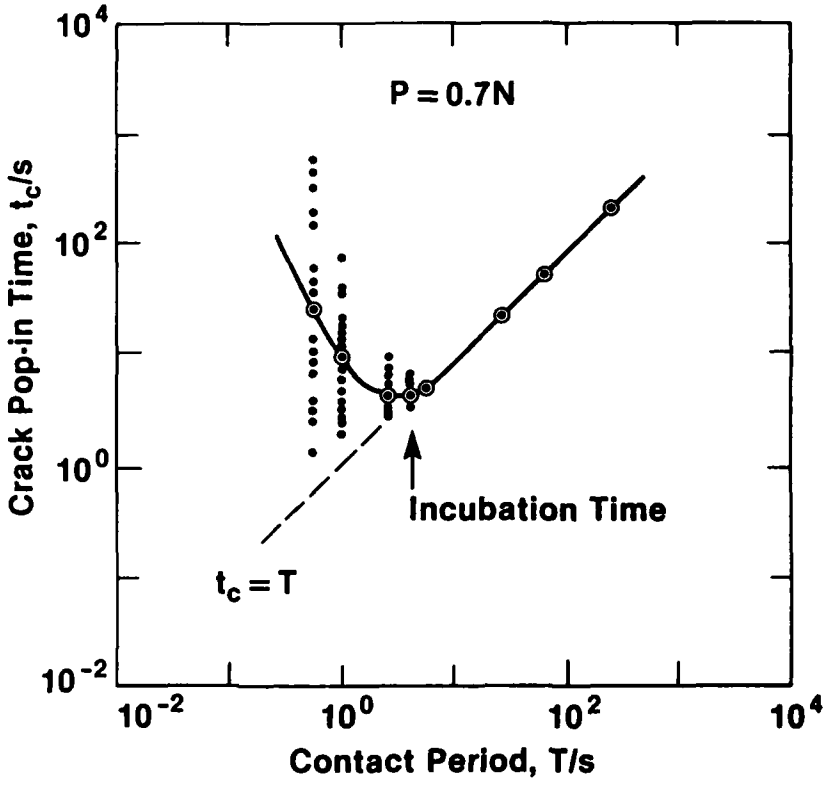

4. Time to fracture as function of contact period, for soda-lime glass in air. Open symbols denote median values at each prescribed contact period. Results indicate an incubation time for development of a critical crack nucleus.

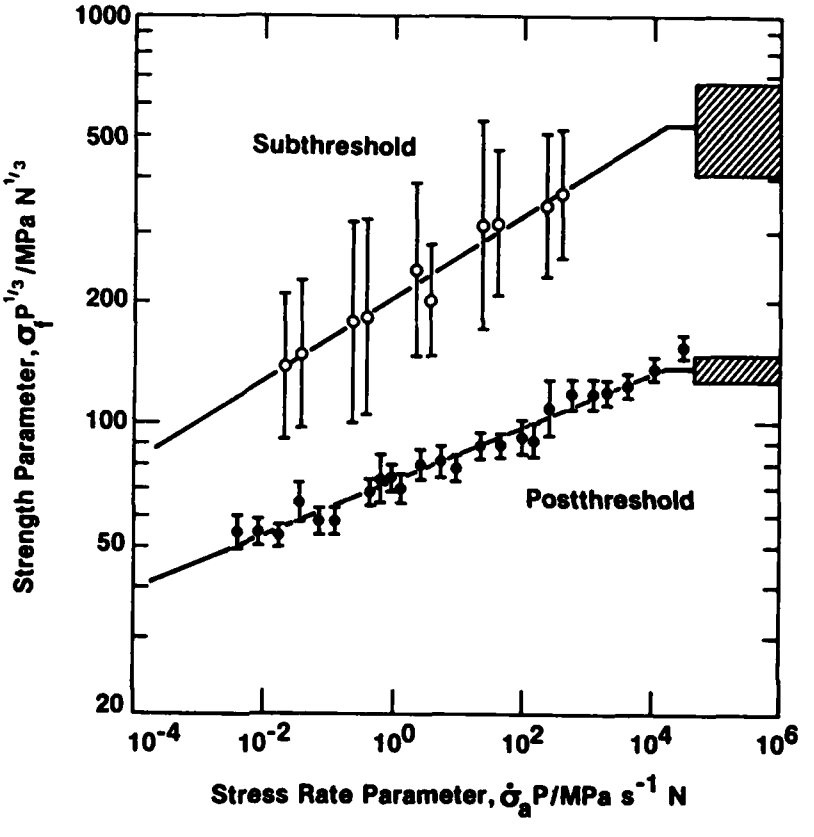

5. Reduced dynamic fatigue plot for soda-lime glass rods containing Vickers indentation flaws tested in water. Shaded bands indicate inert strength levels, error bars are standard deviations. Load range for postthreshold data 0.05 to 10 N (see Ref. 1), for subthreshold data 0.15 to 0.25 N.

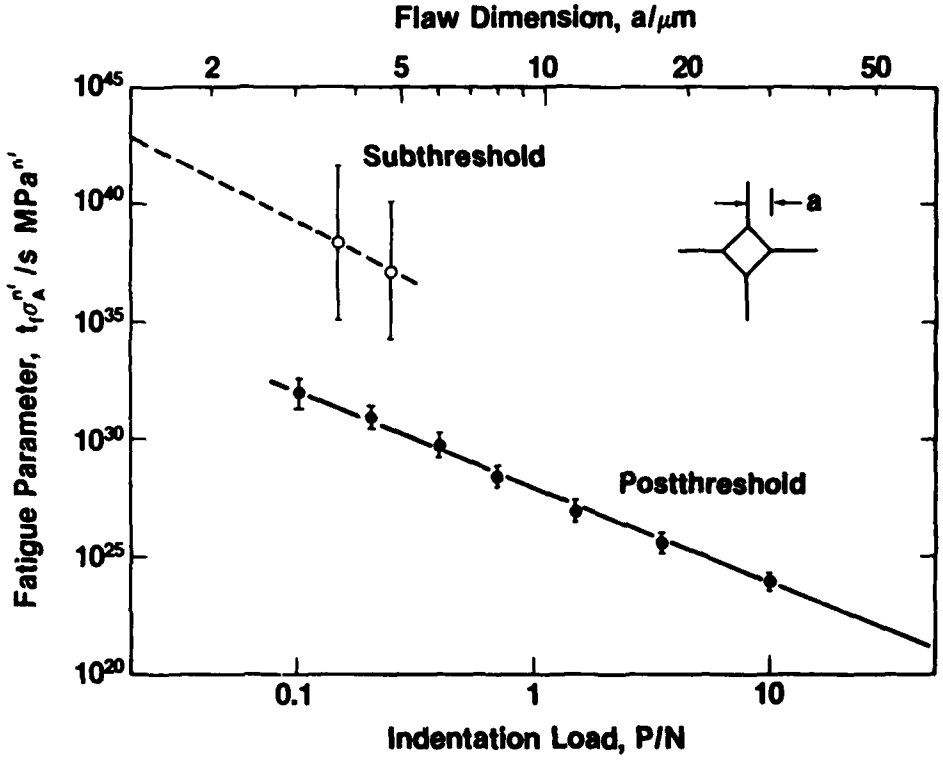

6. Fatigue data from Fig. 5, replotted to show load (or equivalent flaw size) dependence. Error bars are standard deviations.

KINETICS OF SHEAR-ACTIVATED INDENTATION CRACK INITIATION IN SODA-LIME GLASS

B. R. Lawn, T. P. Dabbs* and Carolyn J. Fairbanks

Center for Materials Science
National Bureau of Standards
Washington, DC 20234, USA

*On leave from University of New South Wales

ABSTRACT

The initiation of radial cracks in Vickers indentation of soda-lime glass is found to be strongly rate dependent. For long contact durations the radial cracks pop in during the indentation event, at a reproducible stage of the unloading half-cycle; for short contacts the pop-in occurs after the event, with considerable scatter in delay time. The phenomenon is interpreted in terms of an incubation time to develop a critical nucleus for the ensuing fracture. Increasing either the water content of the environment or the peak contact load diminishes the incubation time. Scanning electron microscopy of the indentation patterns indicates that the sources of the crack nuclei are constrained shear faults within the deformation zone. A qualitative model is developed in terms of a two-step process, precursor faulting followed by crack growth to pop-in instability. Moisture may influence both these steps, in the first by interfacial decohesion and in the second by slow crack growth. No definitive conclusion is reached as to which of the steps is rate-controlling, although it appears that it is the shear across the fault and not the tension across the crack which is vital in driving the initiation. The implications of these results in connection with the basic mechanical properties of brittle solids, particularly strength, are considered.

1. INTRODUCTION

The strength of brittle materials is controlled by the presence of small flaws.[1] It is generally asserted that such flaws are inevitable and ubiquitous, and that they have the characteristics of true microcracks. Structural design with glasses and ceramics has accordingly centered around the laws of crack propagation, the province of "fracture mechanics". However, there is growing evidence that below a threshold size the severity of flaws undergoes an abrupt decrease with an attendant shift in focus to the mechanics of crack initiation.[2-6] Whether these subthreshold flaws retain the essential character of microcracks (albeit within the stabilizing confines of a localized nucleation field) or whether some alternative precursor stress-concentrating process is involved is an issue which remains largely unanswered*.[7] Naturally occurring flaw centers are, by virtue of their small scale (typically $\approx\mu m$), difficult to locate and observe during their evolution to full-scale fracture.

It is in this context that indentation techniques are particularly useful.[8] Flaws can then be generated artificially, with complete control of shape, size and site. Moreover, such flaws bear a strong resemblance to those which develop in structural components from general surface handling, machining and polishing, and in-service particle impact. Insofar as crack initiation from indentation flaws is concerned there has been some revealing,

---

*Or, perhaps more accurately, unquestioned, particularly by those who use fracture-mechanics-based theories to analyze the strength properties of optical fibres.

if limited, progress in the development of a fundamental understanding. A theoretical model of crack "pop-in", based on the instability requirements of a critical nucleus within a highly inhomogeneous elastic/plastic contact field, was first presented by Lawn and Evans.[2] However, that model was somewhat phenomenological in that it made no attempt to specify the source of the nucleus, assuming only that such sources were freely available. Subsequent studies of the indentation fracture event identified the key role of irreversible processes in the contact field as a generator of the driving force for pop in,[9,10] consistent with the general observation that much of the crack formation occurs during unloading of the indenter. A closer investigation of precursor initiation micromechanisms was made in silicate glasses by Hagan and Swain and co-workers,[11-14] building on some earlier observations by Peter.[15] This work showed that the contact deformation zone beneath a Vickers or Knoop indenter consisted of well-defined, closely spaced shear faults, at least in glasses with a high content of network modifier, and that the cracks emanated either directly from the faults themselves or from points of intersection with neighbors.[14] The nature of the shear fault interface in terms of its structural properties remains obscure, although the fact that intrinsically strong glass test pieces can be made to fail from subthreshold indentation flaws at well below theoretical strength indicates that some of the original interfacial cohesion must have been lost.[4,16]

One aspect of indentation crack initiation which has received little attention to date is rate dependence. Rate effects have been shown to be extremely strong in general fracture and deformation properties of several brittle systems, most notably in silicate materials (both amorphous and crystalline) in the presence of water.[17-22] One of the most dramatic illustrations of a kinetic component in the crack initiation is to be found in

the "dynamic fatigue" response of glass test pieces with subthreshold flaws; the strengths in moist environments drop off more rapidly with decreasing stressing rate than for the corresponding flaws with well-developed cracks, notwithstanding the fact that these subthreshold strengths are greater in magnitude (typically by a factor 2 to 4 [4,16]) and are subject to much larger scatter.[16] Thus, quite apart from their bearing on the fundamental micromechanics of fracture initiation, rate processes would appear to be of some importance in determining the limits of practical strength, e.g. with optical fibres.

In this paper we investigate the kinetics of "radial" crack[8] initiation in Vickers-indented soda-lime glass in the presence of moist environments as a function of contact time. This is done with an experimental arrangement which allows for in-situ observation of the contact from below and for control of the load-time characteristics. Post-indentation examination in the scanning electron microscope is used to investigate fine details in the deformation and fracture patterns. It is concluded that the initiation event, although driven to its ultimate well-developed configuration by the tensile component of the indentation stress field, is controlled in its kinetics by a precursor, shear-activated process. This process appears to be one of stress intensification, either by interfacial decohesion or by conventional subcritical microcrack growth.

2. OBSERVATION OF CRACK POP-IN KINETICS

2.1 Experimental Procedure

Figure 1 shows the experimental setup, a somewhat simplified version of earlier indentation arrangements,[9,23] used in this study. As-received

soda-lime glass microscope slides were loaded from above using a standard Vickers hardness indenter. The indenter arm was driven by an electromagnetic coil via a function generator, and the corresponding load-time pulse P(t) monitored by a piezoelectric transducer.[24] In our tests the pulse had the form of a half-sine wave of height P_m and base width T, Fig. 2. A microscope facility enabled an observer to follow the contact event from below the glass slide at all times during and after the loading cycle.

By this means it was observed that the characteristic radial crack pop-in process was highly rate dependent. In particular, the time, t_c, to radial crack initiation was sensitive to the contact duration, T, for a fixed peak load and environment;[25] whereas for sufficiently large T pop-in occurred during the contact (specifically, during the unloading half-cycle), at small T it showed a tendency to prolonged post-contact delay. The radial crack pattern itself showed some variation from the ideal geometry depicted in Fig. 2; the four arms did not always pop-in simultaneously (in which case t_c was measured to appearance of the first arm), and nor did they always appear to emerge exactly from the indentation corners. The appearance of each arm was invariably abrupt, without any apparent precursor growth stage.

Test runs were made to determine the dependence $t_c(T)$, and the influence on this dependence of peak contact load and environmental moisture content. The latter test variable was controlled by simple means: laboratory air of relative humidity 50 ± 5% was taken as a standard environment; extremes of moisture were obtained on the one hand by placing a drop of distilled water on to the prospective indentation site and on the other by enclosing the entire indentation system within a nitrogen gas chamber (although no attempt was made here to ensure optimum "dryness"). The laboratory temperature for these runs was 22 ± 2 °C. Some miscellaneous tests were also run to examine the

potential effects of extraneous variables, such as surface stress in the glass and post-indentation heating, on delayed pop-in kinetics.

2.2 Results

The main results of the kinetic pop-in study are summarized in Figs. 3-5. Figure 3 shows results in detail for a typical test run, in this case in air at load P_m = 0.7 N. An average of 15 indentations was made at each of the preselected contact periods T. The plot indicates median values as well as individual points in order that the data trends be more clearly distinguishable where the scatter is high. It is immediately apparent that the initiation response differs significantly at opposite extremes of the contact time axis:

(i) At long times pop-in occurred reproducibly during the contact at an unload time $t_c \simeq 0.9$ T.

(ii) At short contact times pop-in occurred after indenter release at irregular, extended delay times $t_c >> T$.

The results shown in Fig. 3 suggest the existence of an incubation time for the development of a critical precursor crack nucleus. This incubation time may be defined (somewhat arbitrarily) as the point where the empirically fitted data curve crosses the line $t_c = T$. For contacts shorter than the incubation time the evolution toward a critical nucleus clearly continues after loading, but at a much reduced rate; that is, the component of the indentation stress which drives the nucleation persists in the residual field,

but at a significantly lower intensity than at the peak load configuration. The nucleation event has a stochastical element, as is evident from the scatter in results at small T; at large T attainment of a critical condition is guaranteed, and pop-in occurs spontaneously during indenter withdrawal due to release of some stress constraint.

Figure 4a shows the effect of different peak loads on the kinetics, again in air environment. Over the range of values covered, about one order of magnitude, the load influence does not appear to be strong. Effectively, the results in Fig. 4a may be represented, within the limits of data scatter, by some simple inverse relation between peak load and incubation time. Thus at small T an increased load gives rise to a corresponding reduced (average) pop-in delay. At large T the in-cycle pop-in time does not depend on load. This latter point is illustrated more clearly in the data replot of Fig. 4b, in which the time to fracture is normalized and expanded on to a more sensitive scale. The apparent existence of a load-invariant critical indentation configuration for well-developed nuclei at $t_c = (0.90\pm0.05)\ T$, corresponding to $P_c = (0.30\pm0.05)\ P_m$ on the unload half-cycle, indicates that radial crack propagation is controlled by some characteristic of the stress field, independent of the preceding kinetic formation processes.

The influence of environment is shown in Fig. 5, for a given load. It is immediately clear that the incubation time is highly sensitive to moisture content. Thus whereas the introduction of water has no measurable effect on the response at high T, consistent with the conclusions drawn from the results in Fig. 4, the pop-in time at low T is dramatically reduced.

The following simple tests were also run in an attempt to gain further clues as to the initiation mechanics:

(i) Some indentations which produced well-developed radial crack patterns on unloading were subjected to repeat loading pulses. On reloading, the radial cracks were observed to close up somewhat at the surface, and conversely to open up further beneath the surface (as observed by refocussing the microscope objective, Fig. 1). On reloading beyond the preceding critical unload point P_c the surface closure appeared to be effectively complete, indicating a highly compressive stress in this region.

(ii) Some tests were made on thermally tempered surfaces of a glass of similar composition to that used in obtaining the data for Figs. 3-5. Indentations at air at P_m = 0.7 N, cf. Fig. 3, produced no radial cracks at all within several hours of unloading. This demonstrates that biaxial surface compressions inhibit the initiation process.

(iii) A row of indentations was produced in air at P_m = 0.15 N such that, after an interval of several minutes, the fraction of radial cracks popped in remained small (<< 0.5). After immersing the freshly indented specimen into water at 50 °C for about one minute, crack patterns were observed to have developed at all indentations.

3. SCANNING ELECTRON MICROSCOPY

3.1 Survey of the Technique

Although perfectly adequate for determining the critical pop-in points for radial fracture, optical microscopy proved limited as a means of observing

fine details in the precursor deformation process. Scanning electron microscopy (SEM) was accordingly used to examine indentation sites after the event. The observations were of two types: first, of surfaces simply indented with a Vickers pyramid at prescribed loads in air for a fixed contact period ≈10 s; second, of sections through similar indentations, obtained by positioning the Vickers pyramid at points along a preexisting hairline crack, Fig. 6.[11-15] Examples of the former type are shown in Figs. 7 and 8, and of the latter in Fig. 9.

Many of the important features of the indentation patterns revealed by the micrographs have been discussed at length elsewhere;[14] we simply summarize these features here, placing emphasis on those which bear on the initiation phenomenon. The radial cracks apparently initiate from within the deformation zone (as do subsurface lateral cracks[26]). Within the deformation zone well-defined displacement faults are evident by virtue of the stepped traces they leave on the specimen free surfaces; these traces, approximately parallel to the impression edges in top view and curved below the contact center in side view, correspond closely to maximum shear trajectory surfaces.[11] The shear faults appear to be "ideally narrow",i.e. they do not form as slip bands characteristic of dislocation multiplication processes in metals. They can intersect with neighbors, generally on near-orthogonal trajectories, sometimes producing kinks in the subsurface traces, indicating some degree of continuity across the fault interface. These intersections can give rise to local stress intensifications, as evidenced by the formation of cavities there at higher contact loads.[14]

3.2 Key Features of the Indentation Patterns

The features we would emphasize as pertinent to the initiation process are as follows:

(i) The normal stresses which act across the shear faults are predominantly compressive. Evidence for this is seen in Figs. 7 and 8. In both these micrographs the radial cracks have wide residual openings outside the deformation zone but close up tightly within the inner regions of the zone. Fig. 8 is particularly interesting in this regard, for the contact appears to have "welded" together opposite faces of the preexisting fissure. This evidence reinforces the notion of structural "continuity" across the faults and suggests, moreover, that the compressive stresses must induce significant interfacial cohesion.

(ii) Notwithstanding this predominance of compression within the deformation zone the faults appear to open up slightly, notably at the top surface where some biaxial "stretching" of the upper layers must have occurred to accommodate the increased area of the impression. Such surface openings are enhanced in the sectioned specimens, Fig. 9 (cf. Fig. 7), indicative of surface relaxation effects associated with the sectioning process itself. Thus the shear faults remain planes of weakness in the material, so the cohesion referred to in (i) above must be somewhat less than that representative of the bulk strength.

(iii) The major faults appear to be separated by a characteristic spacing, in this case of order 1 μm, but this spacing is subject to considerable variability. Accordingly, no two indentations, even when produced under ostensibly identical test conditions, produce precisely the same fault pattern; indeed, as is apparent from Fig. 7a the pattern can differ significantly in adjacent quadrants of the same impression.

(iv) The faults are constrained in their sideways expansion on the surface at the indentation diagonals (where the direction of shear strain must change abruptly to accommodate the pyramidal geometry of the indenter) and, to a lesser extent, in their downward extension by mutual intersections (interpenetration becoming increasingly difficult as kinks form[14]). Hence the scale of the critical fault is effectively determined by that of the hardness impression (notwithstanding the variability factor discussed in (iii) above).

(v) The radial cracks appear to generate from the shear faults, but, because such cracks inevitably expand toward the center of indentation (even if only slightly, due to the high compressive stresses within the deformation zone) as well as away from it, the origins themselves are difficult to locate. In many cases there is evidence of more than one initiation attempt at any indentation corner; in the detail surface view of Fig. 7b, for instance, small crack segments approximately parallel to the impression diagonal are seen to run from near the ends of some of the inner faults, only to be arrested at the (weak) interfaces of surrounding neighbors. Thus initiation would seem to originate at or close to the surface extremity of an outer fault where the constraint is high and the potential for obstruction by neighbors is low. This conclusion suggests a certain independence of nucleation centers in

adjacent quadrants, consistent with the fact that radial cracks can occasionally be made to pop-in on both sides of an indentation corner, as in the upper right of Fig. 7a (although the relaxation effect of the first pop-in will more often than not be sufficient to suppress its potential competitor), and with the earlier observation (Sect. 2.1) that the four arms of the radial pattern do not usually form simultaneously.

(vi) As the peak indentation load diminishes into the subthreshold region the scale of the contact reduces to a level comparable with the characteristic fault spacing. Yet the surface impression remains well formed and smooth,[27] suggesting that the faulting mechanism probably continues to operate continually between major slip events, albeit at a much reduced level of severity.

4. CRACK INITIATION MODEL

In this section we seek to establish a qualitative model for the radial pop-in process, consistent with the preceding experimental observations. In particular, we concern ourselves with an explanation of the incubation time, along with its dependence on moisture, stress state, etc. The model is developed in two parts, shear-activated faulting followed by tension-activated crack pop-in.

4.1 Formation of Shear Faults

The contact of a sharp-pointed indenter on a material surface produces a highly concentrated stress field. In the absence of nonlinear, irreversible deformation processes this field would be singular at the contact point. In

characteristically "plastic" materials (e.g. most metals) stress relief occurs readily by the operation of dislocation multiplicative processes (or by some alternative plasticity process, such as twinning). Such dislocations usually generate at low friction levels and penetrate deep into the material, thereby accommodating the large downward displacements at the contact surface over relatively expansive slip distances. In "brittle" materials, however, low-stress regenerative processes of this kind do not operate at ordinary temperatures, and relatively high stress levels, approaching the limits of intrinsic cohesive strength, are needed to drive stress-relieving processes. In this latter case the deformation is more catastrophic in nature across the fault plane, although it is still driven predominantly by the shear component of the contact field. A distinguishing feature of such high-stress modes is the strong localization of the deformation zone about the surface impression, intensified by the geometrical constraints referred to in Sect. 3.2. Shear strain levels are accordingly severe in this class of materials and the tendency to elastic recovery in the impression depth is strong.[28]

The slip process envisaged here for soda-lime glass is one of high-stress, intermittent shear failure along well-defined fault surfaces. As the indenter penetrates, faults are "punched" into the underlying material in the manner of Fig. 10. Minor slippage probably occurs on a much finer scale than the spacing of traces observed in the SEM observations; we have already alluded to this in our previous mention of the smooth surface impression at subthreshold loading (Sect. 3.2), and there is some more direct supportive evidence from high resolution observations of closely-spaced ($<< 1$ μm), shallow, penny-like "shear defects" at low-load Knoop indentations in diamond using transmission electron microscopy.[29] These surface-localized shear

defects cannot in themselves accommodate the buildup of surface displacement at the contact interface so, at some catastrophic point, a major fault develops into the material. Some stress release must accompany the development of any such fault, which subsequently becomes encompassed within the expanding deformation zone. The stress level is then able to build up again, thereby allowing the process to repeat itself.

It was argued in Sect. 3.2 that compressive stresses within the deformation zone must induce some cohesion across the fault interfaces. In this context we may note that Wiederhorn and Townsend[30] showed that tensile crack interfaces in soda-lime glass can heal spontaneously, with strength recoveries ≈80% in shock loading and ≈20% in static loading, the difference in the two cases reflecting the fact that the entry of atmospheric water molecules and the ensuing saturation of primary bonds are rate limited. We might expect a shear fault which develops catastrophically and which sustains intense closure tractions in the way envisaged above to rebond at least as strongly as rapidly loaded tensile cracks. However, the degree of healing will depend on other factors as well, not least the topography of the interfacial walls;[31] for walls in sliding contact this topography is likely to be far from smooth on the molecular scale. Hence the newly formed deformation faults represent planes of substantially recovered structural integrity, yet, at the same time, of potential weakness in the glass.

Taking the analogy with tensile cracks one step further, it can be argued that any entry of water into the shear fault interfaces should cause substantial decohesion, replacing silanol bridging bonds by weak hydrogen bonds. As far as environmental access is concerned it is well known from the literature on grain boundaries in crystalline materials that high energy defect planes can provide rapid diffusion pathways.[32] The kinetics of this

precursor stage in the overall crack initiation process then arise from the rate dependencies of the sequential diffusion and interaction processes. It is interesting to note that Kranich and Scholze[33] arrived at a similar conclusion in their interpretation of the observed time dependence of hardness in glass[22,24]; their discussion centered on a water-induced "softening" effect, in which hydrolytic weakening acts to suppress recovery of indentation diagonals during unloading. Two important characteristic features may thus be associated with our fault model: first, since external water must diffuse into the interfaces via the top surface (where, it will be recalled, there is a tendency to a slight opening), the decohesion depth will be limited, especially at the faster contact rates; second, since it is the shear component of the stress field which creates the fault in the first place, the decohesion of the restored interfacial bonds is presumably also shear-activated.

4.2 Initiation of Radial Cracks

The initiation of a radial crack occurs when a favorably disposed shear fault within the contact field reaches a critical stress intensification. There would appear to be two distinctive ways in which this intensification might be achieved. The first is by classical subcritical growth of a microcrack.[34] In this interpretation it is acknowledged that the microcrack can originate from the edge of a shear fault; however, the kinetics of the pop-in event are essentially due to moisture-enhanced "slow" growth in some tensile region of the field (although this growth could conceivably, at least at its inception, involve some "mixed mode", i.e. combined shear plus tension). The second is by interfacial debonding of the shear faults themselves, as discussed in Sect. 4.1. Again, it is taken that fracture will

originate from the faults, but this time the fault edges are constrained; it is now the shear-activated decohesion process which is rate controlling. The distinction here is not trivial, for the basic rate equations could conceivably have entirely different forms in the two cases, and it is such basic equations which must ultimately provide the starting point for any proper theory of fatigue in the subthreshold region.

At this point it is useful to recall the major features of the kinetic observations that our crack initiation model will need to explain. First, it is necessary to account for the roles of the two test variables, water concentration and indentation load, on the incubation time. Then we should be able to show why at long contact periods the pop-in time is reproducible and insensitive to the test variables and, conversely, why at short contact periods it is not. Again, our model should indicate why the rate of radial crack development <u>after</u> indentation is lower than that <u>during</u> indentation at any given load, and why this rate tends to diminish further as the contact period is decreased.

Consider these points in relation to Fig. 11. This schematic representation, drawn from the SEM observations, shows a fault FF developing from one of its ends into a radial crack FC. The fault is driven by the shear stress SS and the crack by the normal stress NN. A complete evaluation of these two stress terms over the respective planes at any given stage of the indentation cycle is a complex task requiring, among other things, explicit knowledge of the constitutive laws for the deformed material and facility for incorporating details of the contact geometry.[8] Nevertheless, by recognizing that the general indentation field may be subdivided into reversible and irreversible components,[9] simplistic elastic/plastic analyses may be used to determine some of the broader features.[10] Accordingly, Fig. 12 indicates how

the level of the two pertinent stress terms at the contact surface may vary through the cycle. The shear SS, which must be determined largely by the indenter angle (Fig. 10), reaches a maximum value at full loading; on removing the indenter elastic recovery occurs in the penetration depth,[28] effectively reducing the contact angle, thereby leaving a residual stress of diminished magnitude but of same sign acting on the fault. The normal stress NN has a slightly more subtle evolution, owing to the fact that the reversible and irreversible components oppose each other:[10] at full loading the elastic component dominates, and because this term is compressive in the surface region* the net stress is also compressive; on unloading the indenter only the inelastic component remains, and so the normal residual stress is tensile. Thus there is a "crossover point" in the unloading where the driving force on the radial crack plane abruptly becomes positive; this feature is consistent with the observation (Sect. 2.2) that well-developed radial cracks tend to close up at their surface on reloading the indenter beyond the preceding critical unload point (in our case at $P_c = 0.3\ P_m$).

The question now is, are the kinetics controlled by a subcritical stage of the crack growth along FC or by fault decohesion at FF in Fig. 11? Let us attempt to analyze the experimental evidence in terms of these two possibilities:

---

*In the subsurface region beneath the indenter this same component is tensile, the implications of which we shall pursue in the Discussion.

(i) Test variables; role of water and contact load. We have already indicated that both crack growth[17,19] and fault decohesion[33] (Sect. 4.1) are sensitive to water in the external environment. In each case there is a two-step process, diffusion followed by interaction, the rates of which increase in some simple proportion with chemical activity. On the face of it, therefore, both potential models would appear to account for the curve shifts in Fig. 5 to shorter times with increasing moisture content.

A similar conclusion may be drawn concerning the contact load. The main effect of increasing P_m is to increase the fault size, without changing the intensity or geometrical distribution of stresses over the fault surface (similitude principle).[2,10] The stress intensification in turn is expected to increase with fault size, but only modestly (fractional power)[34], for any given diffusion or interaction conditions. This is again consistent with the slow data trends to shorter times at higher loads in Fig. 4.

Hence as far as the basic chemical and stress effects are concerned there is little to distinguish between the two candidate models in accounting for qualitative variations in incubation times.

(ii) Effect of contact period on incubation time. For contact periods T greater than the pop-in time t_c the critical nucleus, whatever its nature, has developed beyond the configuration at which unstable fracture must occur spontaneously in tensile loading. It is evident from Fig. 12 that such spontaneous fracture cannot occur at peak loading, for there the pertinent normal stresses are compressive; the indenter has to be unloaded to $\simeq 0.3\ P_m$ before tensile driving forces may be realized. In this time region, therefore, the pop-in event is determined predominantly by the stress field characteristics (more specifically, by its constraint characteristics), so the

kinetics of the nucleation event itself are not manifest in the data, provided there is always a sufficient density of faults to guarantee a suitable nucleation center.

At $T << t_c$ the development of a critical nucleus is clearly completed after the indentation cycle. It is now the residual components of stress which drive the initiation. As seen from Fig. 12 a positive driving force for fracture exists throughout the post-indentation period, so pop-in occurs immediately the precursor nucleus becomes critical. In this domain, therefore, the kinetics of the nucleation event itself and the variables which control this event are reflected directly in the data. Any factors which militate against exact reproducibility of events from indentation to indentation will likewise reflect in the data scatter. In this regard the variability of the fault patterns noted in the SEM observations (Sect. 3.2) is pertinent, particularly in mind of the notoriously high gradients of stresses (from which the overall crack driving force must ultimately be determined) which characterize the near fields in general contact problems.[8]

Again, it is not clear that any qualitative distinction can be made between models in explaining the transition from in-cycle to post-cycle crack initiation as the contact period diminishes; any rate-limiting process consistent with the dependence on water content and contact load as discussed in (i) above would seem to be capable of accounting for incubation phenomena of this kind.

(iii) Pop-in rate; effect of different stress component, contact period and temperature. We may note from Fig. 3 that, for given environmental and loading conditions, there is an intermediate range of contact periods within which initiation occurs with comparable frequencies during and after the

contact. In the latter case, however, the pop-in time is relatively long, i.e. $t_c >> T$. This implies that the development of a critical nucleus continues after indenter removal, but at a reduced rate relative to that at full load. Reference once more to Fig. 12 indicates that the stress component responsible for providing the initiation driving force must be the shear SS rather than the tension NN, for the latter increases on unloading. Unfortunately, this still does not help us in distinguishing between the models, for both the growth of a microcrack from the fault edge and the decohesion of the fault itself would tend generally to diminish in velocity upon reducing the shear intensification. Of course, the microcrack mechanism would tend also to rise in velocity under the simultaneous action of the increasing tensile loading; whether this tensile component of driving force should be sufficient to dominate the shear contribution, in which case the microcrack hypothesis would no longer comply with experimental observation, can only be answered by a quantitative analysis.

We further recall from Fig. 3 that the time to pop-in tends to increase as the contact period is systematically reduced below the incubation period. This observation is consistent with the argument presented in the preceding paragraph; reducing T is equivalent to reducing the time interval in which the nucleus grows at its fastest velocity.

The fact that immersion of air-indented specimens into hot water rapidly accelerates the pop-in rate (Sect. 2.2) serves to indicate that the appropriate rate-controlling process is thermally activated, as expected for general interfacial diffusion and reaction processes.

5. DISCUSSION

We have presented evidence for strong kinetic effects in the threshold for radial fracture. In particular, we have shown that there exists an incubation time for crack pop-in, and that this time is reduced as the moisture content or peak contact load is increased. We have also presented SEM micrographs which demonstrate the role of shear faults in the precursor initiation process. Two possible models have been considered in our attempts to account for the observations, one based on the notion of microcrack expansion from the edge of a critical fault and the other on the progressive decohesion of the fault interface itself. Both models involve a two-step, diffusion-interaction sequence. Our qualitative interpretations of the data have not allowed us to distinguish between the two models, although it has been established that the vital component of the stress field in driving the initiation is the shear across the precursor fault and not the tension across the ultimate crack.

These results, despite their lack of conclusiveness, are useful in the way they highlight the rapidly changing nature of strength-controlling flaws in the subthreshold region. The emphasis shifts from classical crack extension to deformation fault energetics. On entering the realm of ultra-small scale flaws, therefore, one may need to adopt an entirely new physical base for analyzing such flaw-related properties as strength, wear and erosion, grinding and polishing, etc.[3] For this reason alone it would appear reasonable to advocate more quantitative treatments of the two models discussed above, along with a broader experimental investigation into extraneous variables, in an attempt to obtain definitive answers. Studies of other materials, including "anomalous" glasses,[12] which tend to deform by

densification rather than by slip processes, and crystalline materials, which tend to slip on restricted crystallographic planes, could prove valuable, if only to establish the generality of the phenomenon.

Of the flaw-related properties mentioned above, strength is perhaps the one which has been studied most systematically in relation to the subthreshold transition[4,16]. The most distinctive feature on undergoing this transition from the domain of well-developed cracks is an abrupt increase in the strength level, demonstrating that the subthreshold flaw is not nearly as potent as its postthreshold counterpart as a source of degradation. Nevertheless, the former flaw type does still provide preferred sites for failure in glass surfaces of otherwise pristine condition (e.g. optical fibres), emphasizing the significantly weakened structure of the shear fault interface. The mode of failure envisaged here is one of augmentation of the residual shear stress on the fault by the applied tensile loading, Fig. 13. This augmentation may occur in either of two ways: directly, by enhancing the shear stress itself; or indirectly, by negating the compressive stress. The abrupt strength increase referred to above arises because one now has to initiate the radial crack before any propagation instability can be attained, and to effect initiation the applied loading has first to compensate for the relaxation of shear driving force that occurs during the preceding contact evolution. The fact that the spontaneous pop-in rate is severely retarded in tempered glass (Sect. 2.2) is in line with this description; the surface compression acts in the opposite direction, diminishing the stress intensification rather than enhancing it.

There are two other distinguishing features of the strength properties for subthreshold flaws which bear comment here.[16] The first is the relatively large scatter in results obtained under ostensibly invariant indentation test

conditions. Such scatter is consistent with that observed in the delayed pop-in data in Fig. 3, associated with the variability in the fault patterns as noted in the SEM studies. What causes this variability in the first place is a question that we cannot answer without a deeper understanding of the fault micromechanics, including, presumably, information on the nature and distribution of the underlying slip nucleation centers. The second of the additional features which accompanies the subthreshold transition is the enhanced susceptibility to "fatigue", as reflected in a steeper slope in standard logarithmic strength vs stress rate plots. An increased susceptibility of this kind could be due to a change in failure mechanism, i.e. fault decohesion. However, it is also possible to explain the trend in terms of the microcrack hypothesis; the presence of a strong residual-contact component in the fracture driving force can lead to significant increases in "apparent" crack velocity exponents.[35] Again, quantitative modelling of the candidate processes would seem to be called for.

Throughout our presentation we have been working on the premise that the radial cracks initiate at or close to the indentation surface. The normal stresses on the crack plane become tensile at the surface only after substantial withdrawal of the indenter; in the subsurface regions, however, these same stresses are tensile at <u>all</u> stages of the contact cycle.[10] Thus at higher indentation loads we might expect the stress intensity for initiation to be exceeded during the first half-cycle, with an attendant switch from surface (radial) to subsurface (median) crack formation.[10,26] Such behavioral changes in the geometrical aspects of indentation fracture have indeed been observed.[11,36] The main influence of kinetic effects in this dichotomy is in the radial fracture threshold; the surface regions do of course have direct access to the environment and are accordingly more susceptible to the

rate-sensitive hydrolytic weakening. In this way estimates of the lower limits to indentation-induced pop-in based strictly on equilibrium concepts[2,34,37] could be in serious error, on the nonconservative side in the context of strength design.

Finally, a comment may be made concerning the nature of the shear fault interfaces as envisaged in this study. The major shear displacements take place catastrophically, close to the level of cohesive strength, without dislocation regenerative processes. The resulting net configuration is nevertheless one which might be represented, mathematically at least, by a pile-up of dislocations. Is such a configuration more accurately defined as a slip surface or a shear crack? In ceramics and glasses with intrinsically strong bonding characteristics the distinction between deformation and fracture processes may not always be as clear cut as it is for materials with well-defined yield stresses.

ACKNOWLEDGEMENTS

The authors wish to thank R. F. Cook, E. R. Fuller, B. J. Hockey, D. B. Marshall, R. S. Polvani, M. V. Swain, and R. M. Thomson for many stimulating discussions during this study. R. F. Cook also performed the delayed hot water tests referred to in Sect. 2.2, and R. S. Polvani set up parts of the hardness testing apparatus. Funding was provided by the U.S. Office of Naval Research, Metallurgy and Ceramics Program.

REFERENCES

1. B. R. LAWN and T. R. WILSHAW, "Fracture of Brittle Solids" (Cambridge University Press, London, 1975) Chs. 1 and 2.
2. B. R. LAWN and A. G. EVANS, J. Mater. Sci. 12 (1977) 2195.
3. B. R. LAWN and D. B. MARSHALL, J. Amer. Ceram. Soc. 62 (1979) 347.
4. T. P. DABBS, D. B. MARSHALL and B. R. LAWN, J. Amer. Ceram. Soc. 63 (1980) 224.
5. T. P. DABBS and B. R. LAWN, Comm. Amer. Ceram. Soc. 65 (1982) C-37.
6. D. J. GREEN, in "Fracture Mechanics of Ceramics", edited by R. C. Bradt, A.G. Evans, D. P. H. Hasselman and F. F. Lange (Plenum Press, New York, 1982).
7. B. R. LAWN, J. Amer. Ceram. Soc., in press.
8. B. R. LAWN and T. R. WILSHAW, J. Mater. Sci. 10 (1975) 1049.
9. D. B. MARSHALL and B. R. LAWN, J. Mater. Sci. 14 (1979) 2001.
10. B. R. LAWN, A. G. EVANS and D. B. MARSHALL, J. Amer. Ceram. Soc. 63 (1980) 574.
11. J. T. HAGAN and M. V. SWAIN, J. Phys. D: Appl. Phys. 11 (1978) 2091.
12. A. ARORA, D. B. MARSHALL, B. R. LAWN and M. V. SWAIN, J. Non-Cryst. Solids 31 (1979) 415.
13. J. T. HAGAN, J. Mater. Sci. 14 (1979) 462.
14. J. T. HAGAN, J. Mater. Sci. 15 (1980) 1417.
15. K. PETER, J. Non-Cryst. Solids 5 (1970) 103.
16. T. P. DABBS and B. R. LAWN, Phys. Chem. Glasses 23 (1982) 93.
17. S. M. WIEDERHORN, J. Amer. Ceram. Soc. 50 (1967) 407.
18. S. M. WIEDERHORN and L. H. BOLZ, J. Amer. Ceram. Soc. 53 (1970) 543.
19. D. T. GRIGGS and J. D. BLACIC, Science 147 (1965) 292.
20. D. T. GRIGGS, Geophys. J. R. Astr. Soc. 14 (1967) 19.

21. C. H. SCHOLZ and R. J. MARTIN, J. Amer. Ceram. Soc. 54 (1971) 474.

22. S. P. GUNASEKERA and D. G. HOLLOWAY, Phys. Chem. Glasses 14 (1973) 45.

23. V. R. HOWES, Glass Tech. 15 (1974) 148.

24. C. J. FAIRBANKS, R. S. POLVANI, S. M. WIEDERHORN, B. J. HOCKEY and B. R. LAWN, J. Mater. Sci. Letters 1 (1982) 391.

25. M. WADA, H. FURUKAWA and K. FUJITA, in Proc. 10th Int. Congr. Glass (Ceramic Soc. of Japan, Tokyo, 1974) Vol 11, p. 39.

26. B. R. LAWN and M. V. SWAIN, J. Mater. Sci. 10 (1975) 113.

27. T. P. DABBS and B. R. LAWN, to be published.

28. B. R. LAWN and V. R. HOWES, J. Mater. Sci. 16 (1981) 2745.

29. P. HUMBLE and R. H. J. HANNINK, Nature 273 (1978) 37.

30. S. M. WIEDERHORN and P. R. TOWNSEND, J. Amer. Ceram. Soc. 53 (1970) 486.

31. B. J. HOCKEY and B. R. LAWN, J. Mater. Sci. 10 (1975) 1275.

32. P. G. SHEWMON, "Diffusion in Solids" (McGraw-Hill, New York, 1963) Ch. 6.

33. J. F. KRANICH and H. SCHOLZE, Glastechn. Ber. 49 (1976) 135.

34. S. S. CHIANG, D. B. MARSHALL and A. G. EVANS, J. Appl. Phys. 53 (1982) 312.

35. E. R. FULLER, B. R. LAWN and R. F. COOK, J. Amer. Ceram. Soc., in press.

36. H. ISHIKAWA and N. SHINKAI, Comm. Amer. Ceram. Soc. 65 (1982) C-124.

37. J. T. HAGAN, J. Mater. Sci. 14 (1979) 2975.

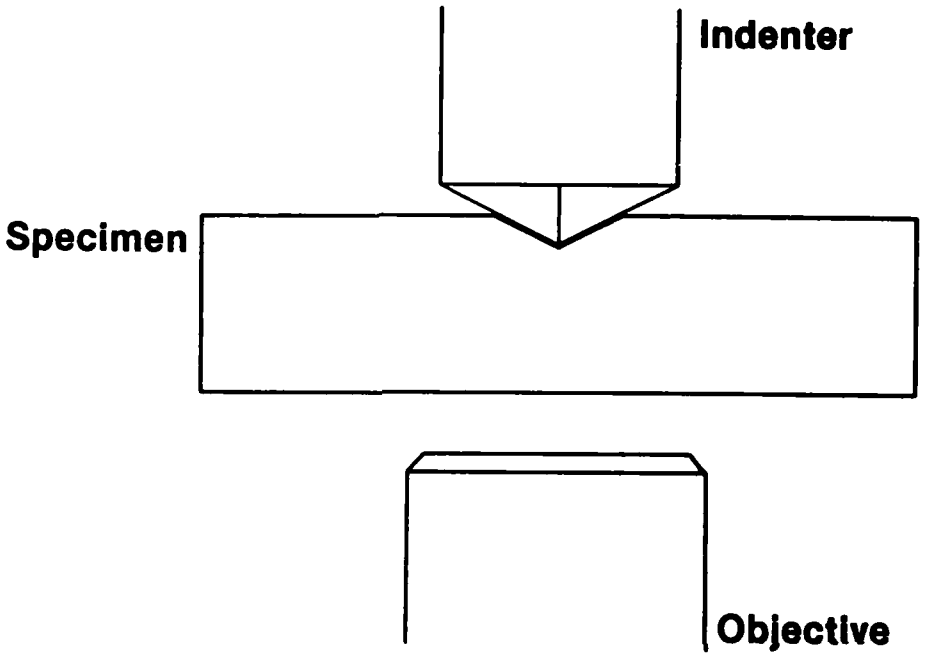

1. Schematic of setup for viewing Vickers indentation in soda-lime glass.

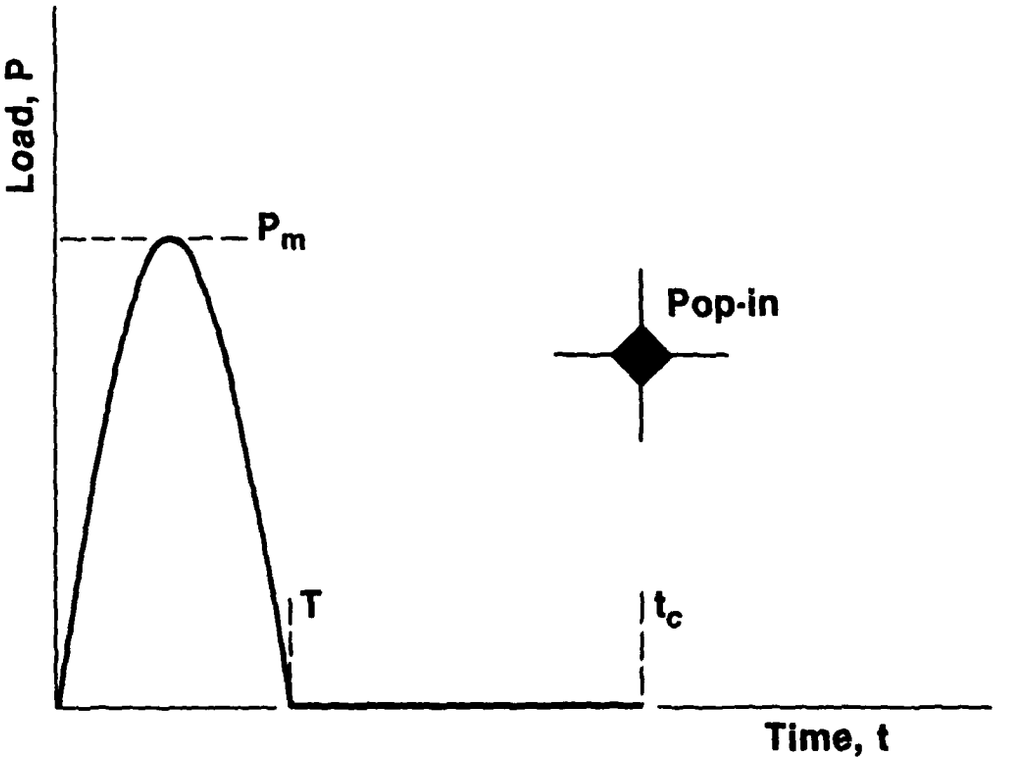

2. Indentation load pulse parameters. Experiment measures time to radial crack pop-in, t_c, as function of contact period, T, at fixed peak load, P_m.

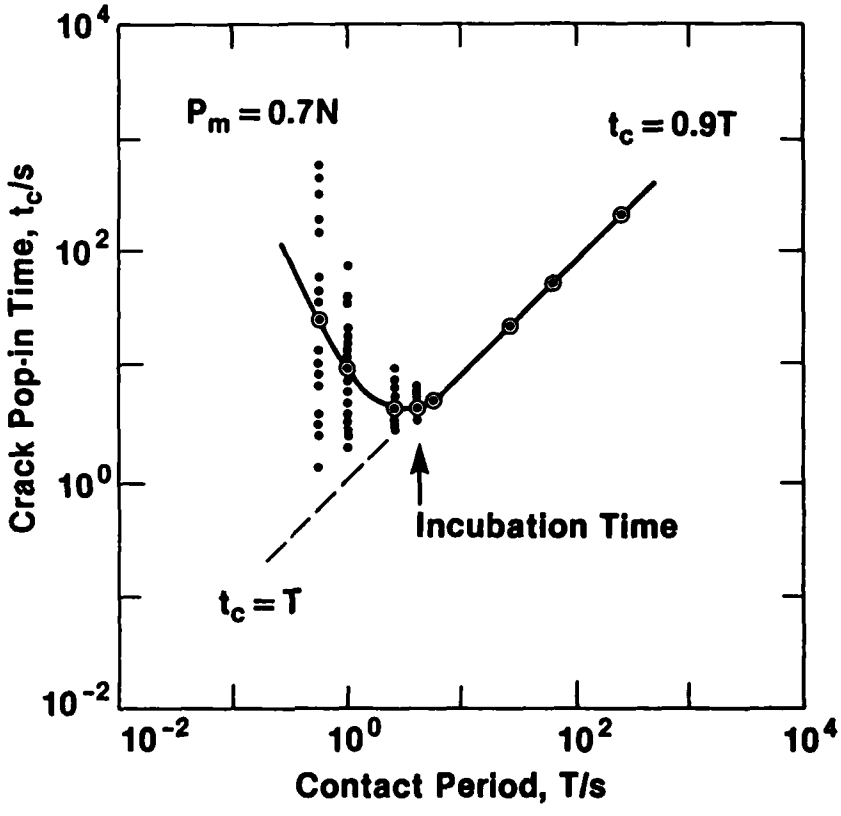

3. Time to fracture as function of contact period, for soda-lime glass in air at fixed indentation load. Open symbols denote median values at each prescribed contact period. Data suggest an incubation time for development of a critical crack nucleus.

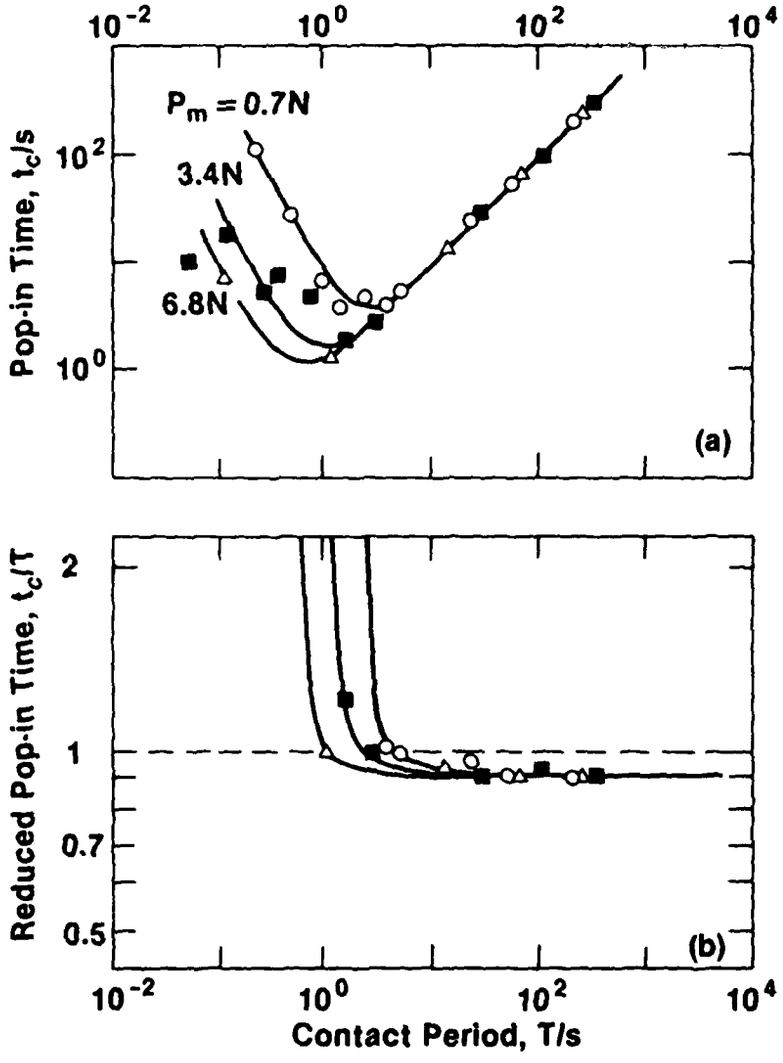

4. Time to fracture as function of contact period, for soda-lime glass in air at three indentation loads. Only median values of pop-in times are plotted. Plot (b) is a replotted version of (a), demonstrating more sensitively the tendency to an equilibrium pop-in condition at longer contact periods.

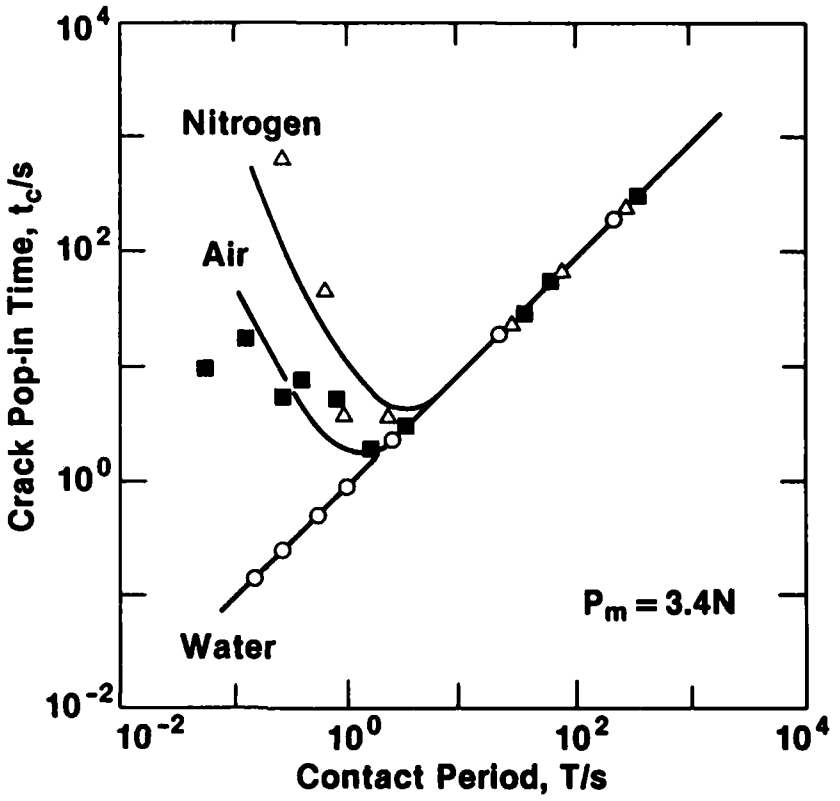

5. Time to fracture as function of contact period, for soda-lime glass at fixed indentation load in three environments. Only median values of pop-in times are plotted.

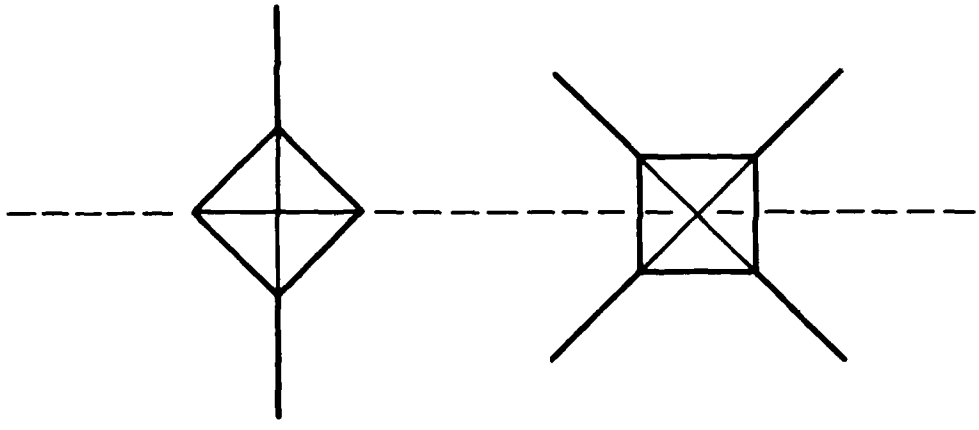

6. Schematic of two indentation orientations at preexisting crack (dashed line) for obtaining section views.

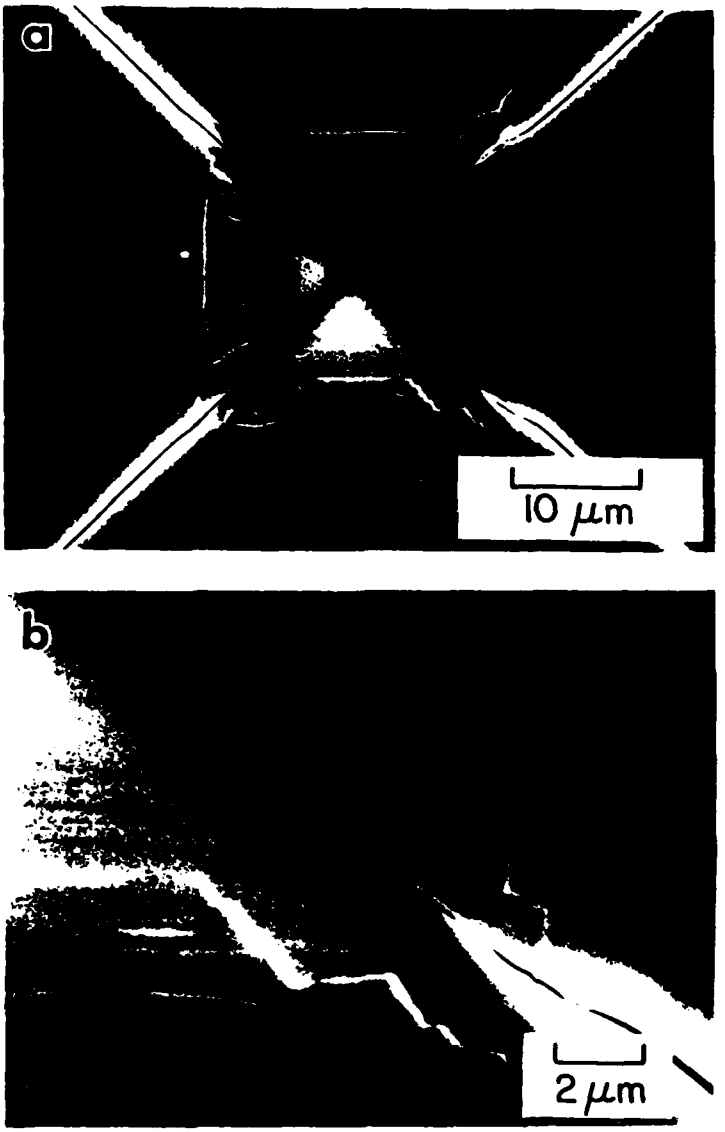

7. **Scanning electron micrograph of Vickers indentation in soda-lime glass. Surface view.** Indentation load P_m = 4.0 N. **Micrograph (b) is an enlarged detail of right lower impression corner region in (a).**

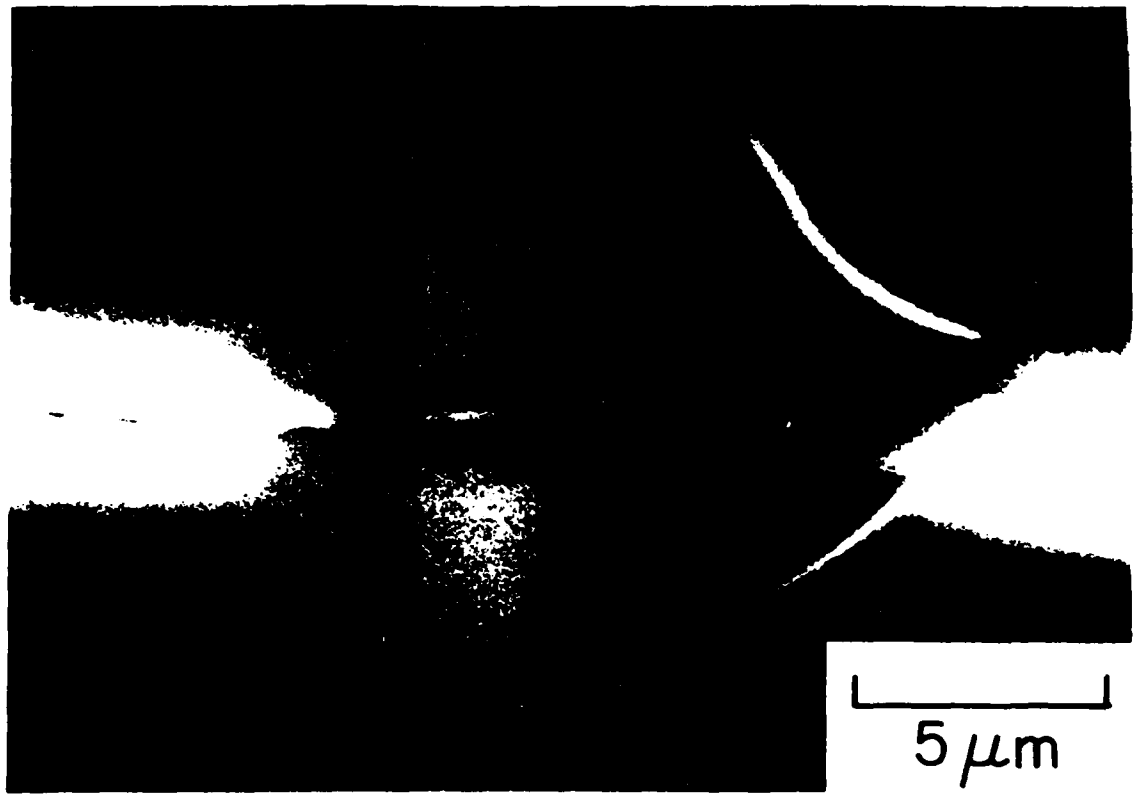

8. Scanning electron micrograph of Vickers indentation across preexisting crack in soda-lime glass. Surface view. Indentation load P_m = 1.0 N. Note apparent "welding" of pre-crack interface within compressive deformation zone.

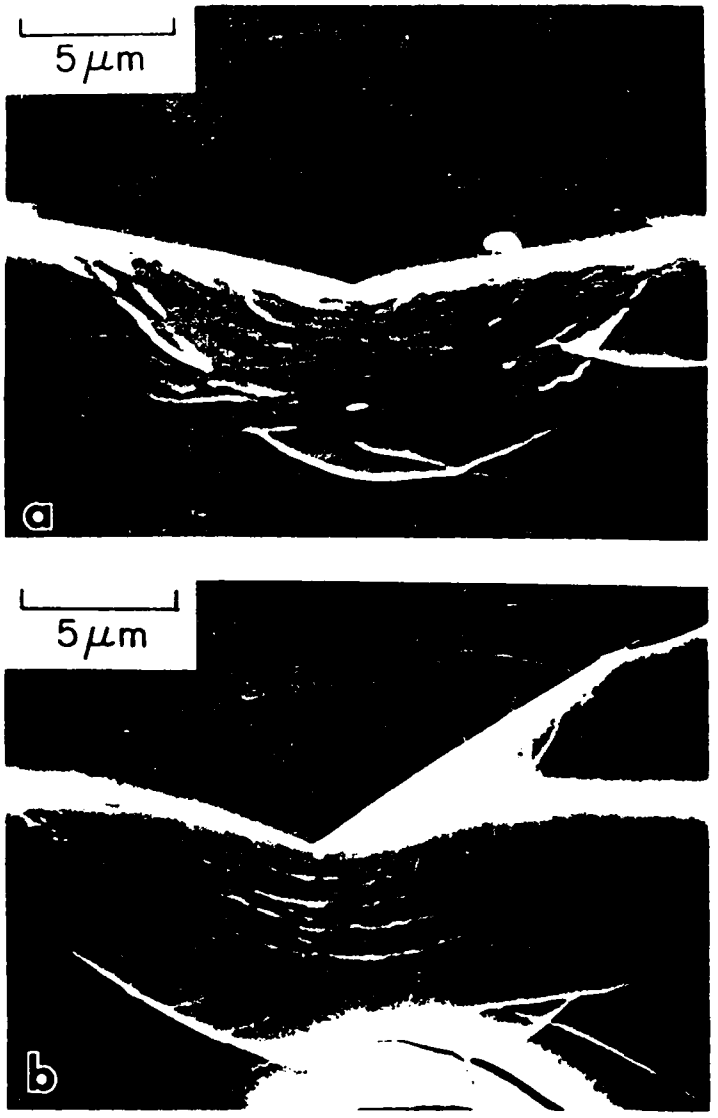

9. Scanning electron micrograph of Vickers indentation in soda-lime glass. Surface plus section view: (a) 90° orientation, (b) 45° orientation. Indentation load P_m = 2.0 N.

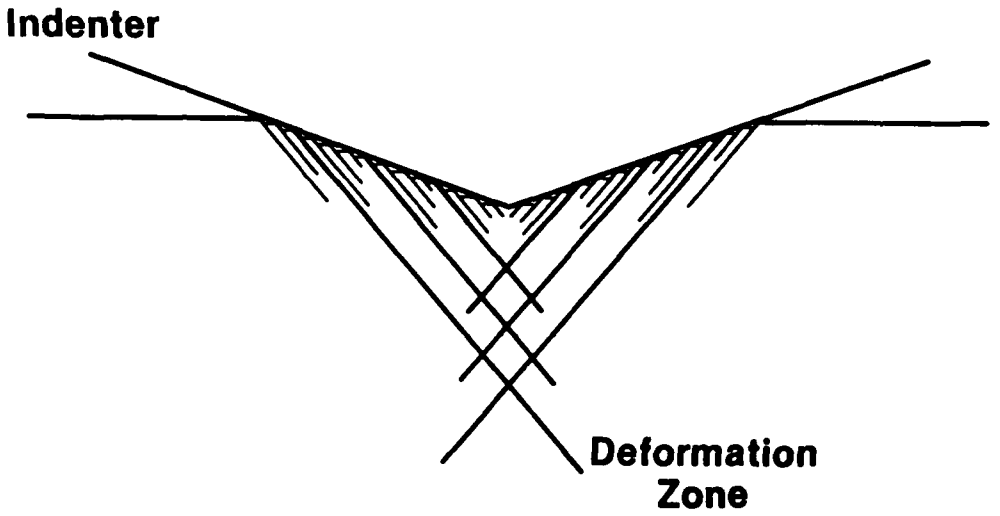

10. Model of fault formation beneath Vickers pyramid, showing how shear displacements accommodate the penetrating indenter. Minor slip is shown occurring between major faults.

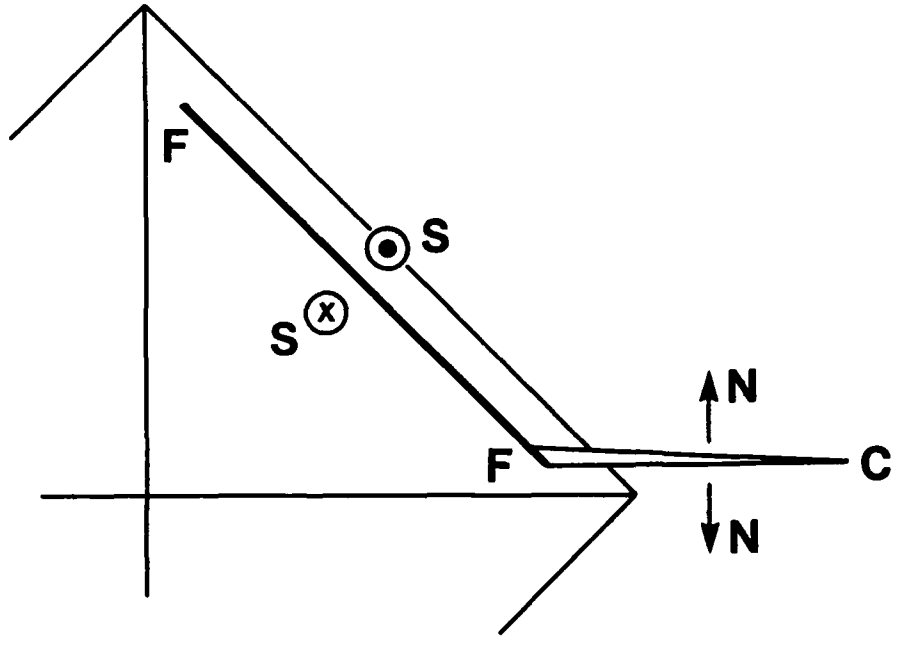

11. Model of radial crack initiation FC from fault FF, in one quadrant of Vickers impression. Shear SS and normal NN stresses provide driving forces for fault and crack respectively.

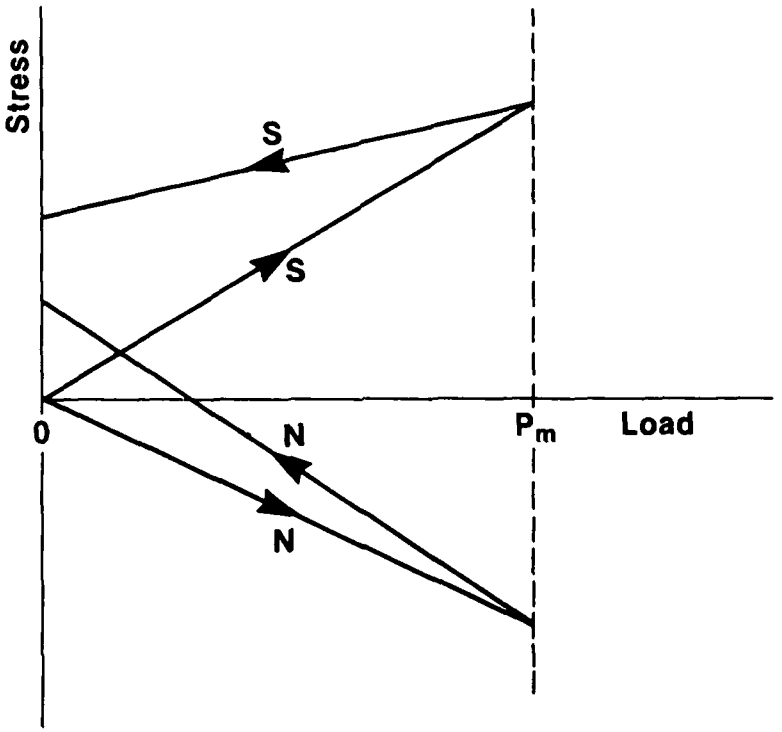

12. Intensity variation of shear SS and normal NN stresses (Fig. 11) through indentation cycle. Whereas during the unloading half-cycle SS simply reduces in magnitude to residual level, NN actually reverses sign, at $P \approx 0.3\ P_m$, enroute to its ultimate tensile state.

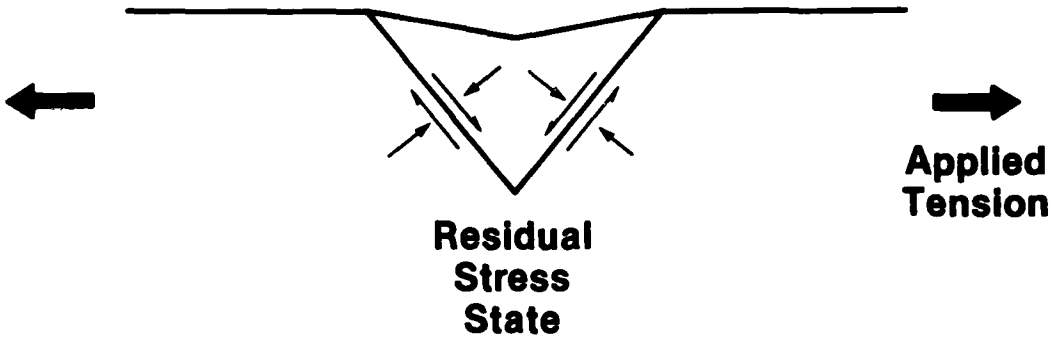

13. Schematic showing augmentation of residual stress configuration at indentation fault by applied tensile field. The tensile load may be resolved into components at the fault plane which reinforce the residual shear and negate the residual compression.

UNIVERSAL FATIGUE CURVES FOR CERAMICS USING INDENTATION FLAWS

H. Multhopp, R.F. Cook,* B.R. Lawn

Center for Materials Science, National Bureau of Standards,
Washington, DC 20234

*On leave from the University of New South Wales

In a recent series of papers[1-6] a methodology has been developed, using controlled indentation flaws, for evaluating crack velocity parameters from fatigue* strength data. The initial work,[1,2] on glass, established the fracture mechanics basis of the approach from which these evaluations could be made, with emphasis on the exceptional degree of accuracy attainable. An attempt was subsequently made to generalize the fracture mechanics formulation, taking into account the residual contact stresses about the flaws, by numerical integration of the fatigue differential equations.[3] The validity of the ensuing solutions was then tested on a glass ceramic in a case study.[4] Following this, a systematic investigation was made of the role of flaw size in the failure mechanics, once more using glass as a model test material.[5] It was thereby shown that data over an extensive range of indentation loads could be conveniently reduced onto a "universal fatigue curve" for each material. The scheme for the data reduction was analogous to that originally proposed by Mould and Southwick[7], except that now the plotting parameters could be related explicitly to intrinsic material properties. Finally, a more complete theoretical analysis of the underlying fatigue equations, following the realization that solutions could be derived in closed form, was presented as a basis for placing the procedure on a more rigorous footing.[6]

In the present paper we indicate how the universal fatigue curves may be used to make comparative evaluations of different ceramic materials. Evaluations of this kind are often difficult to make, owing to the

---

*The term "fatigue" here referring to the time dependence of strength as function of applied stress or stressing rate.

variability in natural flaw distributions. We illustrate the approach by considering results for two ceramics of technological importance, alumina* and silicon carbide**, in relation to the glass ceramic*** data reported earlier[4].

Accordingly, controlled-flaw fatigue tests were run as follows.[4] Specimens were prepared as bars with polished surfaces for 4-point flexure. Each bar was indented at the center of its prospective tensile face with a Vickers pyramid so as to generate a "well-developed" radial crack pattern. The indentation loads chosen were 20 N for the glass ceramic, 10 N for the silicon carbide, and 20, 10 and 5 N for the alumina; this use of more than one load in the last case was simply to provide a self-consistent check of the universal plotting scheme. The fatigue tests were run in water at specified stressing rates; inert strengths for baseline reference were similarly run in dry nitrogen or silicone oil. Simple beam theory was used to calculate the maximum tensile stress in each specimen from the breaking load.****

---

* AD 96, Coors Porcelain Co., nominal grain size 10 μm.

** NC 203, Norton Co., grain size 4 μm.

*** Pyroceram C9606, Corning Glass Co., grain size 1 μm.

**** For the alumina bars, which were received in thin substrate form, it was necessary to include a specimen thickness correction term in the strength evaluation. This correction never exceeded 6%.

The measured strengths, σ_f, are plotted as a function of stressing rates, $\dot{\sigma}_a$, in Fig. 1, with indentation load, P, incorporated into the coordinates in accordance with the universal fatigue relation for controlled flaws,[5]

$$\sigma_f P^{1/3} = (\lambda_P' \dot{\sigma}_a)^{1/(n'+1)} \quad . \tag{1}$$

Here n' and λ_P' are load-independent parameters for a given material/environment system, obtainable from slope and intercept on the logarithmic plot. Each data point in this figure represents the mean and standard deviation of 5 to 15 tests at each specified value of $\dot{\sigma}_a P$. The solid lines are least-squares fits to the data for each material, and the shaded bands are appropriate inert strength levels.

Figure 1 has immediate value as a graphic indicator of relative material properties. Thus, for any given combination of flaw severity (characterized here by P) and time dependence in the applied stressing (characterized by $\dot{\sigma}_a$), it is clear that silicon carbide, followed by alumina, has the superior strength properties. From a more quantitative standpoint, it can be shown[6] that the slope and intercept parameters in Eq. (1) relate explicitly, via a set of "transformation equations", to the exponent and coefficient in a power-law crack velocity function. Likewise, the height of the inert strength plateau relates to the material toughness.[8] Accordingly, the universal plotting scheme contains all the information for complete characterization of both the kinetic and the equilibrium fracture responses for ceramic systems. A more extensive treatment of this kind of characterization will be presented elsewhere.[9]

Another feature which is evident in Fig. 1 is the relative degree of scatter in the data for the three materials. This scatter trend appears to correlate with grain size (see earlier footnote). For alumina, the material with the greatest variability, microstructural influences were readily apparent as disruptions to the ideal radial crack geometry.[10] Such complications, while clearly not conducive to optimal accuracy in fracture parameter evaluations, may nevertheless take us one step closer to the configurations of naturally occurring flaws, thereby giving us added confidence in applying results from controlled indentation tests to real materials.

ACKNOWLEDGEMENTS

The authors are grateful to A.C. Gonzalez and S.W. Freiman for helpful discussions in connection with this work. Funding was provided by the U.S. Office of Naval Research, Metallurgy and Ceramics Program.

REFERENCES

1. B. R. Lawn and D.B. Marshall, J. Amer. Ceram. Soc. 63 (1980) 532.
2. P. Chantikul, B. R. Lawn and D. B. Marshall, ibid. 64 (1981) 322.
3. B. R. Lawn, D. B. Marshall, G. R. Anstis and T. P. Dabbs, J. Mater. Sci. 16 (1981) 2846.
4. R. F. Cook, B. R. Lawn and G. R. Anstis, ibid. 17 (1982) 1108.
5. T. P. Dabbs, B. R. Lawn and P. L. Kelly, Phys. and Chem. Glasses 23 (1982) 58.
6. E. R. Fuller, B. R. Lawn and R. F. Cook, J. Amer. Ceram. Soc., in press.
7. R. E. Mould and R. D. Southwick, ibid. 42 (1959) 542, 582.
8. P. Chantikul, G. R. Anstis, B. R. Lawn and D. B. Marshall, ibid. 64 (1981) 539.
9. R. F. Cook and B. R. Lawn, *Proceedings of Symposium on* "Methods for Assessing the Structural Reliability of Brittle Materials", Edited by S. W. Freiman (A.S.T.M. Special Technical Publication), in press.
10. A. C. Gonzalez, H. Multhopp, R. F. Cook, B. R. Lawn and S. W. Freiman, ibid.

FIGURE CAPTIONS

1. Universal fatigue curves for three ceramics, tested in water. Vickers indentation loads P = 5 N (circles), 10 N (squares) and 20 N (triangles).

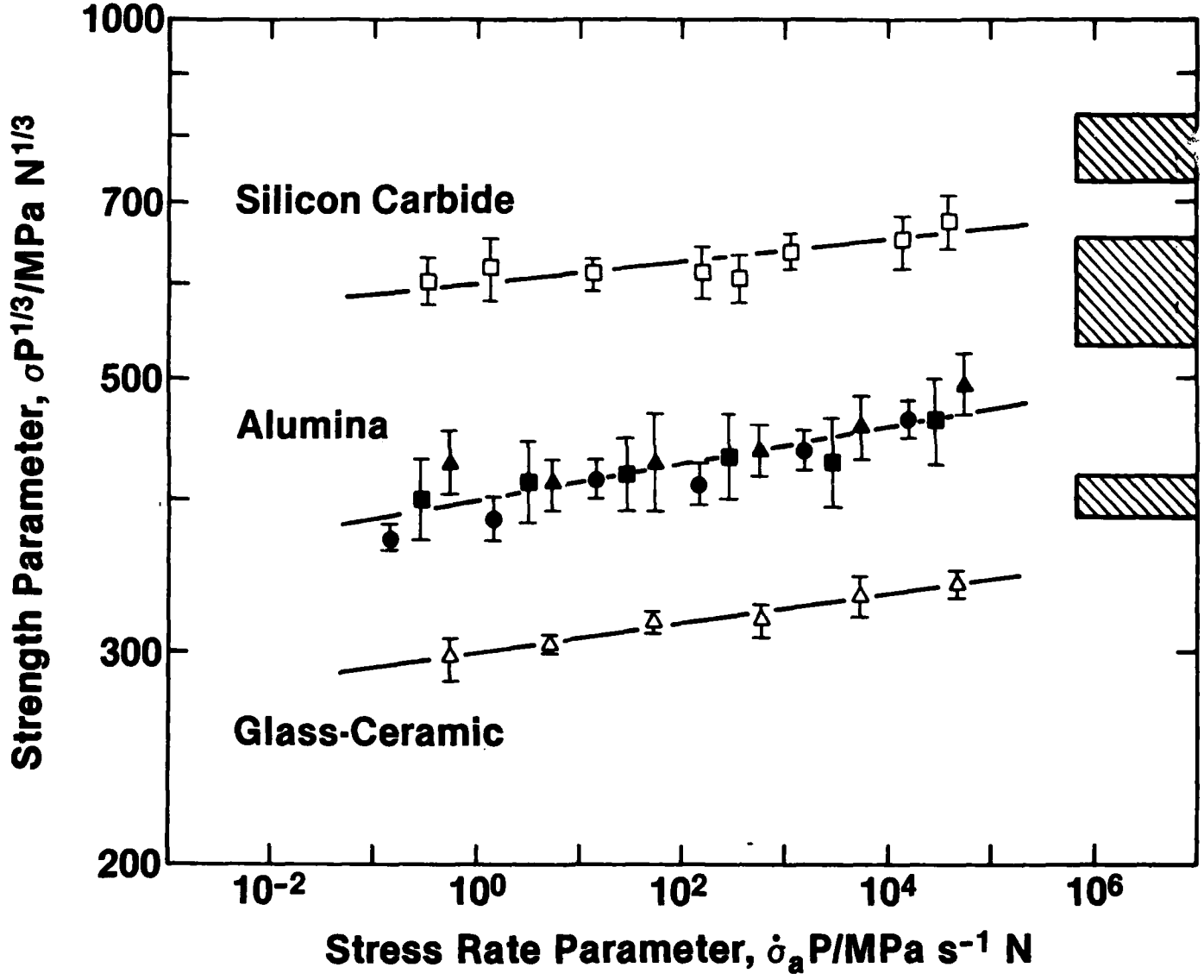
1000
700
500
300
200
Silicon Carbide
Alumina
Glass-Ceramic
Strength Parameter, σP^1/3/MPa N^1/3
10^-2
10^0
10^2
10^4
10^6
Stress Rate Parameter, σ̇aP/MPa s^-1 N

A MODIFIED INDENTATION TOUGHNESS TECHNIQUE

R.F. Cook* and B.R. Lawn

Center for Materials Science
National Bureau of Standards
Washington, DC 20234, U.S.A.

*On leave from the University of New South Wales

ABSTRACT

A modified indentation technique for measuring toughness is described. The method retains the elastic/plastic basis of previous contact fracture descriptions, but eliminates explicit reference to residual stress parameters in the toughness formulation. Accordingly, improved correlations between indentation data and "conventional" K_c values are obtained, even for materials (e.g. anomalous glasses) with non-ideal deformation responses.

Indentation methods are now widely used for determining toughness characteristics of brittle glasses and ceramics. These methods fall into two main categories: (I) tests in which K_c is evaluated from direct measurements of crack size as a function of indentation load[1,2]; (II) tests where the indentation crack serves as a controlled flaw in a flexural specimen, so that K_c is determined by a strength measurement.[3,4] Estimates of absolute accuracy levels run at 30-40% for both categories, for materials with "well-behaved" indentation patterns.[2,4]

A critical factor in any indentation toughness determination is a proper accounting of the residual contact stresses in the fracture mechanics formulae. These stresses play a primary role in driving the cracks at all stages of growth, both during and after the indentation cycle. Existing models of the fracture processes derive from oversimplistic elastic/plastic analyses[5-7], necessitating the "calibration" of the residual field terms from "standard" materials of known toughness.[2,4] Implicit in all these models are certain assumptions concerning the geometrical similitude of the indentation patterns from material to material. As we shall indicate, cases arise where such similarity principles are no longer applicable, leading to unacceptable error levels in the toughness estimates. In light of this problem, we shall propose a "modified" indentation testing approach, a "hybrid" of the two methods categorized above, which avoids specific reference to residual stress terms altogether.

We begin by outlining the basis of the two existing methods. In the first, Fig. 1a, the characteristic crack size c_o is measured, usually from surface radial traces, at given indentation load P. Direct observation of the

crack evolution during the actual contact process shows that the bulk of the surface growth occurs on unloading, i.e. as constraining elastic stresses are removed.[5] Under such conditions the crack approaches its immediate post-indentation configuration in a state of stable equilibrium. Then we may write[2]

$$K = \chi P/c_o^{3/2} = K_c \tag{1}$$

where the parameter χ characterizes the intensity of the residual driving force, as our toughness equation. Strictly, measurements of c_o after the event should be carried out in an inert environment, for the crack may be susceptible to further, subcritical extension in the persisting contact field.

In the second method, Fig. 1b, the indentation crack is subjected to an applied stress σ_a. The system remains in equilibrium in inert test environments, so that the stress intensity factor now becomes[6]

$$K = \chi P/c^{3/2} + \psi\sigma_a c^{1/2} = K_c \tag{2}$$

where ψ is a crack geometry parameter. This state of equilibrium is maintained by stable growth of the crack with increasing stress until failure occurs at the maximum in the $\sigma_a(c)$ function; thus, at $d\sigma_a/dc = 0$ Eq. (2) gives

$$\sigma_m = 3K_c/4\psi c_m^{1/2} \tag{3a}$$

$$c_m = (4\chi P/K_c)^{2/3} \tag{3b}$$

In this type of test the most accessible variables are P and σ_a, so one usually eliminates c_m from Eq. (3) to obtain[4]

$$(256\chi\psi^3/27)^{1/4} (\sigma_m P^{1/3})^{3/4} = K_c \qquad (4)$$

In this case toughness evaluations can be made without ever having to measure a crack dimension.

The usefulness of Eqs. (2) or (4) for K_c determinations thus rests with our ability to specify the material dependence of the residual parameter χ. For an ideal elastic/plastic material in which the indentation process can be represented by an "expanding cavity" model[8], this dependence is relatively straightforward; we obtain $\chi \propto (E/H)^{1/2}$ approximately, where E is Young's modulus and H is hardness.[7] Embodied in this idealization is the assertion that the plastic component of the deformation is a constant volume process, characterized by a well-defined yield stress. Not all brittle materials deform in this way, however. So-called "anomalous" (network former) glasses and porous or phase-transforming ceramics can accommodate the indentation volume, at least partially, by structural densification. Such densification modes produce much lower residual stress levels in the constraining elastic material about the indentation, with consequent reductions in the appropriate χ values.[9] Similar reductions may be expected in softer ceramics which minimize elastic constraints by allowing yielded material to "pile up" around the penetrating indenter, as occurs in most metals.[10] Additional, post-indentation relaxation of the χ term may be effected by subcritical growth of lateral cracks,[4,11] mechanical removal of the contact deformation zone,[3] specimen heating,[12] etc.

In selecting our standard materials for calibrating the toughness equations we naturally seek candidates for which the deformation response is close as possible to the ideal.[2,4] In general, such a calibration will provide us with an upper bound to χ for any subsequent test specimen. This in turn will tend to bias the indentation-determined toughness values above the "true" values. An extreme example of this is shown in the data in Table 1 for two glasses, soda-lime and borosilicate, which are respectively normal and anomalous in their indentation behavior.[9] Whereas the K_c values from indentation[2,4] and "conventional" (double-cantilever beam)[13] determinations agree to within 25% for the normal glass, there are differences of greater than a factor of 2 for the anomalous glass. Discrepancies of this magnitude are not exactly conducive to comparative materials evaluation.

It is clear from the above discussion that the indentation approach will benefit by any modification which minimizes reliance on the χ parameter. Reference to Eq. (3) shows that such reliance can be eliminated altogether if we replace P by c_m as a test variable; our new toughness equation then follows directly from Eq. (3a),

$$(4\psi/3)\sigma_m c_m^{1/2} = K_c \qquad (5)$$

The modified procedure represents a hybrid of the two earlier methods, in that both a crack size and a strength measurement are required. Of course, the fact that χ does not appear explicitly in Eq. (5) does not mean that residual stresses play an insignificant role in the indentation test; χ is simply incorporated into a directly measurable quantity, via. Eq. (3b).

It is possible to measure c_m directly by setting up a microscope facility onto the strength test apparatus, and monitoring the crack extension to the failure point.[6,14] However, this is not a practical arrangement for most routine materials testing laboratories. An alternative procedure is to use "dummy" indentations, as in Fig. 2.[15] Thus, more than one (3, in the present tests) Vickers indentations are placed on the prospective tensile surface, within the inner span, of a 4-point bend specimen. Ostensibly, all such indentations should experience a near-identical stress history during the bend test, provided the separations are sufficiently large that interactions with neighbors do not occur. In practice, the inevitability of slight inhomogenieties in the loading system ensures that failure occurs from just one of the indentations, leaving intact dummies available for the measurement of the critical crack dimensions.

The results of tests using the modified procedure are shown as a plot of $\sigma_m c_m^{1/2}$ against K_c for several materials in Fig. 3. The vertical error bar on each data point represents standard deviation bounds for measurements on 12-15 specimens. The data cannot be fitted to a straight line through the origin, as required by Eq. (5), implying that the crack geometry parameter ψ does not satisfy the similitude requirements. Nevertheless, a linear best fit

$$K_c = A\,\sigma_m c_m^{1/2} + B \qquad (6)$$

with A = 2.02 and B = -0.68 does intersect all error bars, and should therefore serve as a convenient empirical calibration function for evaluating the toughness of other materials. Moreover, the data points for the soda-lime

and borosilicate glasses now fall almost identically on the representative line, so the gross departures from universal indentation behavior evident in Table 1 do indeed appear to have been largely eliminated.

In weighing up the merits of our technique we need to be aware of any attendant disadvantages. We have replaced P with c_m as a test variable, and crack dimensions are notoriously susceptible to measurement errors (particularly on the small scale of typical indentation patterns). We recall from our derivation of Eq. (3) that the failure condition is approached via a maximum in the $\sigma_a(c)$ function, so small variations in stress levels on the dummy indentations could lead to substantial variations in crack sizes. It is therefore important to adopt a consistent experimental methodology in the calibration scheme of Fig. 3, to minimize the influence of any systematic component in such variations.

Accordingly, the modified indentation method should be seen as supplementing rather than replacing its predecessors. It is certainly to be preferred for any material suspected of deforming by other than constrained plastic flow. It might also be used effectively where stress relaxation processes can occur, e.g. at elevated temperatures. The relative lengths of the crack arms perpendicular and parallel to the tensile direction in Fig. 2 then provide an immediate indication of the intensity of the residual stress influence. If the former arms show no signs of having expanded during the strength test it can be taken that the residual field is now reduced to insignificant proportions (in which case the indentation toughness formulation would need to be entirely restructured[6]).

ACKNOWLEDGEMENT

Funding for this work was provided by the U.S. Office of Naval Research, Metallurgy and Ceramics Program.

REFERENCES

1. A.G. Evans and E.A. Charles,"Fracture Toughness Determinations by Indentation," J. Am. Ceram. Soc., 59 [7-8] 371-72 (1976).
2. G.R. Anstis, P. Chantikul, B.R. Lawn, and D.B. Marshall, "A Critical Evaluation of Indentation Techniques for Measuring Fracture Toughness: I," J. Am. Ceram. Soc., 64 [9] 533-38 (1981).
3. J.J. Petrovic and M.G. Mendirattta; pp. 83-102 in Fracture Mechanics Applied to Brittle Materials. Edited by S.W. Freiman. A.S.T.M. Spec. Tech. Publ., No. 678, Philadelphia, 1979.
4. P. Chantikul, G.R. Anstis, B.R. Lawn, and D.B. Marshall, "A Critical Evaluation of Indentation Techniques for Measuring Fracture Toughness: II," J. Am. Ceram. Soc., 64 [9] 539-43 (1981).
5. D.B. Marshall and B.R. Lawn, "Residual Stress Effects in Sharp Contact Cracking: I," J. Mater. Sci., 14 [8] 2001-12 (1979).
6. D.B. Marshall and B.R. Lawn, "Residual Stress Effects in Sharp Contact Cracking: II," J. Mater. Sci., 14 [9] 2225-35 (1979).
7. B.R. Lawn, A.G. Evans, and D.B. Marshall, "Elastic/Plastic Indentation Damage in Ceramics: The Median/Radial Crack System," J. Am. Ceram. Soc., 63, [9-10] 574-81 (1980).
8. R. Hill, The Mathematical Theory of Plasticity; Ch. 5. Oxford University Press, London, 1950.
9. A. Arora, D.B. Marshall, B.R. Lawn, and M.V. Swain, "Indentation Deformation/Fracture of Normal and Anomalous Glasses," J. Non-Cryst. Solids, 31 [3] 415-28 (1979).
10. D. Tabor, Hardness of Metals; Ch. 7. Clarendon Press, Oxford, 1951.

11. B.R. Lawn, D.B. Marshall, and P. Chantikul, "Mechanics of Strength-Degrading Contact Flaws in Silicon," J. Mater. Sci., 16 [7] 1769-75 (1981).

12. D.H. Roach and A.R. Cooper, unpublished work.

13. S.M. Wiederhorn, "Fracture Surface Energy of Glass," J. Am. Ceram. Soc., 52 [2] 99-105 (1969).

14. D.B. Marshall, "Controlled Flaws in Ceramics: A Comparison of Knoop and Vickers Indentation," J. Am. Ceram. Soc., 66 [2] 127-31 (1983).

15. R.F. Cook, B.R. Lawn, and G.R. Anstis, "Fatigue Analysis of Brittle Materials Using Indentation Flaws: II," J. Mater. Sci., 17 [4] 1108-16 (1982).

Table 1. K_c evaluations for two glasses (MPa $m^{1/2}$) using conventional and indentation (Fig. 1) techniques

Glass	D.C.B.	Indentation I	Indentation II
Soda-lime (normal)	0.75	0.8	1.0
Borosilicate (anomalous)	0.77	1.6	1.2

FIGURE CAPTIONS

1. Schematic of established indentation methods: (I) direct crack size method; (II) controlled flaw/strength method.

2. "Dummy" indentation method. Specimen breaks from one indentation, leaving survivors on surface from which c_m can be measured.

3. Results of tests using modified indentation toughness method, for selected glasses and ceramics.*

*a. Schott-Ruhrglas (GMBH)

b. Schott-Ruhrglas (GMBH)

c. Schott-Ruhrglas (GMBH)

d. Plessey, Australia

e. Channel Industries

f. Synroc B, Australian Atomic Research Establishment

g. Pyroceram C9606, Corning

h. AD96, Coors Porcelain

i. NC 203, Norton

j. F99, Freidrichsfeld GMBH

(I)

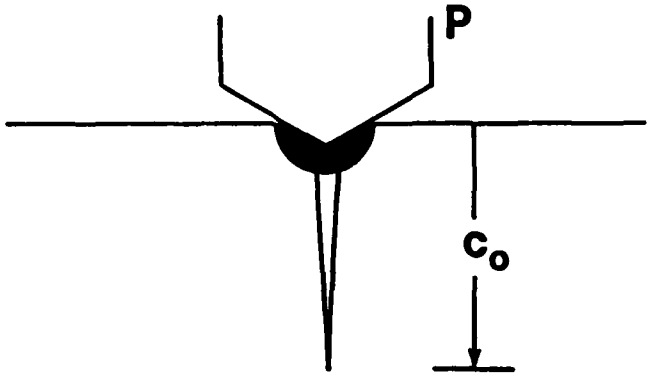

(II)

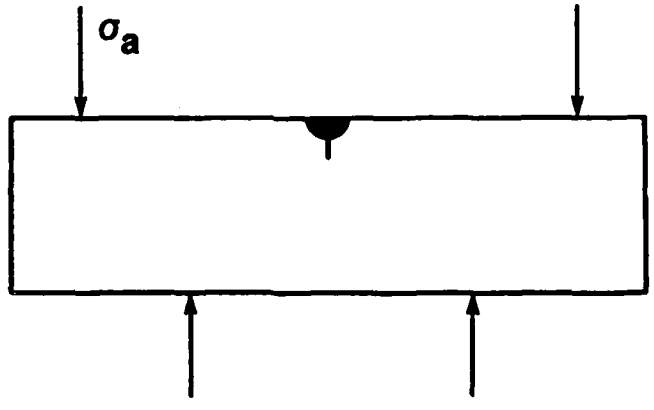

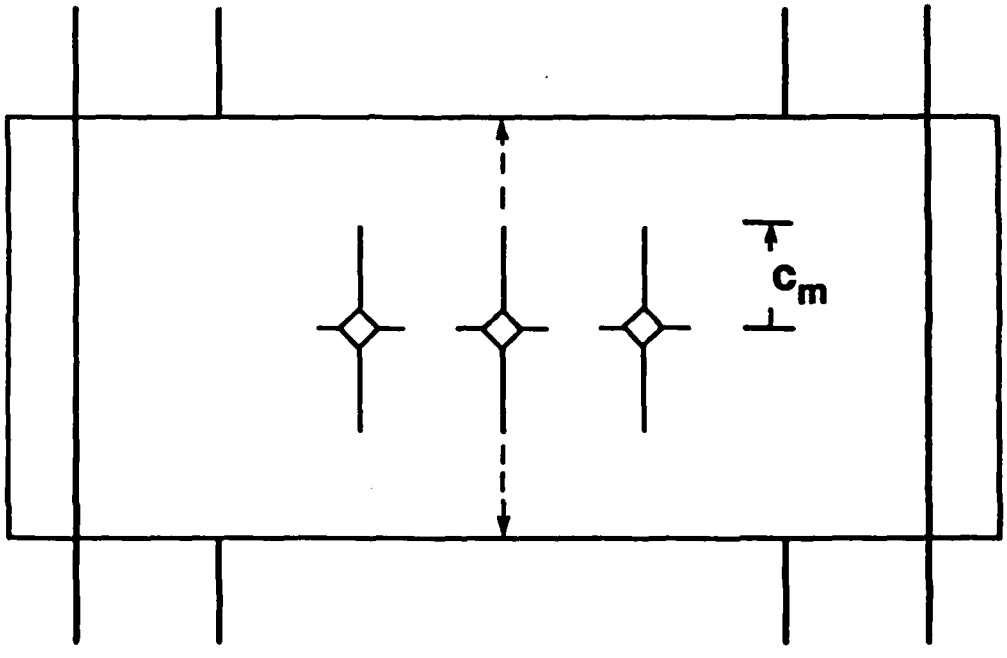
c_m

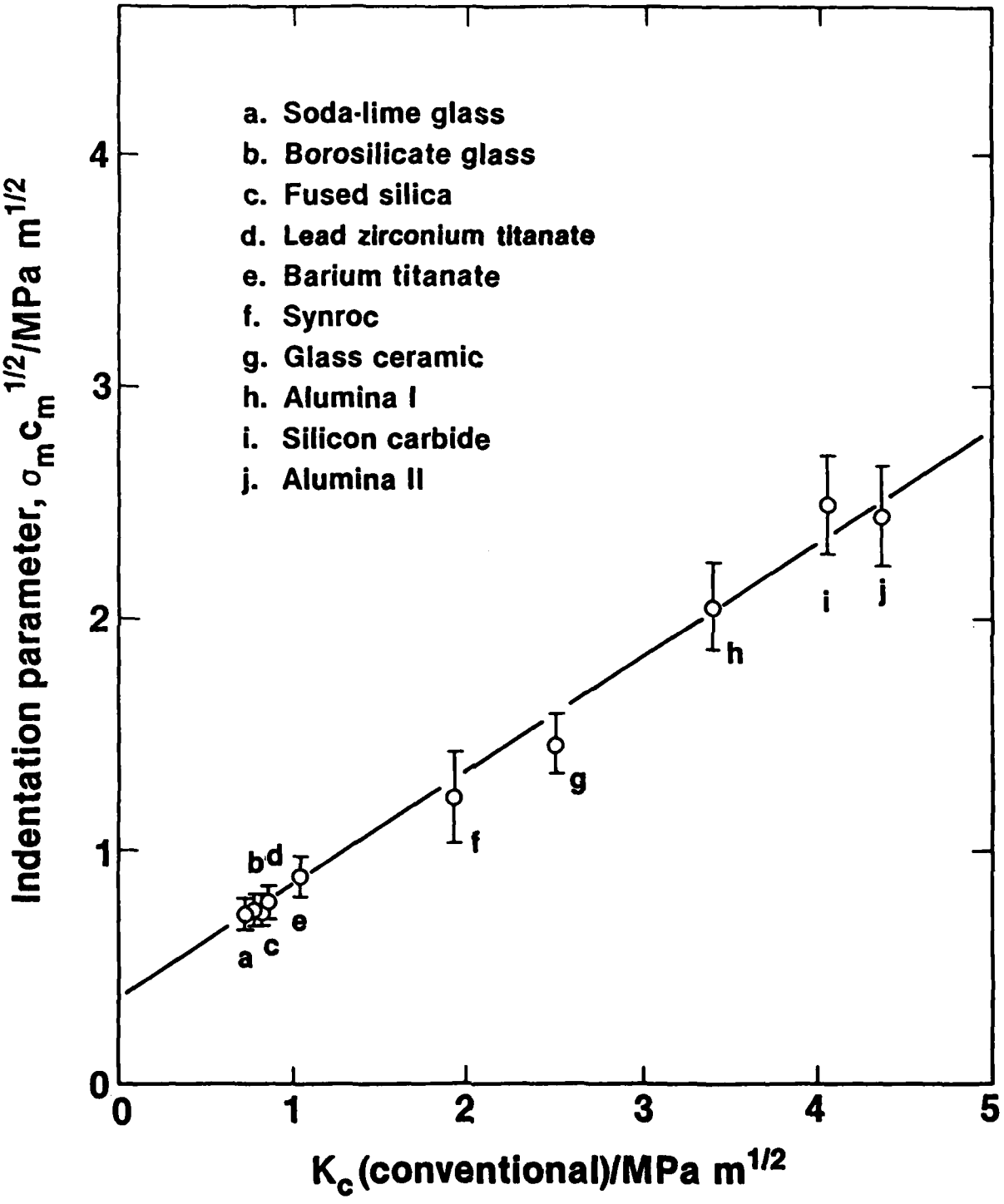
a. Soda-lime glass
b. Borosilicate glass
c. Fused silica
d. Lead zirconium titanate
e. Barium titanate
f. Synroc
g. Glass ceramic
h. Alumina I
i. Silicon carbide
j. Alumina II
Indentation parameter, $\sigma_m c_m^{1/2}$/MPa m$^{1/2}$
K_c(conventional)/MPa m$^{1/2}$
0
1
2
3
4
5

END

DATE
FILMED

11-83

DTIC